Design and Development of IGBT-Based Pulse Voltage Generator for Insulation Testing

by

Yatong Yu

A thesis

presented to the University of Waterloo

in fulfillment of the

thesis requirement for the degree of

Master of Applied Science

in

Electrical and Computer Engineering

Waterloo, Ontario, Canada, 2009

Author's Declaration

I hereby declare that I am the sole author of this thesis.

This is a true copy of the thesis, including any required final revisions, as accepted by my examiners.

I understand that my thesis may be made electronically available to the public.

Abstract

With the desire for energy conservation and lower costs, the application of pulse-width modulated (PWM) voltage source converter (VSC) drives has grown at an exponential rate. However, due to their high switching frequency and high *dv/dt*, increased dielectric stresses and thermal stresses are applied to the insulation system of the motors, which may lead to the failure of the insulation. In order to test the performance of the motor insulation under the above complex stress conditions, an IGBT-based pulse voltage generator which can produce high voltage square wave and PWM waveforms has been successfully developed in this research.

The generator consists of IGBT switches and other wave shaping components. The special cascade connection circuit design enables the generator to produce the stable high voltage square wave and PWM waveforms. A microcontroller-based trigger signal generator is used to trigger the power electronic switches in the generator. In order to avoid false triggering from electromagnetic interference (EMI), optical fibre cables are used to connect the trigger signal generator to the switches which are located in a high electric potential area. The generator can produce square wave and PWM waveforms with a peak voltage up to 15 kV and with a switching frequency of 600 Hz to 6 kHz. The fundamental frequency of the PWM waveform is 20 Hz to 1200 Hz, the rise time is less than 200 ns, and the pulse width can be varied up to several milliseconds.

A 4 kV_{rms} form wound model stator coil was tested under different voltage waveforms: power frequency, exponential decay pulse, square wave, and sinusoidal pulse-width modulated (SPWM) waveform. Infrared images and the maximum temperature rise of the coil under different electrical stresses were recorded. The results show that both the square and SPWM voltage waveforms cause a significantly higher temperature rise than the power frequency and exponential decay pulse voltage waveforms. Since the actual VSCs generate transients similar to those of the square and PWM voltage waveforms, it is recommended that the stator coil insulation be analyzed using PWM voltage waveforms in order to simulate actual conditions.

Acknowledgements

I am grateful to my academic supervisor, Dr. Shesha Jayaram, for her help, support, and guidance throughout the duration of this work.

I would like to thank my readers Dr. Edward Cherney and Dr. Magdy Salama, for their valuable comments towards my work.

I would like to thank Dave Messervey, and Ramtin Omranipour along with the research group at GE, Peterborough, Canada for providing coil samples.

Thanks my friends of the high voltage group: Dr. Ali Naderian, Dr. Isaias Ramirez, Dr. Fermin Espino-Cortés, and Dr. Saeed Ul-Haq for helping. I would also like to thank other past and present members of the HVEL group, include: Gowri, Emad, Chitral, and Ganesh for their company during these years.

Thanks to Murched Ajami, Jin Hyun Chang and other under graduate research assistants for their contribution to the work.

To my loving daughter Jessica
To my loving wife Wei Huang

To my mother and mother-in-law

Table of Contents

List of Tables

List of Figures

Chapter 1
Introduction

Industrial motors are the largest end users of electricity in modern society. In North America, about 70% of the electricity consumed by industry is used to power motors. Over the past 20 years, induction motors have dominated the motor market, and about 90% of industrial motors are AC induction motors [1]. To a large extent, this dominance is due to tremendous gains in the technology and packaging of signal and power electronics during this period, which have resulted in smaller and less expensive adjustable speed drives (ASDs), sometimes called variable speed drives (VSDs).

An adjustable speed drive basically consists of a rectifier, a DC link, and an inverter, which converts the 60Hz AC from the utility power source to the AC of a selected frequency. Such power electronic-based ASDs for medium and high voltage induction motors emerged in the early 1980s. The first medium-voltage ASD was a current source converter (CSC) type, in which a reactor was used as a DC link to provide a DC current. Since the current source converter ASDs are bigger, less efficient and have a higher cost than voltage source converter (VSC) ASDs, they are being replaced by voltage source converter ASDs in a wide range of applications. In voltage source converter ASDs, capacitors are used as a DC link to provide a constant DC voltage.

High-speed power electronic switches, such as gate turn-off thyristors (GTOs), insulated gate bipolar transistors (IGBTs), metal-oxide-semiconductor field effects transistors (MOSFETs) or integrated gate commutated thyristors (IGCT) rectify the DC voltage to square-wave pulses with an adjustable pulse width, in which the fundamental frequency of the output voltage can be adjusted by changing the trigger signal of these switches. This combination of signal and power electronic techniques has overcome the shortcomings of the induction motor with respect to speed control.

The applications of induction motors fed by voltage source converters have therefore significantly increased over recent years and now dominate the market. However, the new pulse width modulated (PWM) voltage source ASDs provide a more complex voltage waveform to the motors than the power frequency sinusoidal voltage waveform; thus, concerns about the adverse effects of such drives on the motor insulation has increased as the applications of drives based on PWM voltage has increased.

The PWM voltage waveform consists of a group of voltage pulses with a fast rise time and varying pulse widths. Several studies have shown that the PWM voltage waveform causes enhanced electrical and thermal stresses on the motor coil [3, 4, 5] that leads to premature stator damage or failure. Unfortunately, the motor manufacturing industry has neither test standards nor test facilities that addresses the issue of enhanced stresses caused by solid state switching drives. Suitable testing equipment is therefore needed for the qualification and acceptance of electrical insulation systems in motors fed by ASDs.

The main objective of this thesis is to design and develop an IGBT-based pulse voltage generator that can produce high voltage square wave and PWM waveforms for qualification and acceptance testing of electric rotating machines fed by voltage source converters. The following sections in this chapter provide background knowledge about the adjustable speed drives, the structure of motor insulation systems, and the enhanced electrical and thermal stresses caused by the PWM voltage waveforms. A review of updated industry-standard insulation test methods and previous designs of high pulse voltage generators are also presented.

1.1. Adjustable speed drives

The development of adjustable speed drives has dependent strongly on the development of power electronic components. Fig. 1.1 shows the progress of power electronic devices in the last half-century. The era of power electronics began with the invention of the first commercial thyristor developed by General Electric (GE) in 1958 [6]. These semiconductor devices were originally designed for use in

communication systems. Since then, the development of power electronic devices and their associated circuits has led to steady improvement in the ratings of thyristors and their operating frequency, eventually resulting in the extension of their application to motor control systems and power systems.

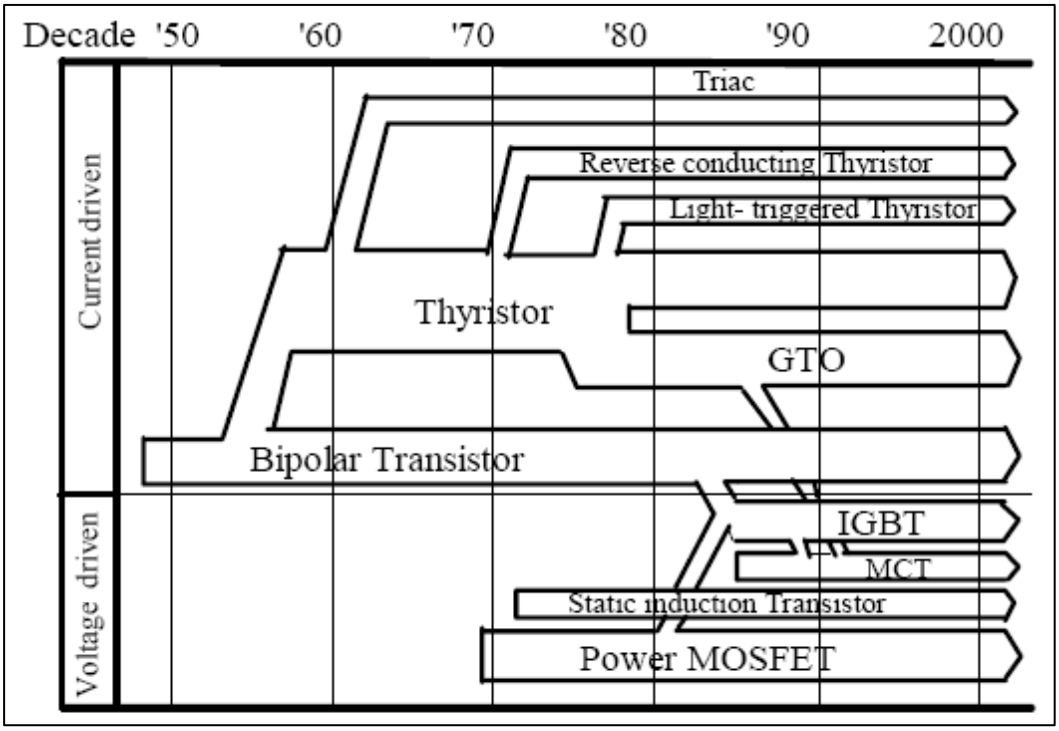

Fig. 1.1: Development of power electronic devices [6].

Fig. 1.2 shows the development history of motors and their power electronic drive systems. From the late 1950s to the early 1980s, high-power thyristors have been used as controllable rectifiers to control the speed of DC motors. By 1975, the first turn-off semi-conductor component was developed; since then, various types of high-voltage, high-power, and high-speed power electronic controllable switches have been developed and made available on the market, including MOS-controlled thyristors (MCTs), MOSFETs, GTOs, IGBTs, and IGCTs. These revolutionary power electronic elements, combined with modern communication signal techniques, has led

to the arrival of the variable frequency converter, which can be used as an adjustable speed drive for all types of AC motors.

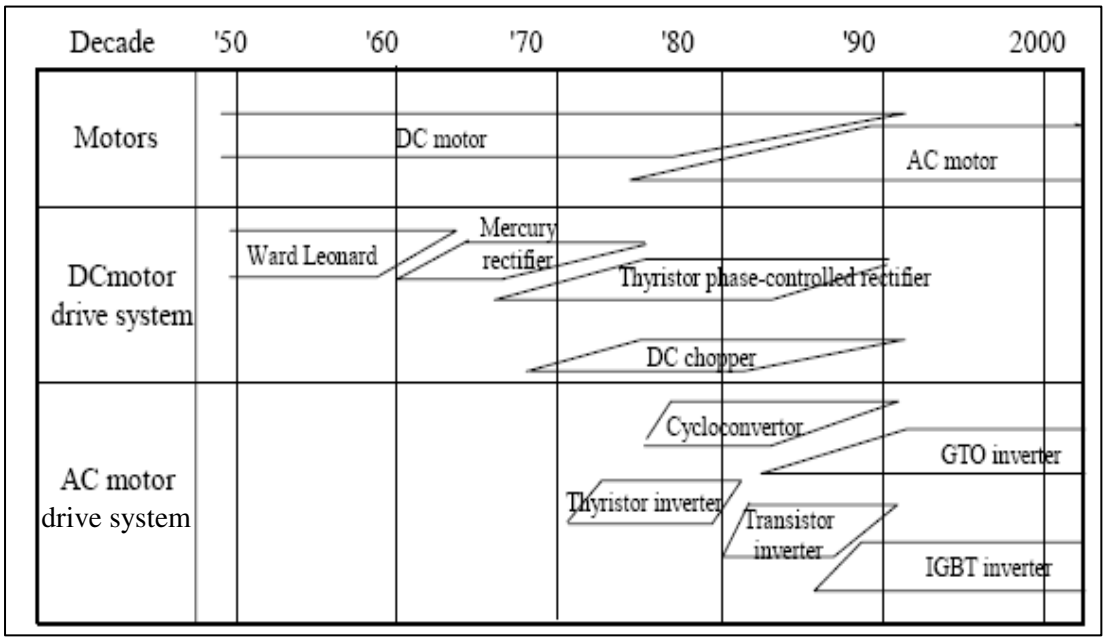

Fig. 1.2: Development history of motors and drive systems [6].

Power electronic-based adjustable speed drives can be classified into two main categories [8]: CSCs and VSCs. In current source converters (Fig. 1.3.), the DC term is a regulated current, and DC inductors are selected to provide the current source. The immediate output is a pulsed current whose fundamental component is controllable in magnitude, phase angle, and frequency through the adjustment of a modulating signal. Output capacitive filters are required in order to eliminate current harmonics from the output current. Thus the voltage and current applied to the motor are quasi-sinusoidal, which is less harmful to the motor insulation system. However, because of the heavy and bulky DC-link choke and the possible occurrence of resonances between the capacitive filter and the motor inductances, current-source converters are less frequently used in industrial applications. The main applications of this type of converter are in active power filters and high-power AC motor drives in which the motors are fed with a long connecting cable.

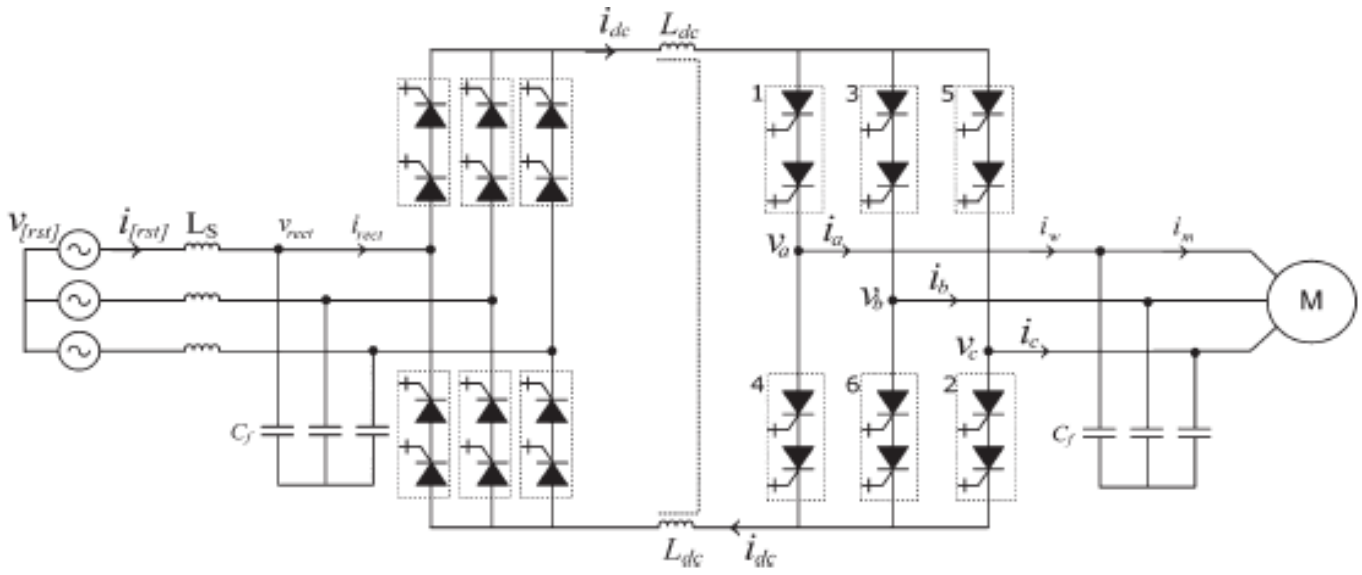

Fig. 1.3: Current source converter with PWM rectifier and inverter [49].

On the other hand, in VSCs (Fig. 1.4), capacitors are used for the DC-link rather than the heavy and bulky DC-link choke to provide a constant DC regulated voltage. The output voltage of a VSC is a chain of pulsed voltages, and the local average voltage (the average voltage per switching period) of each pulsed voltage in the chain is controlled by the IGBT switches. In a SPWM converter, which is one of the most commonly used in motor drives, the local average voltage of the output voltage is a sinusoidal waveform (also called a fundamental component). Because VSCs are smaller, lower cost, more reliable, and more efficient than CSCs, they have dominated the motor drive market. The main disadvantage of VSCs is the generation of high *dv/dt* transients and high frequency harmonics, which may cause enhanced electrical and thermal stresses on the motor insulation system and thus results in premature failure of the motors.

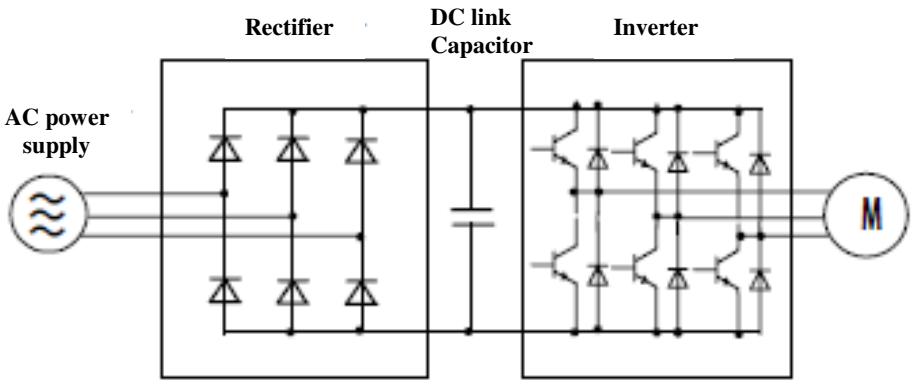

Fig. 1.4: Voltage source converter with diode bridge rectifier and PWM inverter.

1.2. Stator insulation system

The design considerations for a motor insulation system include both electrical properties and mechanical properties, such as dielectric stress, resistance to partial discharge, corona protection, desired thermal class, and durability [10]. Motor stator insulation is a kind of laminated insulation, which contains multiple layers of insulation made of various materials; conductive layers such as conductive tape for slot corona protection; and stress grading coatings. Fig. 1.5 shows both structures of random-wound and form-wound stator insulation systems.

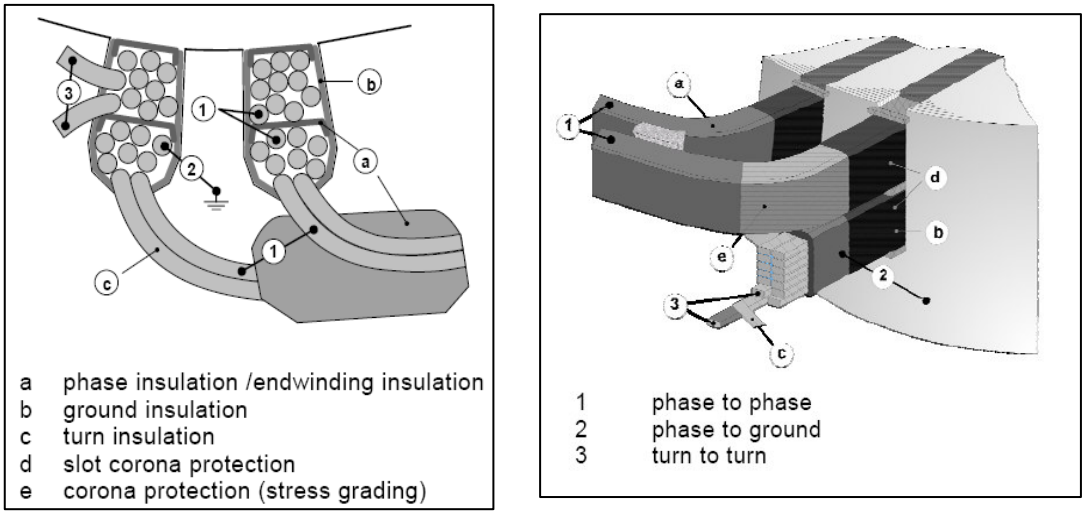

Fig. 1.5: Structures of random-wound and form-wound motor insulation system [28].

The innermost layer is enameled magnet wire coating. In form-wound medium and high voltage motors, several insulation tapes may be needed to cover the magnet wire in order to enhance the turn insulation level. The turn insulation has two purposes: to insulate between turns and to provide good adhesion between the conductor and the impregnating resin. Sometimes the turn insulation may contain conductive additives in order to decrease the partial discharge (PD) activity close to the conductors.

Moving outward from the turn insulation, the next layers are the ground wall and slot insulation and the phase insulation layers. The ground wall and slot insulation provides electrical insulation between the motor winding and the motor core. The phase insulation separates the wire bundles of the different phases in the core slot and coil overhang. Both serve as electrical insulation as well as mechanical protection.

For medium and high voltage motors, the slot portion of the coil is wrapped with layers of conductive armour tape. The main function of this low-resistance layer is to provide a good contact between the coil and the core, eliminating possible partial discharge (PD) and hence the erosion caused by the PD. They also provide protection against vibration damage. The conductivity of the armour tape is constant at about 10^{-2} to 10^{-5} S/m, thus avoiding short circuiting of core laminations and Eddy current [50]. At the end of the coil, which has a rated voltage above 4.16 kV, layers of voltage stress grading material is used to force the electric field uniform, preventing the occurrence of slot discharges due to sharp changes in voltage or the concentration of the electric field.

1.3. Enhanced electrical and thermal stresses by PWM-VSCs

PWM converters work with switching frequencies of up to 20 kHz. A PWM voltage waveform is a chain of square pulsed voltage with pulse widths varying at a specific mode in one fundamental cycle. Fig. 1.6 shows a typical PWM waveform recorded at the terminal of a motor stator fed from a PWM-VSC. The continuous strikes of fast transient voltage clearly increase the electrical and thermal stresses on the insulation system of the motor coil. These problems result from the PWM

waveform, which can be characterized according to its varying pulse width, rise time, fall time, peak value, and switching frequency.

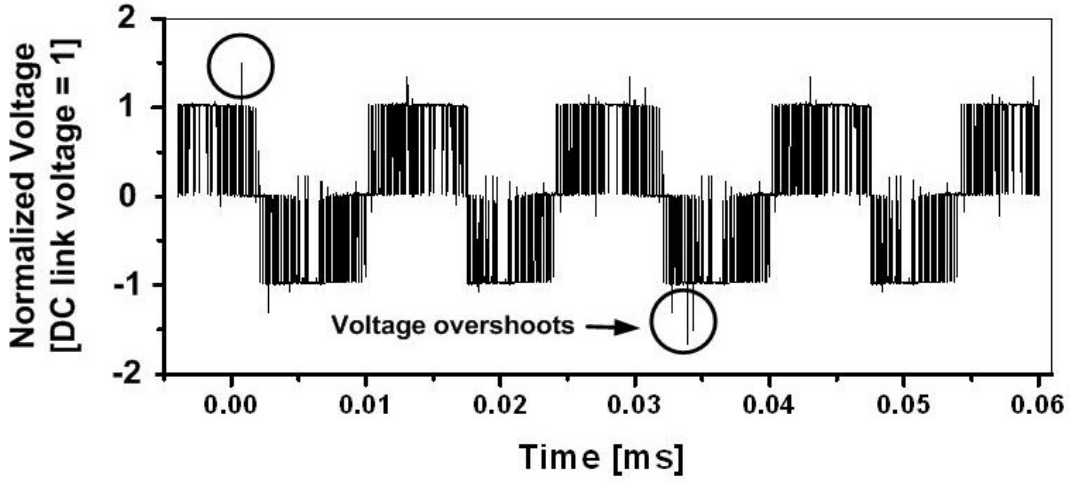

Fig. 1.6: A typical PWM voltage waveform measured at a motor terminal.

The high repetition rate pulse voltage with high *dv/dt* transients causes increased dielectric loss [14,15], space charge injection or charge accumulation in the insulation [16], and higher partial discharge activity [17, 18]. All these parameters have a negative effect on the insulation system of the motor and result in additional heating within the motor insulation system, causing a general or local temperature rise. Enhanced thermal stress is thus applied to the motor insulation system, which may lead to failure of the motor.

Additionally, the enhanced thermal stress on the insulation system of the motor may be caused by the high frequency harmonic content in the PWM voltage waveform. As mentioned before, the motor insulation system is a laminated structure that contains multiple layers of insulation composed of various materials, conductive tape for the elimination of slot discharges, and semi-conductive stress grading coatings. Each of these materials has its own characteristic frequency response; some insulation materials are sensitive to high frequencies, some of them are not so sensitive to high frequencies.

When the multiple sinusoidal voltages of the various frequencies of PWM waveforms are applied simultaneously to the motor insulation system, some of the frequency-sensitive materials in the laminated insulation system generate more heat under the high frequency harmonic stress. Additionally, in a laminated insulation system of motor coils, the diversity of the frequency response characteristics of the materials also changes the voltage distribution along the insulation layers. The voltage distribution under a high frequency harmonic is not the same as the voltage distribution under a power frequency voltage, which is strategically designed. Some layers in the laminated insulation system, such as the conductive armour layers, may be subject to increased voltage drop and therefore generate more heat, which results in a local temperature rise.

In summary, the insulation system of a motor that is fed by a voltage source converter is not exposed to the traditional power frequency sinusoidal voltage, but instead to a more complex voltage waveform, which may cause increased voltage stress and thus a higher level of thermal stress on the motor insulation, resulting in the premature failure of the motor. The increased stresses caused by PWM-VSCs are a function of the varying pulse width, rise time, fall time, crest value, and switching frequency of the PWM waveform and also of the impedances and frequency response characteristics of the feeding cable and the coil.

1.4. Review of insulation tests for rotating machinery

Insulation tests are designed to evaluate the condition of the electrical insulation in the design, qualification, acceptance, and maintenance of rotating machinery. The current test methods in IEEE and IEC standards [19-28] include an insulation resistance/polarization index measurement, a high potential test, a voltage-endurance test, a turn insulation test, and a high repetition rate impulse test. These tests are briefly described as follows:

- Insulation resistance/polarization index measurement [19]: Insulation resistance measurement has been used for more than half a century to evaluate the condition of electrical insulation. With the carefully maintained record of periodic measurements, accumulated over months and years of service, this

easy method is valuable as a measure of some aspects of the condition of the electrical insulation, such as contamination, absorbed moisture, or severe cracking. However, since the insulation resistance is not related directly to the dielectric strength (unless the defect is concentrated), it is impossible to show clearly that the insulation system of a motor is acceptable. Further, this index measurement is not sensitive to internal insulation defects.

- High potential test: In this test, a voltage higher than the rated voltage is applied to the test object for a specified time (usually 1 minute) for the purpose of determining the dielectric strength of the insulation system. The high potential test can use a power frequency source, a direct current source, or a very low frequency. According to the IEEE standards for stator coils, the power frequency AC test voltage is 1000 V_{rms} plus twice the rated voltage. Alternatively, the DC test voltage is 1.7 times the power frequency AC rms test voltage; the very low frequency AC test voltage is 1.63 times the power frequency AC rms test voltage.
- Voltage-Endurance test [25, 27]: The voltage duration test is designed for the stator coil of large motors and generators. An AC voltage higher than the rated voltage is applied to the stator coil for a long time (250 or 400 hours).
- Turn insulation test: Turn insulation tests are designed for testing the dielectric strength of turn insulation under transient voltage stress. Experience has shown that turn insulation failure can be caused by steep-front surges such as lightning strikes and breaker operations. Thus, in IEEE Std 522-2004, the recommended test voltage is one that has a frequency several orders of magnitude above the power frequency.
- High repetition rate impulse test: In IEC technical specification 60034-18-42, a repetitive impulse or a sinusoidal voltage at a frequency above 1000 Hz is recommended for evaluating the performance of an insulation system in rotating electrical machines that are fed by voltage source converters. This technical specification attempt to address concerns about the enhanced stresses caused by solid state switching devices.

1.5. Previous designs of power electronic based pulse voltage generator

A variety of techniques have been used to overcome the voltage limitations of power electronic switches and to achieve the high voltages needed by using relatively low voltage switches. The most common approaches are either connecting the semiconductor switches directly to the load, or connecting them to the load through signal or series-connected pulse transformers.

Kim et al. introduced a type of Marx circuit in order to generate a high voltage pulse power supply [37]. They claimed that their design can produce up to 200 kV pulse voltage with a repetition rate of up to 1000 pulses per second (PPS). The rise time of the pulse voltage is less than 1 μs, and the pulse width is up to 4 μs.

Fig. 1.7 shows the topology of the 20-stage Marx circuit described in their paper. Each stage is made of an IGBT stack, two diode stacks, and a capacitor. When the IGBT stacks are off, the capacitors (C_1~C_{20}) are charged by a common DC source through an inductor (L_1). If the IGBT stacks are turned on at the same time, the charged capacitors are simultaneously switched into a series configuration, delivering a pulse voltage to the load. In this transient moment, the inductor (L_1) acts as an isolator to separate the DC source from the high voltage output of the generator.

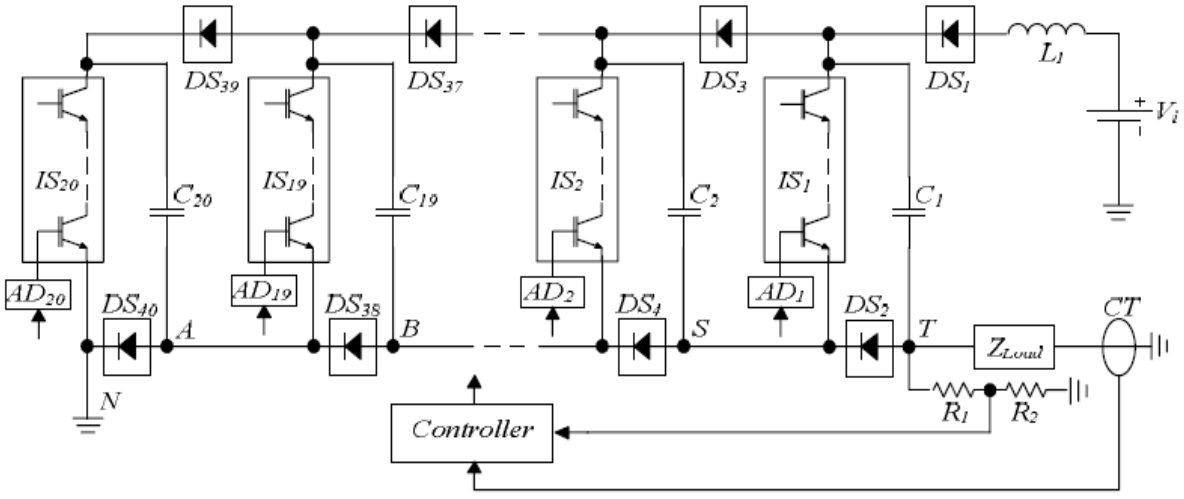

Fig. 1.7: A 20-stage Marx circuit.

Although this approach can successfully produce a high voltage pulse at a specific repetition rate, it can not be used to generate high voltage square and PWM waveforms due to the following limitations.

- One limitation is the pulse width. As previously mentioned, an inductor is used to isolate the DC source from the high voltage output at the moment when the IGBT stacks are turned on. According to the characteristics of the inductor, the inductor can isolate only transient voltage. If the IGBT stacks remained on for a longer period, or in other words, if this Marx circuit produced a wider pulse, the inductor would short-circuit, which might damage the DC source.
- Another concern about this Marx circuit is the risk of an unsynchronized switching operation problem. Because this circuit is actually a series configuration, the simultaneous operation of the switches is critical. If one or more switches in the IGBT stacks fail to operate simultaneously, all the IGBT stacks would then fail. Trigger circuits, protection circuits, and electromagnetic compatibility (EMC) should therefore be designed precisely, which means higher cost and lower reliability.

Redondo et al discussed a modular pulsed generator based on low voltage MOSFET switches and step-up pulse transformers [39]. Their generator produces up to 15 kV / 1 A with a 5 μs width at a 10 kHz repetition rate and a pulse rise time of less than 1 μs. A total of three individual stacked modules are used in the generator, each consisting of a modified forward converter that drives a step-up pulse transformer. The secondary side of the transformer in each module is connected in series with the one in the following module. The concept of the circuit in the generator is shown in Fig. 1.8.

The advantage of this generator is that it can produce a high pulse voltage by using low voltage MOSFET switches without any risk of switch failure. However, because pulse transformers are used in the generator to boost the voltage, the output waveforms are distorted due to leakage inductance and the residual capacitance of the transformer coils. The pulse width is also limited by the transformer for the same

reason. Another disadvantage is that the MOSFET driver circuits are supplied by batteries, which limit the continuous operation time of the generator. Therefore, although this approach provides a safe method of generating a high voltage pulse using low voltage power electronic devices, it can not be utilized to build a test facility that can generate high voltage square wave and PWM waveforms.

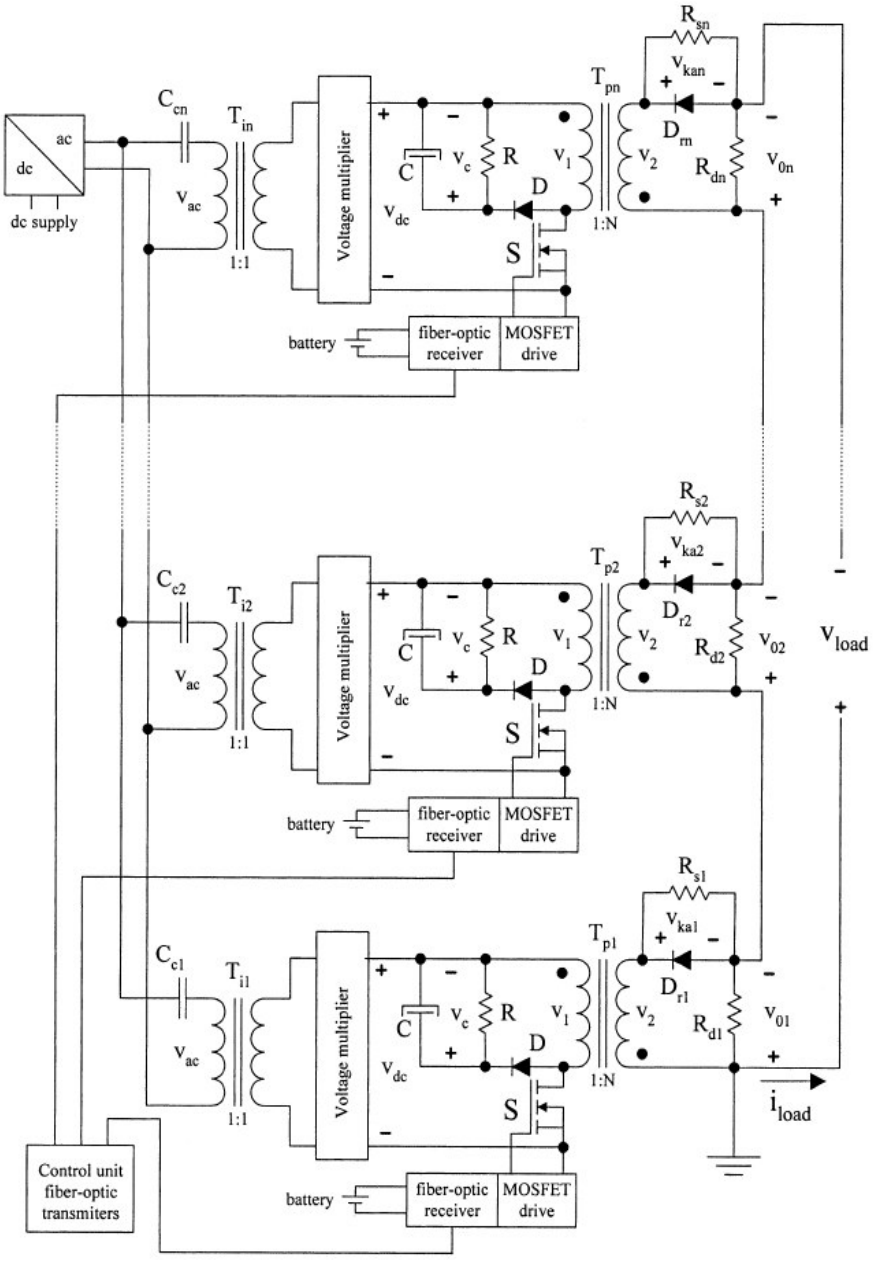

Fig. 1.8: Modular pulse power generator.

1.6. Thesis objectives and organization

A critical consideration in the design, manufacture, maintenance, and evaluation of a rotating machinery insulation is that any insulation test that is used should reflect the actual operating conditions to which the rotating machines are exposed when they are operating. As discussed and reviewed, the motors fed by power electronic-based voltage converters are affected by increased electric and thermal stresses due to varying pulse widths, a fast rise time, a high switching frequency, and the impedance of the feeding cable and motor coil. Until now, most insulation test methods and test facilities are traditional, which have been derived from the initial design of rotating machinery in which the motors are operated at a single power frequency. Thus, the difference between the test conditions of the motors and their actual operating conditions is highly significant. The current test methods and facilities are not directly related to the motor's dielectric strength under a PWM waveform and therefore cannot evaluate the performance of the motor insulation system effectively.

Current laboratory research has utilized fast repetitive exponential decay waves and single high frequency sinusoidal waves and has attempted to analyse the premature failure mechanism of motor insulation fed by a PWM voltage waveform. Although the results have shown that fast repetitive exponential decay or high frequency voltages have a negative impact on the motor insulation system, these factors may be only part of the problem. In fact, the failure mechanism of the motor coil is a result of a combination of a number of factors [34]. The fast repetitive exponential decay type of pulsed voltage or single high frequency sinusoidal waveforms are not the exact voltage waveforms which the motors are exposed to when they are fed by voltage source converters. These test waveforms contain only one or part of the adverse factors, not all of them. The accuracy of the evaluation results obtained by using these voltage waveforms is therefore highly dubious.

To improve the insulation system of large high voltage form-wound motors, motors should be tested with a voltage waveform similar to the waveform under which the motors are operated. This requirement would also be suitable for qualification and acceptance tests of electrical insulation systems.

The main goal of this thesis is thus to design and build an insulation test apparatus capable of generating high voltage square and PWM waveforms for the purpose of testing rotating machinery and other power system equipment insulation. The objectives of this thesis are therefore as follows:

- Design and build an IGBT-based pulse voltage generator capable of generating high voltage square wave and PWM waveforms. The peak value of the output voltage is up to 15 kV, which is suitable for insulation tests on motors rated to 13.8 kV (phase-to-phase). The rise time of each pulse in the waveforms is about 200 ns.
- Simulate and test the performance of the IGBT based pulse voltage generator with different loads.
- Compare the insulation performance of a form-wound coil under different voltage waveform stresses.

Accordingly, the thesis is organized as follows:

- Chapter 1 reviews background knowledge about adjustable speed drives, motor insulation systems, the enhanced stress caused by PWM voltage waveforms, current insulation test methods, and previous pulse voltage generator designs.
- Chapter 2 discusses the design of the main circuit and structure, including the mechanism of waveform generation, component selection, local IGBT switch driver circuits, cascade circuit design, the optical fibre signal transmission channel, and some structural insulation issues.
- Chapter 3 introduces the design of microcontroller-based square wave and PWM waveform trigger signal generator, including hardware and firmware.
- Chapter 4 presents the results of the simulation based on PSIM software as well as the experimental results produced by utilizing the generator on a variety of test objects. The insulation tests on a 4 kV motor coil with

different waveforms and an analysis of the results obtained are also provided in the chapter.

- Chapter 5 presents a summary of the conclusions and offers suggestion for future development and applications of the high voltage pulse generator.

Chapter 2

Cascade Connection Design for Generation of High Voltage Square and PWM Waveforms

This chapter presents the main circuit design of the IGBT-based pulse voltage generator. The generator consists of 10 stages connected in cascade; each stage can generate square and PWM waveforms independently. When the operations of all stages are controlled simultaneously, a high voltage square or PWM waveform is generated.

2.1 Mechanism of high voltage square pulse generation

Both square and PWM waveforms can be described as a chain of square pulses. The rise time, fall time, and pulse width determine the maximum achievable repetitive frequency of the pulse chain. The basic circuit for high voltage square wave and PWM wave generation is shown in Fig. 2.1. In Fig. 2.1(a), R_{con} represents the equivalent resistor of the connecting wire which is very small. R_1 is the wave shaping resistor, C_1 is the DC link capacitor, and C_{tr} represents equivalent capacitor that is the combination of residual capacitance of the wave shaping resistor and the load capacitance.

First, the capacitor C_1 is charged to voltage V_1. When the switch turns on (Fig 2.1(b)), C_{tr} is rapidly charged by the capacitor C_1, and the voltage across C_{tr} increases fast, thus the rising part of a square wave pulse is formed. During the turn-on period, the voltage V_{OUT} can be expressed as:

$$V_{OUT} \approx V_1\{1-\exp[-t\times(C_1+C_{tr})/R_{con}C_1C_{tr}]\} \qquad (2.1)$$

Since $C_1 >> C_{tr}$, the rise time of the square pulse is mainly determined by R_{con} and C_{tr}.

When the switch is on, capacitors C_1 and C_{tr} discharge through resistor R_1 as shown in Fig 2.1(c). The crest part of the square pulse is formed in this period. The voltage V_{OUT} in this period can be expressed as:

$$V_{OUT} \approx V_1 \exp[-t_W/R_1(C_1+C_{tr})] \qquad (2.2)$$

where t_W is the on-time of the switch SW_1. If t_W is much less than $R_1(C_1+C_{tr})$, the pulse width can be mainly decided by the on-time of the switch SW_1.

When the switch is off as shown in Fig 2.1(d), the capacitor C_{tr} discharges through R_1. This forms the falling part of the square pulse. The voltage V_{OUT} can be expressed as the equation (2.3). The equation shows that the fall time of the square pulse is determined by R_1C_{tr}.

$$V_{OUT} \approx V_1 \exp(-t/R_1C_{tr}) \qquad (2.3)$$

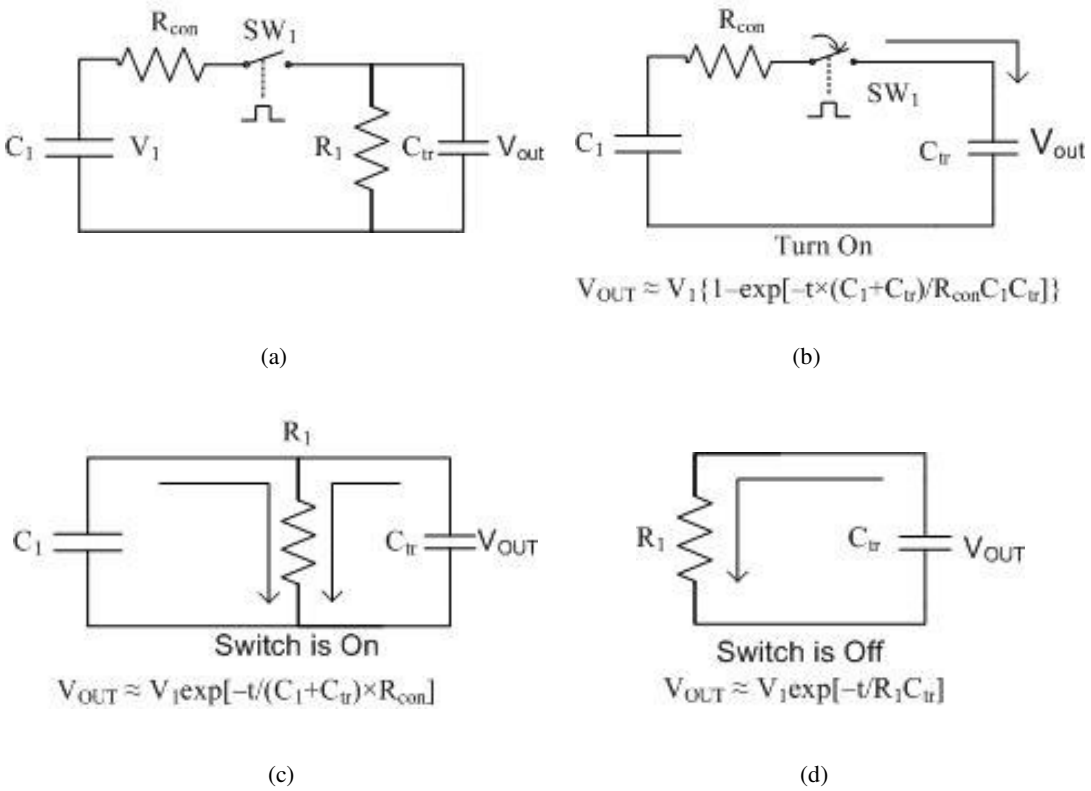

Fig. 2.1: Basic circuit for high voltage square wave and PWM wave generation.

With the properly selected values of resistors the capacitors, a square voltage pulse can be generated by turning the switch on and off. If the capacitor is charged from a stiff DC source, a square wave or a PWM wave can be produced by continuously turning on and turning off the switch in a prescribed mode.

2.2 Cascade connection and switch selection

Fig. 2.2 shows the capabilities of some power electronic devices that are available. The power transistors MOSFET, GTO, IGBT, and IGCT are some of the fast switches that can be used in the generation of high voltage square wave and PWM waveforms due to their high voltage rating.

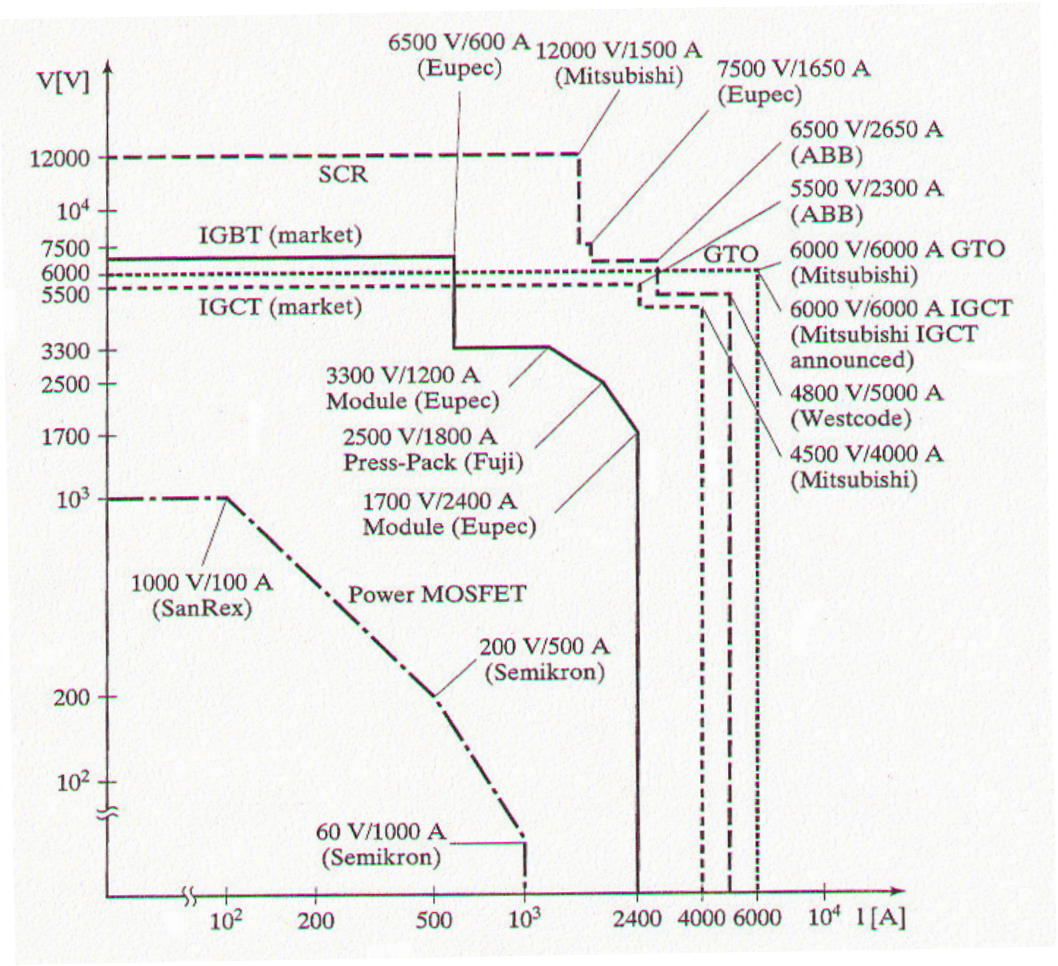

Fig. 2.2: Summary of power electronic components capabilities.

Because the majority of high voltage power electronic switches are also designed with correspondingly high current ratings, the cost of these high voltage switches are very high. Since high current capacity is not required for insulation testing, it is economical to build the generator based on the components that have relatively low voltage and low current ratings, and consequently, lower in cost.

A low cost discrete IGBT switch (IXMH16N170) is selected for building the IGBT-based pulse voltage generator in this research. This IGBT switch is manufactured by IXYS Inc. The voltage and current ratings are 1700V and 16A respectively. The typical turn-on time is around 93ns, and the typical turn-off time is 490ns. So theoretically, the maximum switching frequency can reach 1.7 MHz which is far higher than the operating frequency required for the motor insulation testing.

One way to enhance the voltage handling capability of low voltage switches is to connect low voltage switches in series, as shown in Fig 2.3(a). Although a lot of applications of this method are reported to be successful [29, 37], the possibility of non-uniform voltage distribution along the chain of switches can not always be avoided. The non-uniform voltage distribution in the series connection could be caused by two reasons.

One reason is that the steady-state and transient characteristic of each individual switch in the chain may not be identical due to variations that come about during manufacture. Therefore, the switches take a different share of the total voltage in the steady-state. For the same reason, the switches in a series chain may not turn-on and turn-off at the same time during switching transients even if the gating signals are applied simultaneously to all the switches. In order to equalize voltage sharing of series switches, in its steady-state as well as during switching transients, external shunt RC circuits are need on all switches in the chain. However, the use of these circuits may lead to distortion of the generated waveform.

The second reason is that the non-synchronized operation of the switches may be caused by the difference in gate driving signal circuits and the electromagnetic interference on these circuits.

Failure to simultaneously turn-on or turn-off all the switches may cause damage to the switches in the series connection. This comes about when a switch in the chain

closes later than the other switches; or if a switch opens earlier than other switches, the total output voltage appears across the out of phase switch, resulting in a damage of the switch. Hence, as soon as the switch fails (permanently short-circuited in most cases), the remaining switches must be able to withstand the total voltage that otherwise would be shared by all switches, which may lead to failure of other switches in the series connection.

A good solution to eliminate the risk of switch failure in the series connection is to utilize the cascade connection as shown in Fig 2.3(b). The cascade connection consists of several isolated stages which are similar to the circuits shown in section 2.1(see Fig.2.1). Each stage consists of a DC source, a switch, a diode, and a low inductance wave shaping resistor. The outputs of all stages are connected in cascade. As mentioned in section 2.1, each stage can generate waveforms independently by turning on and turning off the switch. If the switches in all stages turn-on and turn-off simultaneously, the total output voltage is the sum of the voltage of all stages. For N stages, the peak value of the output voltage can be theoretically $N \times V_1$, where, V_1 is the voltage of the DC source in each stage.

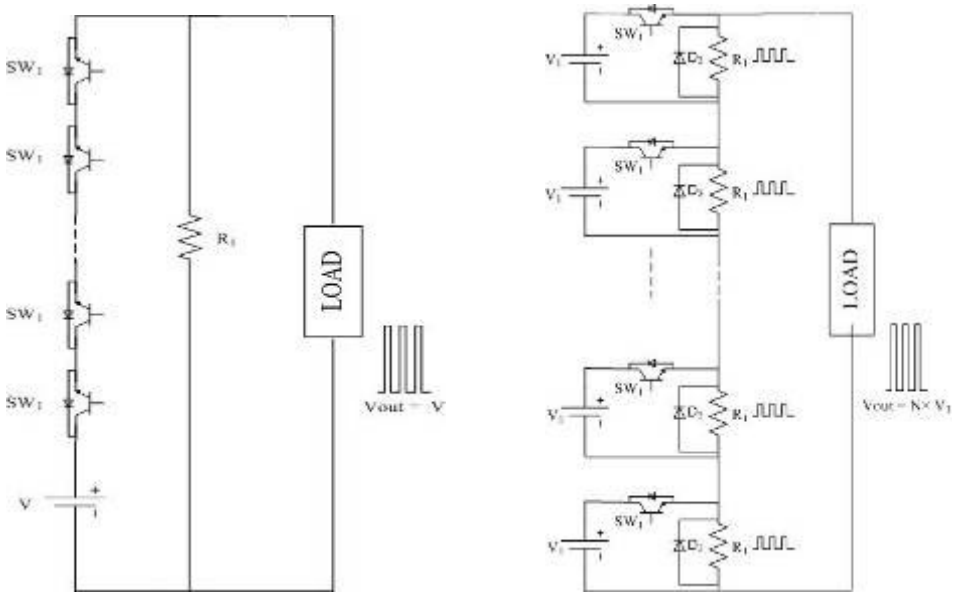

(a) Series connection (b) Cascade connection

Fig. 2.3: A comparison of a series connection and a cascade connection.

In the series connection, every switch works simultaneously to share the high DC source voltage V, hence, synchronized operation is critical. Whereas in the cascade connection, the generator is divided into several independent stages and each IGBT switch operates at the stage voltage V_1 (=V/N), which is in the range of the rated voltage of the switches. Thus, for the cascade connection, synchronized operation is not as important as the series connection. The unsynchronized operation only affects the value of the output voltage, but do not cause failure of the switches.

Fig. 2.4 shows the worst case scenario caused by an unsynchronized operation. As shown in Fig. 2.4, assuming that one switch is open while other switches are closed. The load current bypasses the wave shaping resistor of "open switch" stage through the free-wheeling diode D_3. In this case, the voltage across the switch can be expressed as: $V_{SW} = V_1 + V_{D3}$, where V_{D3} is the forward voltage of free-wheeling diode D_3. Since V_{D3} is very low, which is less than one volt, the voltage across the switch is still in the range of its rated voltage, So, no switch will be damaged. The only problem caused by the unsynchronized operation is that the total output voltage would decrease from $N \times V_1$ to $(N-1) \times V_1$.

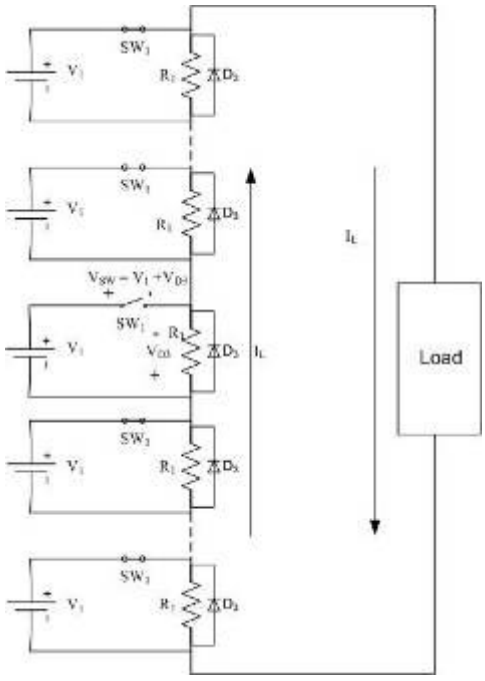

Fig . 2.4: A possible worst case of switching situation in a cascade connection.

2.3 Improved cascade connection design

As mentioned in section 2.2, the cascade connection can eliminate the risk of failure of the switches in generating high voltages. However, in the cascade structure shown in Fig. 2.3(b), each stage in the generator needs a separate DC source and these DC sources have to be isolated from each other, which increases cost, and the control circuits for all these DC sources are complicated. In order to lower cost and increase reliability, an improved cascade connection is designed based on the original cascade connection described in section 2.2. Fig. 2.5 shows the topology of the improved cascade connection design. In this new design, the DC sources in the original cascade connection are replaced by capacitors. Instead of a common high voltage DC source to charge the capacitors in all stages, and a second IGBT switch SW_2 in all stages is used to control the charging of the capacitors (C_1). The function of switch SW_1 in the new design is the same as that in original design, Fig. 2.2.

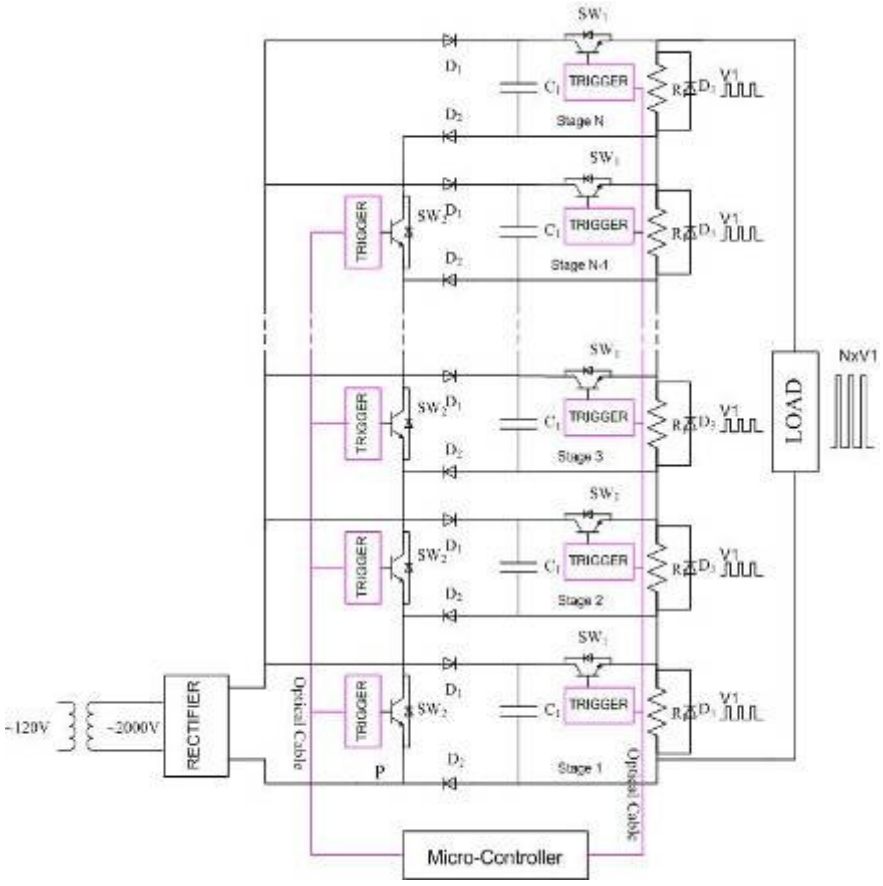

Fig. 2.5: Topology of the improved cascade connection.

Therefore the total operation of the generator is divided into two processes; namely, charging and discharging, which are alternatively controlled by two groups of the switches, SW_1 and SW_2.

During the charging process, switches SW_1 in all stages are off, and the switches SW_2 in all stages are on; the capacitors C_1 in all stages are charged in parallel by the common DC source as shown in Fig. 2.6. Because the charging circuits designed for each stage are the same, each stage has the same charging time constant τ_C , where $\tau_C = R_C \times C_1$, and R_C is the internal resistance of the DC source and connecting wires.

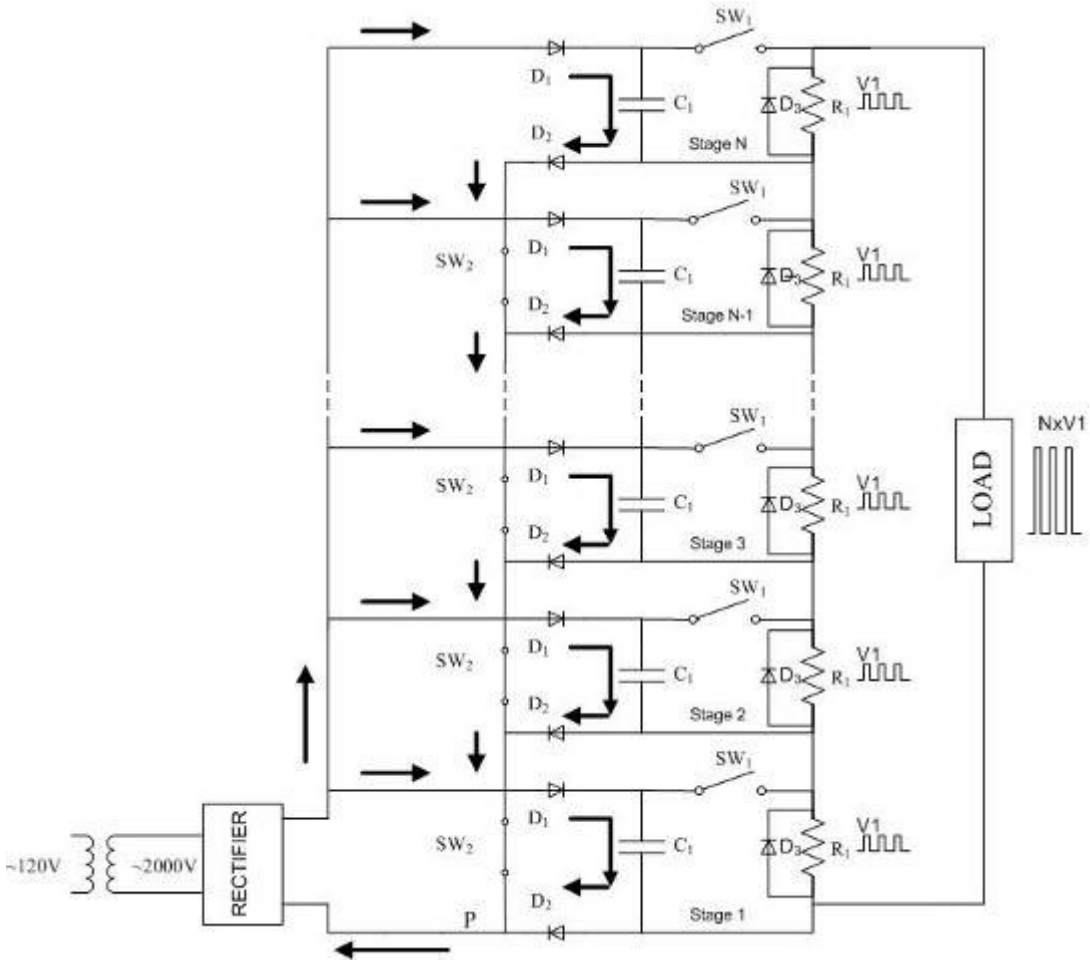

Fig. 2.6: Charging process.

During the discharging process, the switches SW_2 in all stages are off, and the switches SW_1 in all stages are on. The capacitors in all stages are discharged through the wave shaping resistors as shown in Fig. 2.7. As described in section 2.2, if the IGBT switches SW_1 in all stages turn-on and turn-off at the same time, the total output voltage at the load side is the sum of voltage across R_1 in each stage.

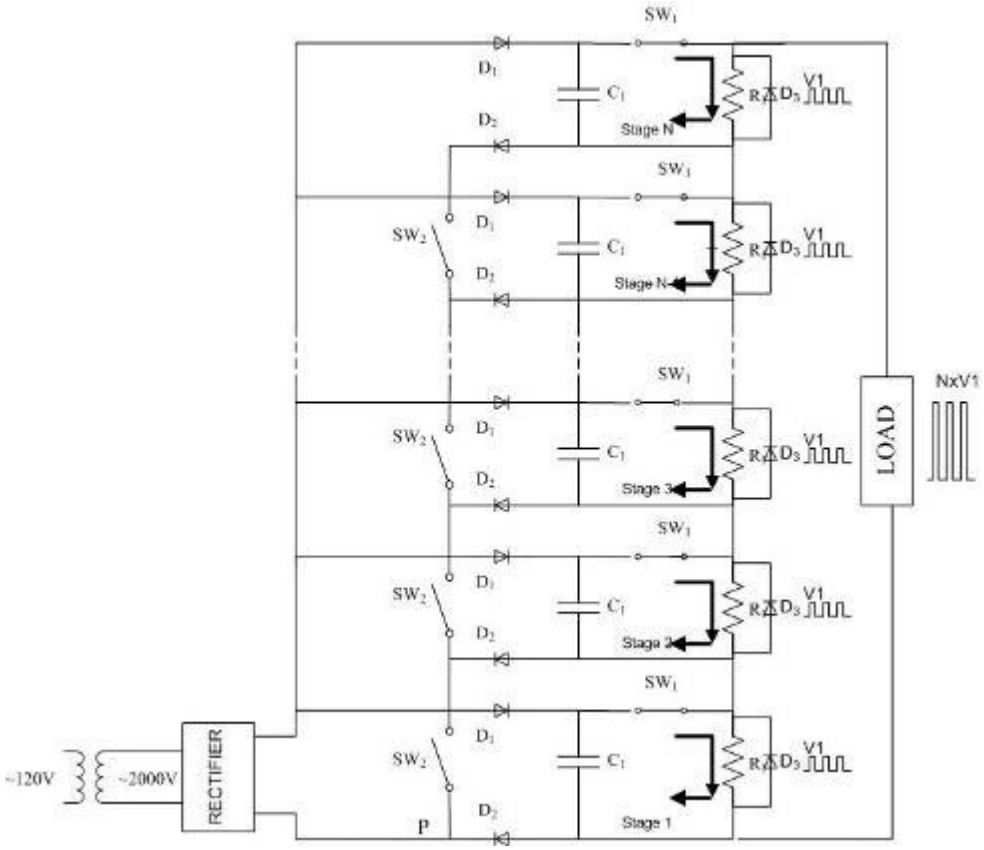

Fig. 2.7: Discharging process.

Both charging and discharging processes are controlled by a microcontroller-based trigger signal generator. In order to avoid short circuiting of the DC source, the charging and discharging operations must run alternatively; for example, when the switches SW_1 are on, the switches SW_2 should be off, and vice versa. Thus, two trigger signal groups, which are used for driving switches SW_1 and switches SW_2 respectively, must be interlocked from each other.

2.4 Trigger and control system

The block diagram of the trigger and control system is shown in Fig. 2.8. The trigger and control system of the generator consists of a microcontroller-based trigger signal generator, local drive circuits, and trigger signal transmission channels. The trigger signal generated by the trigger signal generator is divided into two interlocked signals; one signal is to control the operation of switches SW_1 to produce the desired waveform, and another signal is to control the operation of switches SW_2 to charge the capacitors in all stages. Two op-amp buffers are used to amplify the interlocked signals and drive two groups of optical cable communication channels and each group contains 10 optical channels.

The function of the trigger signal generator is to generate square wave or PWM waveform trigger signals, determine the running mode and operation sequence, and provide a control interface for waveform parameter setting. A microcontroller chip is selected for the purpose. The trigger signal generator and its auxiliary circuits including the buffer circuit and the interlock circuit are introduced in Chapter 3.

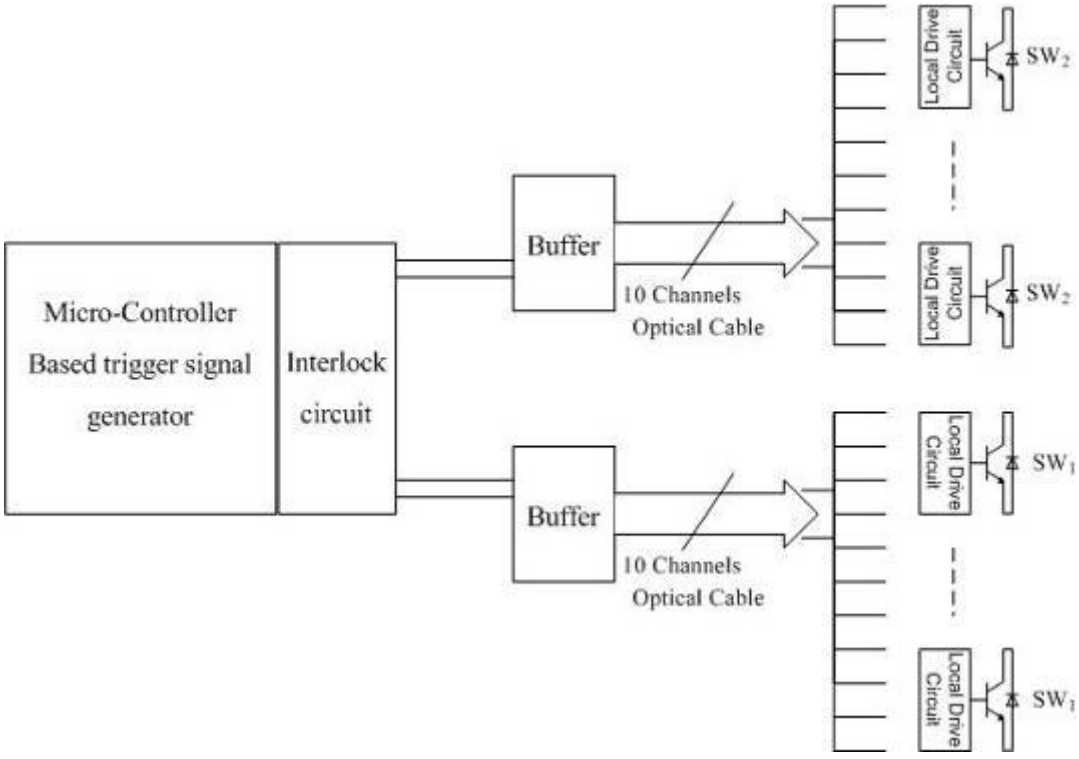

Fig. 2.8: Block diagram of trigger and control system.

The local drive circuits amplify the trigger signal to a high level that is required to operate the IGBT switches and drive the IGBT switches successfully into the “on” or “off” state. These local drive circuits are very important. The characteristic of the local drive determines the characteristic of the IGBT switches.

TD351 is an advanced gate driver for IGBT, which is made by STMicroelectronics. It can provide up to 1.7A sink and 1.3A source drive currents [30]. Fig. 2.9 shows the detailed internal schematic of TD351. The input of TD351 is compatible with optical-couplers and pulse transformer. The input voltage is internally clamped at about 5 to 7 volts. When connected to an open collector optical-coupler, the resistive pull-up resistor can be connected to either the reference output voltage pin VREF or to the voltage supply.

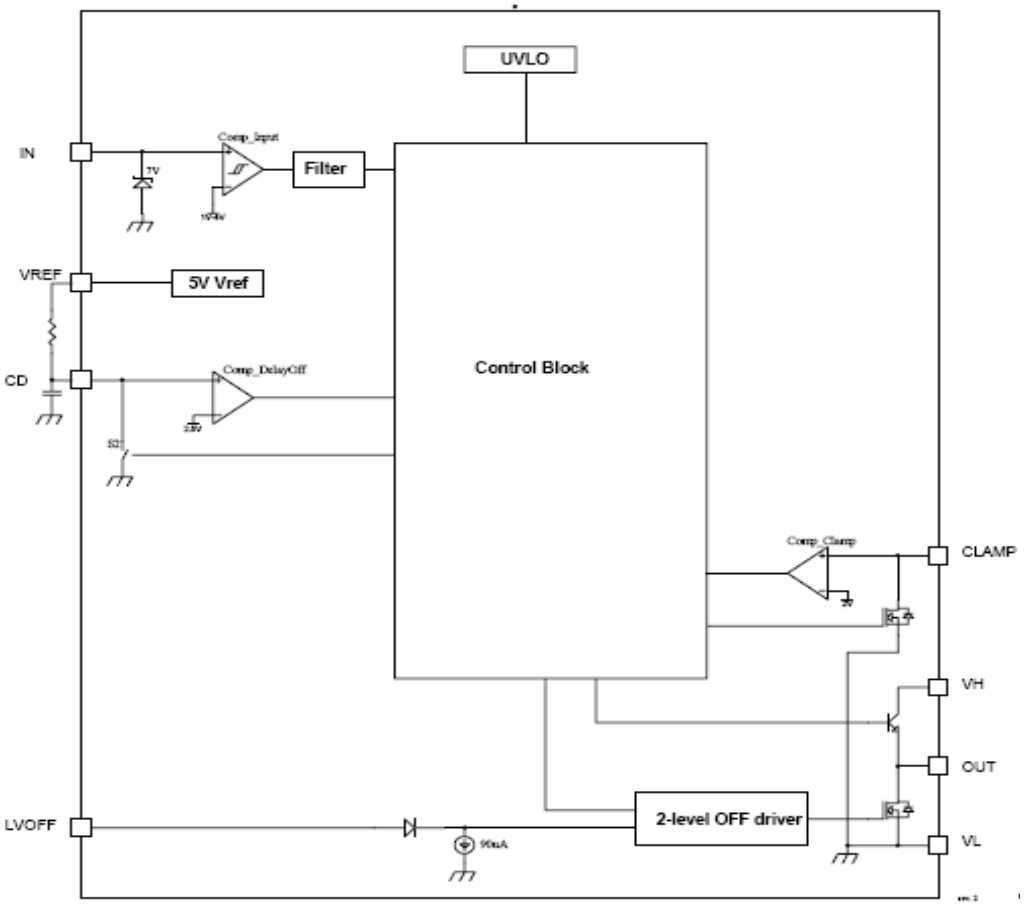

Fig. 2.9: Detailed internal schematic of TD351.

Fig. 2.10 shows the schematic of the local drive circuit. The signal from the fibre optic receiver is fed into an optical couple, TLP250. Then the output of the optical couple is connected to the input pin of IGBT drive, TD351. The gate on-state voltage value is +12V, and the gate off-state voltage value is -12V. The gate resistance is 15 Ω. Thus, the approximate maximum drive current is [(12+12)/15] = 1.6A, which is within the operating current range of TD351.

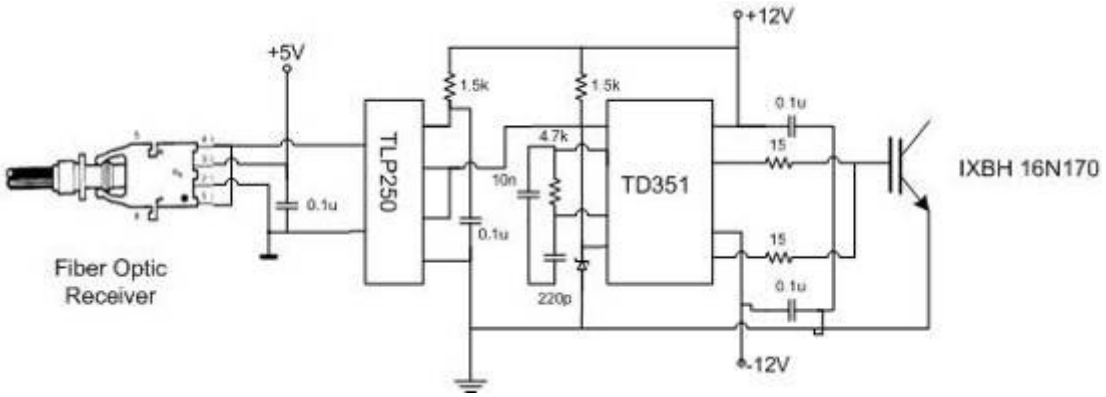

Fig. 2.10: Local drive circuit.

Each stage of the high voltage generator has two IGBT switches; hence, two local drive circuits are needed in each stage to drive the two groups of switches SW_1 and SW_2. Because the electric potential of every stage is not the same, the stages must be isolated from each other. In this design, isolation transformers are used not only to provide power to each drive circuit in each stage, but also to isolate each stage. The connections of the power supplies for each drive circuit are shown in Fig. 2.11. The isolation transformers are connected in cascade. The low voltage DC sources, which supply the local drive circuit, are therefore isolated from each other. There are two chains of cascade connected isolation transformers in the design, which are used to provide local drives for IGBT switches SW_1 and SW_2.

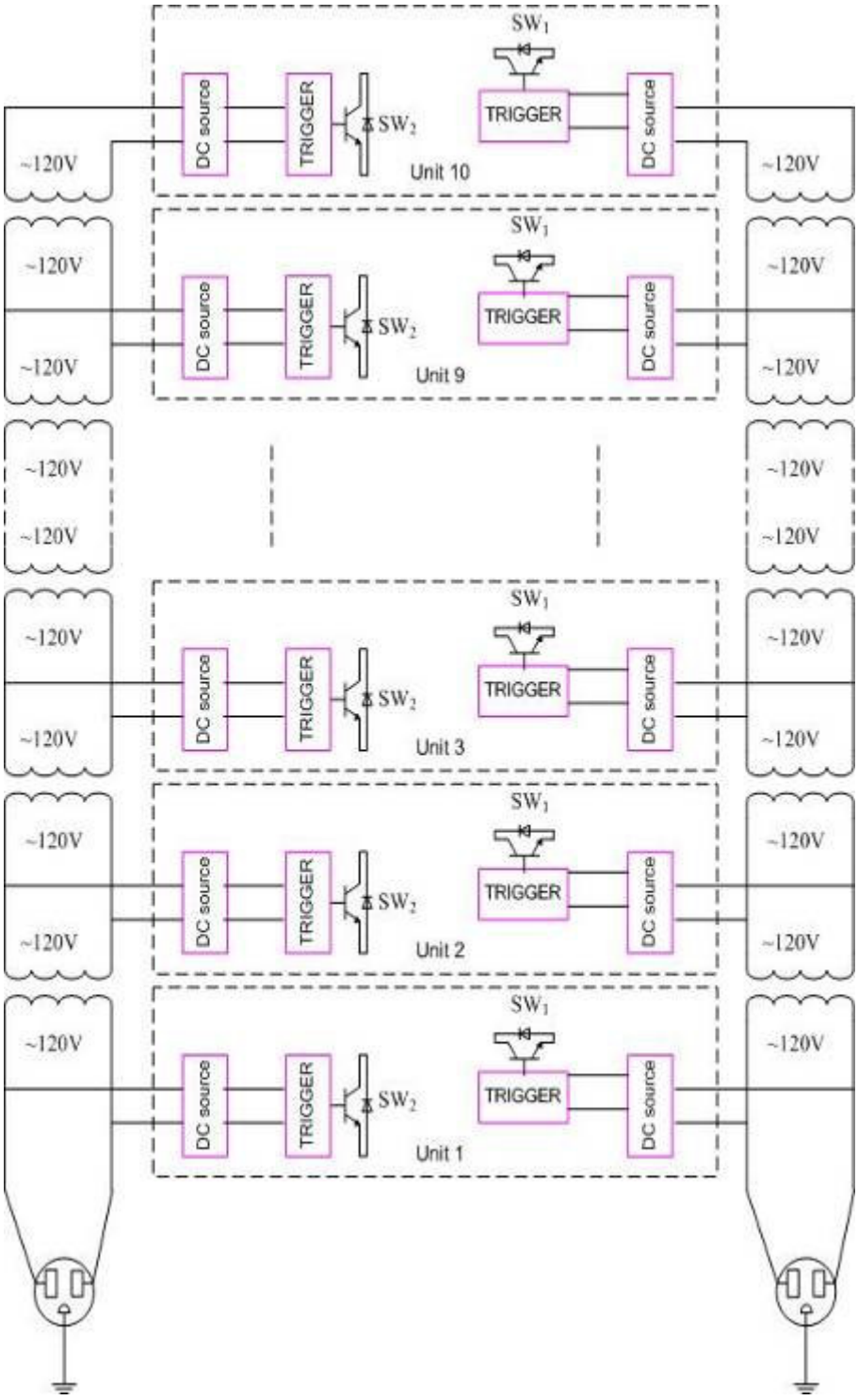

Fig. 2.11: Connection of power supplies for local drive circuit.

To decrease size, toroidal transformers are selected for the isolation transformer in the generator. The parameters of the transformer are shown in Table 2.1.

Table.2.1: Characteristics of theToroidal Transformer

Power (VA)	Frequency (Hz)	Primary (V)	Secondary (V)	Isolation level (V)
100	60	120	120	2000

The trigger signal transmission channels provide a communication connection between trigger signal generator and the local drive circuits of each IGBT switch. These channels also isolate the electromagnetic sensitive trigger signal generator from the local drive circuits which are located at high voltage potential. Thus, the ability to shield against the electromagnetic interference (EMI) is enhanced.

Optical fibres are used as trigger signal transmission medium. The communication channel interface connection is shown in Fig. 2.12. The communication channel consists of an optical transmitter, an optical receiver, and an optical fibre. The transmitter transforms the electrical signal to an optical signal and the receiver then transforms the optical signal to original electrical signal again. The transmitter is connected to the trigger signal generator, and the receiver is a part of local drive circuit. The signal rate of the channel is 5MBd and the maximum propagation data delay of the optical channel is 145ns.

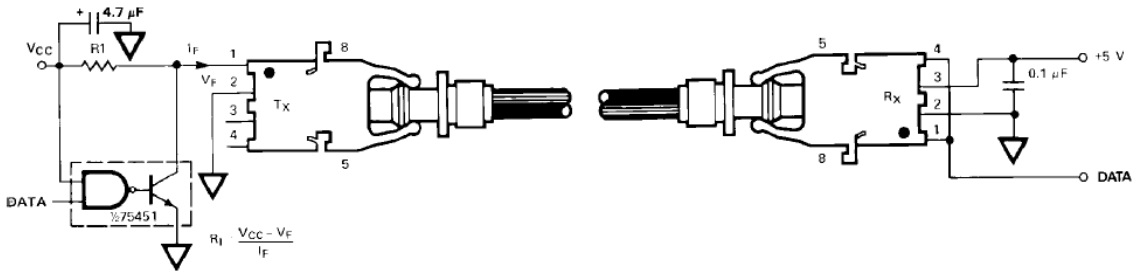

Fig. 2.12: Communication channel interface circuit.

2.5 Structural design of the generator

The IGBT-based pulse voltage generator consists of ten waveform generating stages connected in cascade. Since each stage is working at a different potential, the stages need to be insulated from each other.

In generator structural design, all components in one stage, which are at same potential, are installed on a fibreglass board, see Fig. 2.13. The fibreglass board is made of glass epoxy laminate that has extremely high strength and excellent electrical insulation. The dielectric strength of the board is 550 vpm(Volts/mil) or 21.65kV/mm.

In order to generate a good waveform with a controlled fall time, low inductance resistors are selected for wave shaping. Four resistors are connected in parallel to match the high energy generated in wave shaping. Each resistor is 600W rated, over the operating temperature of -55° to 150°. The inductance of each resistor is less than 80nH. The heat sink is designed to transfer heat to the ambient to keep the temperature within the specified maximum.

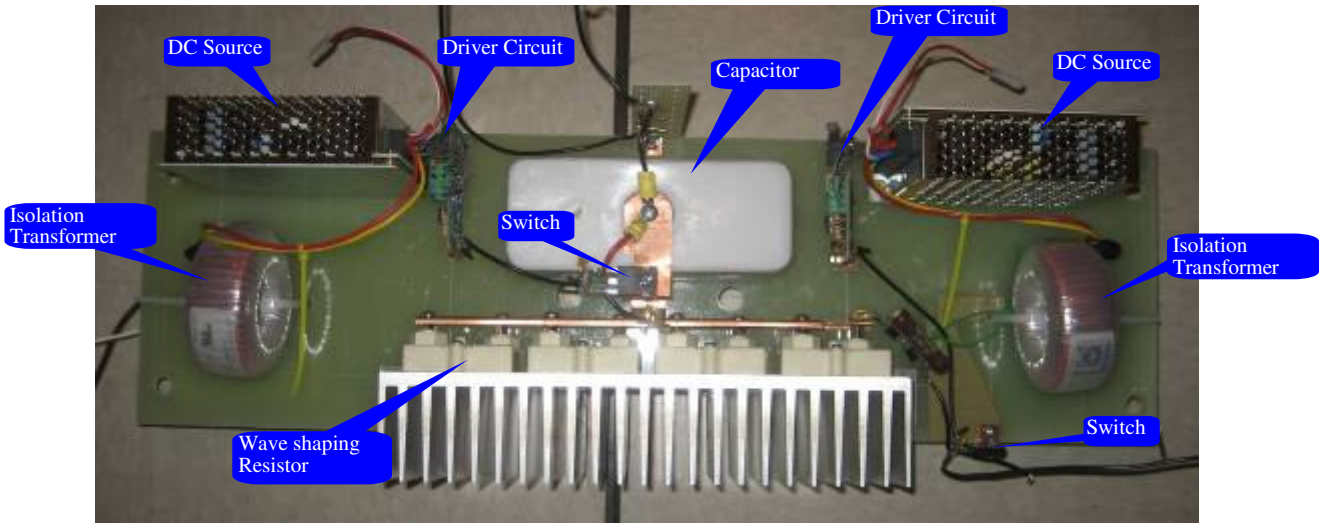

Fig. 2.13: Photograph showing waveform generating stage.

Ten waveform stages are mounted together forming a multi-storey structure. Each stage is mounted over another and supported by an aluminum U-channel, see Fig. 2.14. Because the metal supports are mounted on high insulation strength fibreglass board, the stages are insulated from each other. Any electrical or signal related connections between the stages are connected through isolation transformers or optical fibres.

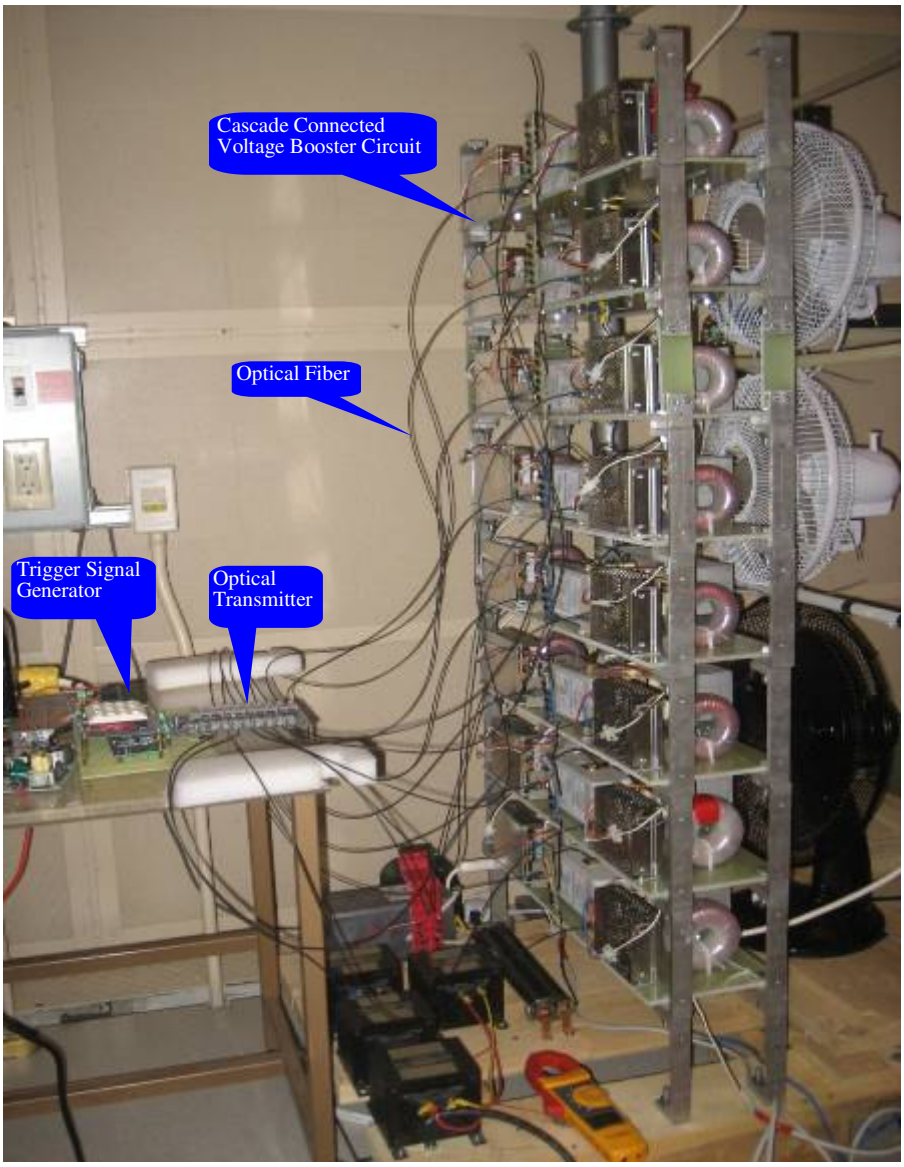

Fig. 2.14: Photograph showing the IGBT based pulse voltage generator.

Chapter 3
Trigger Signal Generator Design

In Chapter 2, the design of the main circuit and structure of the IGBT-based pulse voltage generator is discussed. When the gates of the switches are triggered by either square or PWM waveform trigger signals, high voltage square wave and PWM waveforms are produced. In this chapter, the design of the trigger signal generator is introduced.

As an insulation test apparatus, the IGBT-based pulse voltage generator needs to have multiple functions and a flexible control mode to match different insulation test requirements. The requirements and functions of the trigger signal generator can thus be described as follows:

- It can produce square wave and PWM waveform trigger signals according to different settings: the frequency of the square wave and the switching frequency of the PWM waveform needs to be adjustable.
- It provides an interface so that the operator can select the running mode (automatic or manual, continuous or intermittent), waveform type, and running time for the test.

3.1 Hardware design

To realize the requirements and functions described, an 8-bit PIC microcontroller chip PIC16F877A is used as the core control element in the generator. This sophisticated Harvard architecture-based single integrated computer is low cost, easy to program, and multi-functional.

Fig. 3.1 shows the schematic diagram of the trigger signal generator. The generator consists of a microcontroller and its auxiliary circuit, a signal interlock circuit, a buffer circuit, an input current monitor, and an output for operation of an interlock.

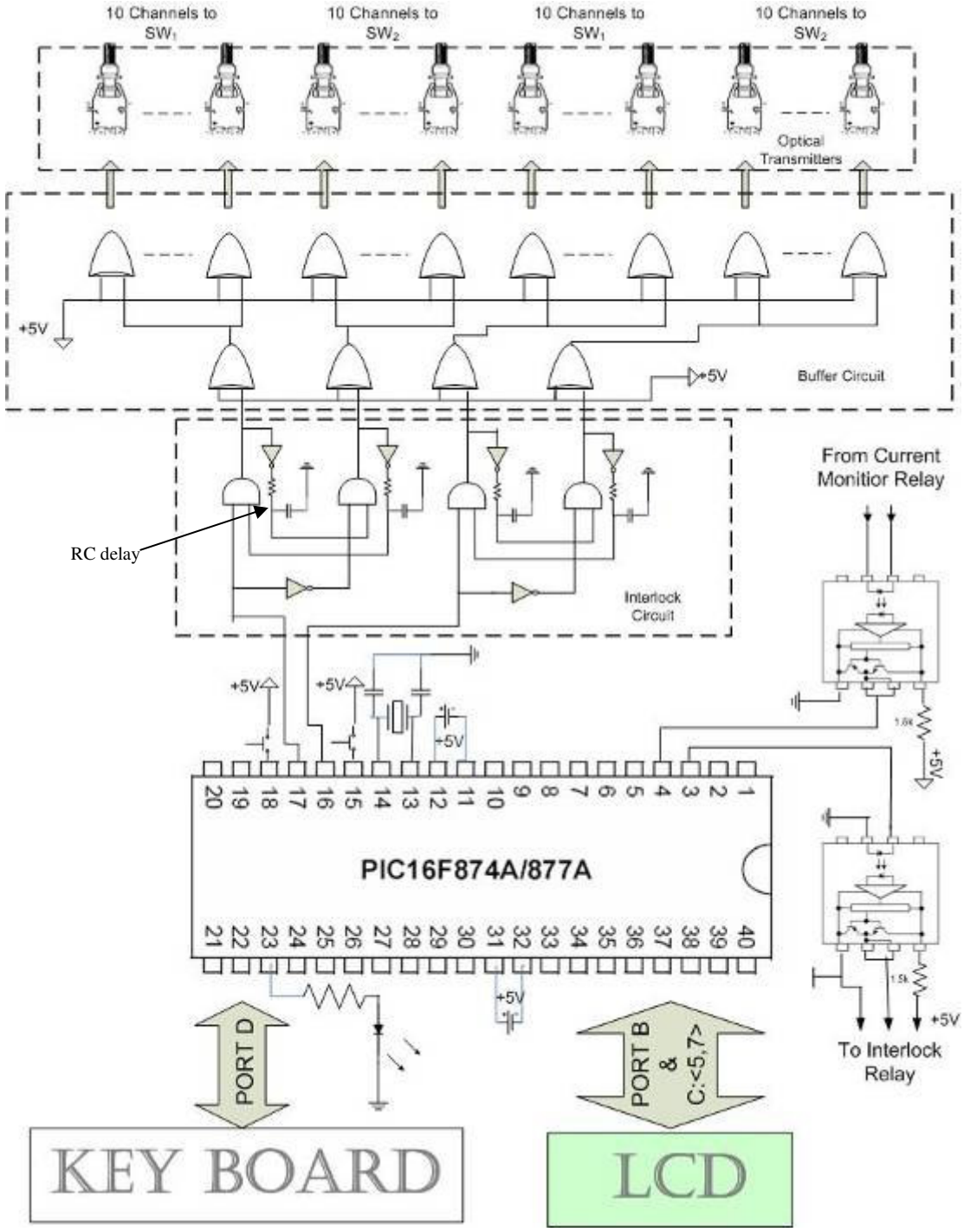

Fig. 3.1: Schematic diagram of the trigger signal generator.

3.1.1 Microcontroller PIC16F877A and its auxiliary circuit

Fig. 3.2 shows the diagrams of the microcontroller chip PIC16F877A. The main features of the chip are:

- ***Operating frequency:*** DC – 20MHz
- ***Flash program memory*** (14 bit words)***:*** 8K
- ***Data memory*** (bytes)***:*** 368
- ***Interrupts:*** 15
- ***Timers:*** 3
- ***I/O ports:*** Ports A, B, C, D, E
- ***Capture / Compare / PWM modules:*** 2
- ***10-bit A/D modules:*** 8 input channels
- ***Analog comparators:*** 2
- ***Instruction set:*** 35 Instructions
- ***Packages:*** 40 pins

Table 3.1 lists the I/O port and pin assignments of the (micro control unit) MCU in the generator. The pins and their respective names are selected in order to minimize the complexity of the program and the hardware setup.

Table 3.1: PIC Microcontroller Chip I/O Port and Pin Assignments.

Name	Port	Pin number	Description
LCD_DATA	Port B.0 ~ Port B.7	33 ~ 40	Pins are set to transfer data between MCU and LCD
E	Port C.7	26	LCD Enable control line
RW	Port C.6	25	LCD Read / Write control line
RS	Port C.5	24	LCD Register Select control line
LED	Port C.4	23	LED output, on while the output waveform is generating
KEYPAD	Port D.0 ~ Port D.3	19 ~ 22	Pins are set to read user input from the keypad
	Port D.4 ~ Port D.7	27 ~ 30	Pins are set as keypad scanning output
PWM1	Port C.1	17	PWM or square wave output 1
PWM2	Port C.2	16	PWM or square wave output 2
MSWITCH	Port C.3	18	Manual switch
SSWITCH	Port C.0	15	Stop switch. Halts the test when the button is pressed
INTERLOCKOUT	Port A.1	3	Operation interlock output
MCURRENT	Port A.2	4	Current monitor relay signal input

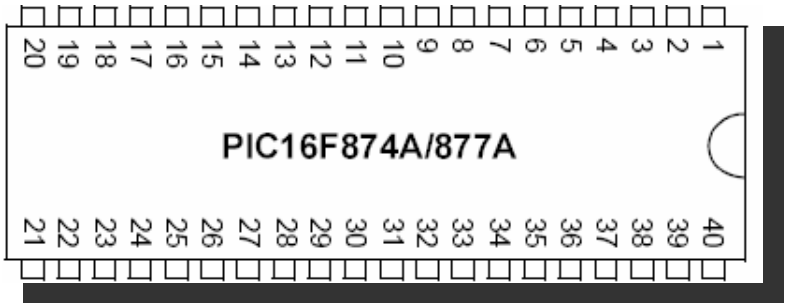

(a) Pin diagram of PIC16F877A.

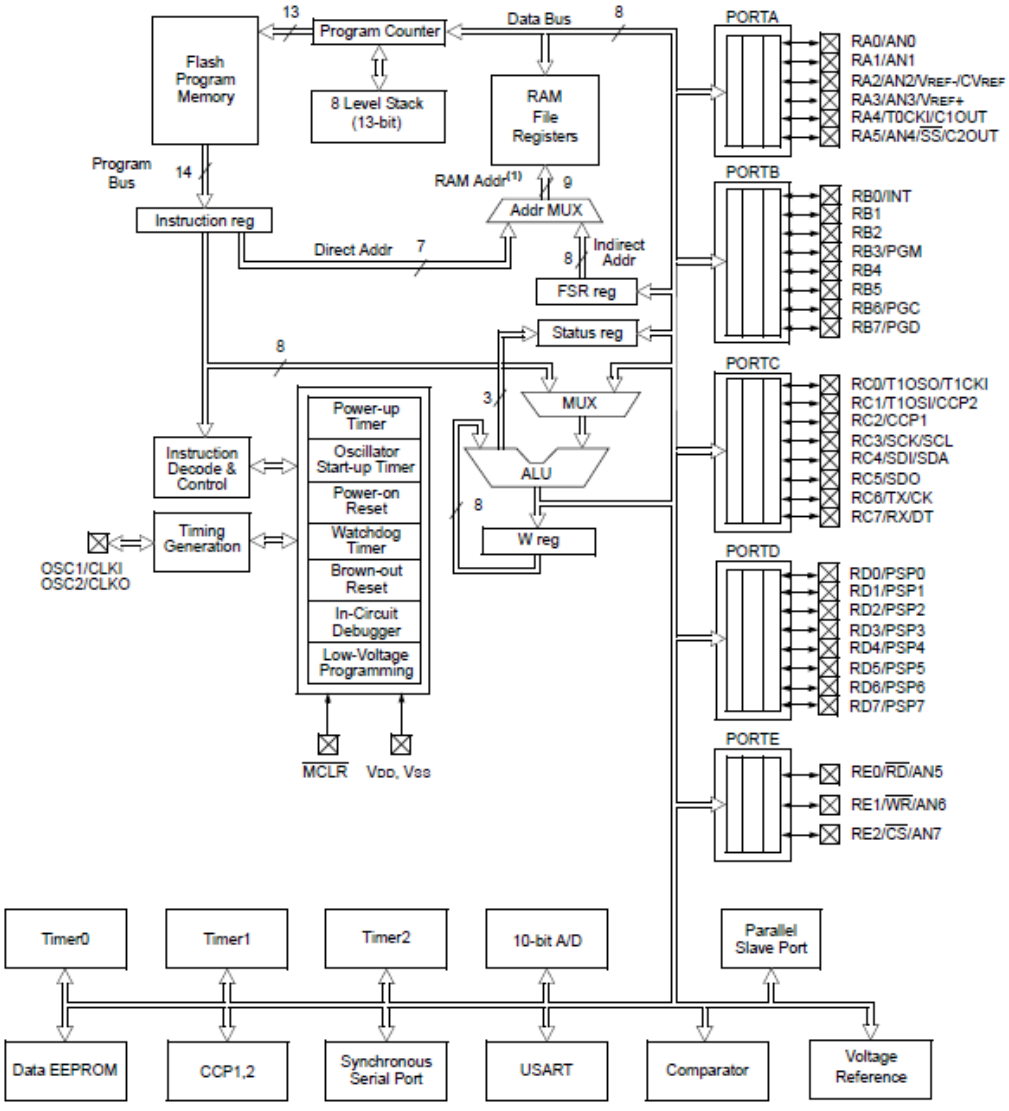

(b) Block diagram of PIC16F877A.

Fig. 3.2: Diagram of the microcontroller chip PIC16F877A.

PORTC is an 8-bit wide, bidirectional port. The 8 pins (port C.0 to port C.7) of PORTC are multiplexed with an alternate function for the peripheral features on the chip. Setting the Port/Peripheral selection registers permits port C.1 and port C.2 to be set in normal input / output pin mode, capture module input mode, compare module output mode, or PWM module output mode.

In this design, ports C.1 and C.2 are set as the normal output when the square wave is generated. The status of the port pin is controlled by the firmware. To generate a bipolar square waveform, the output of port C.1 is set to be opposite to the output of port C.2. When port C.1 is high, port C.2 is low, and vice versa. The differential of the two port pins is a bipolar square wave.

When the generator is set to generate the PWM waveform, both port C.1 and port C.2 are set as the PWM module output. Two independent two-level unipolar PWM waveforms can be generated at port C.1 and port C.2. To generate a three-level bipolar PWM waveform, the fundamental components of these two output signals are phase shifted by 180° with respect to each other. The differential of the two outputs is the three-level bipolar PWM waveform.

As an operational safety consideration, the discharging switch SW_1 is designed to be normally closed, whereas the charging switch SW_2 is designed to be normally open. Thus, when no waveform is being generated, the trigger signal of SW_1 is always high, and the trigger signal of SW_2 is always low.

Port C.0 is set as the “stop” signal input. When the stop button is pushed, port C.0 is pulled high, and the generator stops generating the waveform and trips the power supply of the IGBT-based pulse voltage generator.

Port C.3 is set as the manual “start” signal input. In manual mode, when the start button is pushed, port C.3 is pulled high, and the generator begins to generate the desired waveform.

A 4×4 keypad is used to input the settings. Fig. 3.3 shows the wiring diagram of the keypad. The keypad is connected to PORTD. The columns are connected to port D.4~D.7 as column scanning output. The rows are connected to port D.0~D.3 as row input. Each active row has a 10 kΩ pull-up resistor connected to Vcc.

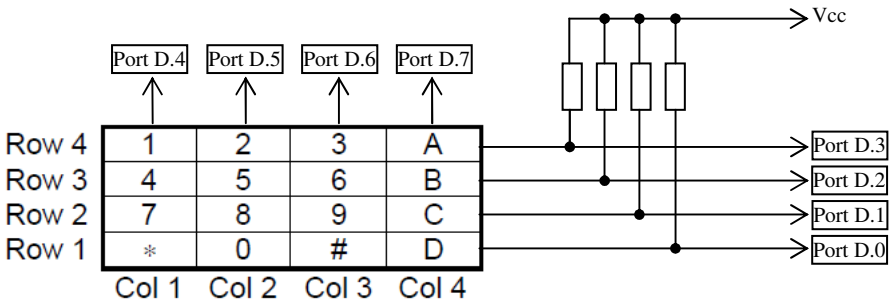

Fig. 3.3: Wiring diagram of the keypad.

A 2×16 intelligent liquid crystal display (LCD) module is selected for displaying the orders, settings, and status of the generator. A 14-pin access is provided, including 8 data lines, 3 control lines, and 3 power lines. The block diagram of the LCD is shown in Fig. 3.4. Pins 1 and 2 (Vss and Vdd) are the power supply lines. Pin 3 is connected to a variable voltage supply and it is used to alter the contrast of the display. Pin 4 is a register select control (RS) line that is connected to port C.5. When this line is low, data bytes transferred to the display module are treated as commands, and the data bytes read from the display indicate their status. Setting the RS line to a high level permits character data to be transferred to and from the display module. Pin 5 is a read/write control line connected to port C.6. This line is pushed low to write and pulled high to read. Pin 6 is the enable line, which is used to initiate the actual transfer of the commands or character data between the module and the microcontroller. Pin 6 is connected to port C.7. Pins 7 to 14 are the 8 data buses connected to port B of the microcontroller.

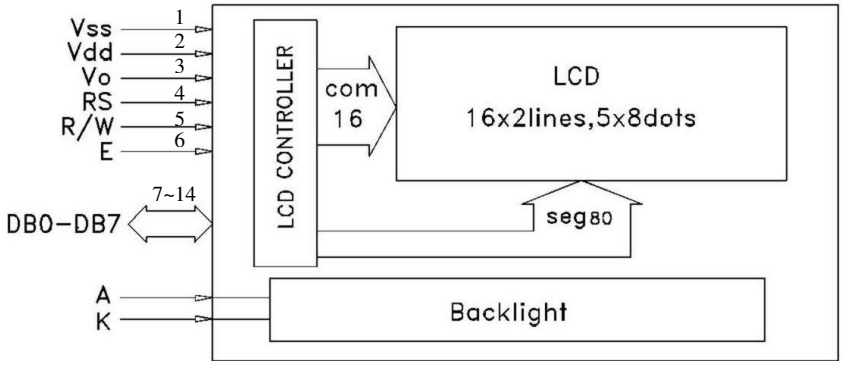

Fig. 3.4: Block diagram of LCD.

3.1.2 Interlock and buffer circuits

As mentioned in chapter 2, each stage in the main circuit (Fig. 2.5) needs two IGBT switches, and the trigger signals of these two switches must be interlocked to avoid a short circuit in each stage. Thus, the trigger signal generated from the microcontroller (port C.1 or C.2) is divided into two interlocked trigger signals in the interlock circuit of the generator; one used to drive SW_1 and the other to drive SW_2. As shown in Fig. 3.1, "and" gate and hex inverter chips are used to realize the interlock function. To eliminate possible signal overlap due to interference, an RC delay circuit is designed in order to insert a "zero gap" between the two signals. Both SW_1 and SW_2 are in the off state during the period of the "zero gap". A RC delay circuit is used to adjust the duration of the "zero gap".

The waveform signals are then sent to the buffer circuit. The circuit includes 4 buffer units. Each buffer unit amplifies the power of the waveform trigger signal and drives ten waveform trigger signal channels. These waveforms are transformed into light signals by the optical transmitters. Optical fibre channels transmit the trigger waveforms to local IGBT switch drives to control the IGBT switches in the improved cascade connection circuit.

3.2 Firmware

The software for the square waveform and PWM waveform trigger signal generator is written in the assembly language of the PIC microcontroller. Fig. 3.5 shows the flow chart of the program. The program has two subroutines: the square mode cycle subroutine and the PWM mode cycle subroutine. These two subroutines can be selected through the keypad.

Main Program

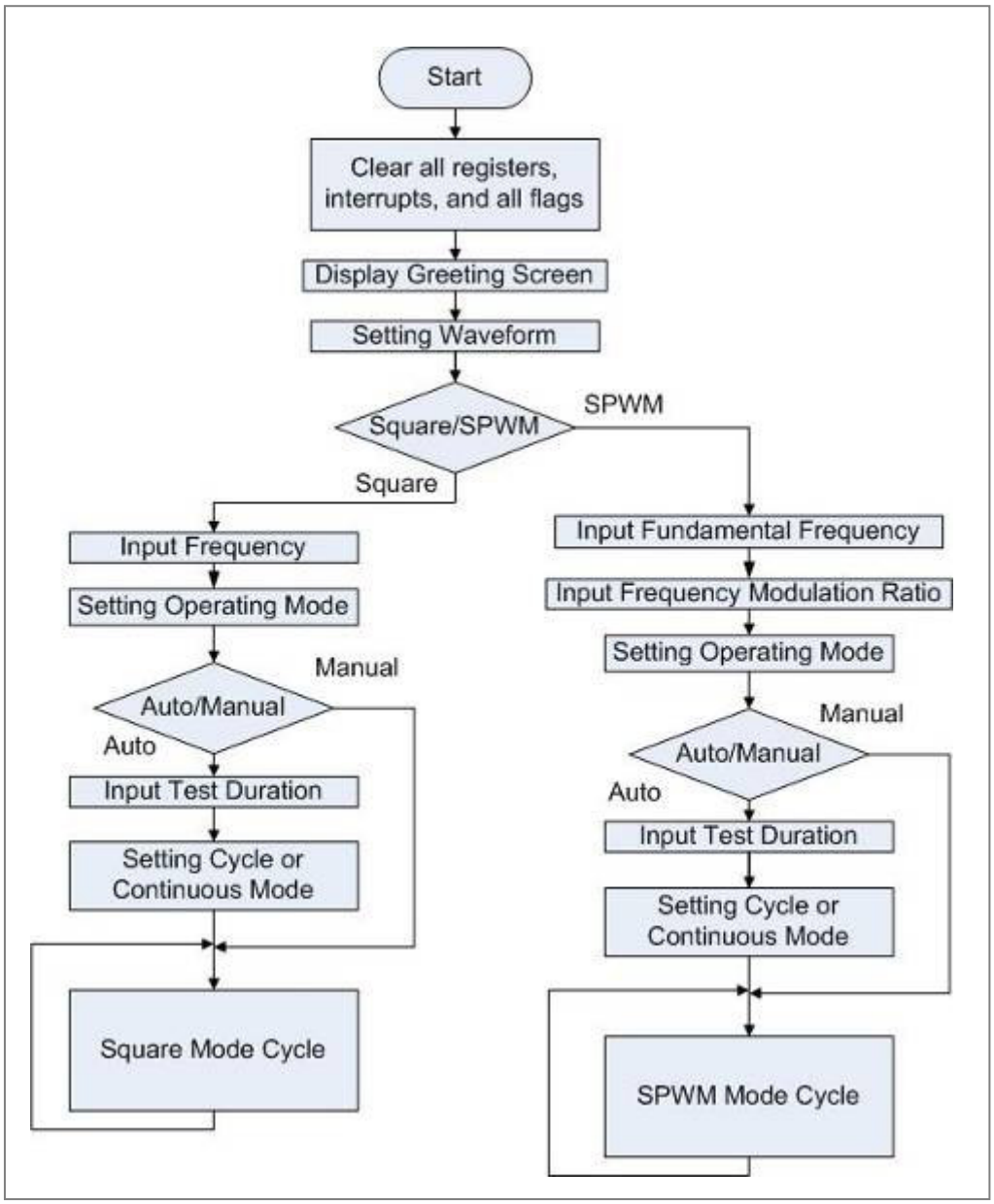

Fig. 3.5: Flow chart of the main program.

3.2.1 Square wave signal generation

Timer0 module timer/counter is used for square wave generation. Timer0 has an interrupt function that can generate an interrupt service routine at a set time to change the status of the waveform output at port C.1 and port C.2 (pins 16 and 17, Table 3.1).

Once Timer0 is set to timer mode, the TMR0 register increments every instruction cycle time multiplied by the prescaler value. Timer0 interrupt is generated when the TMR0 register overflows from a set value to 00h. Fig. 3.6 is a block diagram of the Timer0 module and the prescaler that is shared with the watch dog timer.

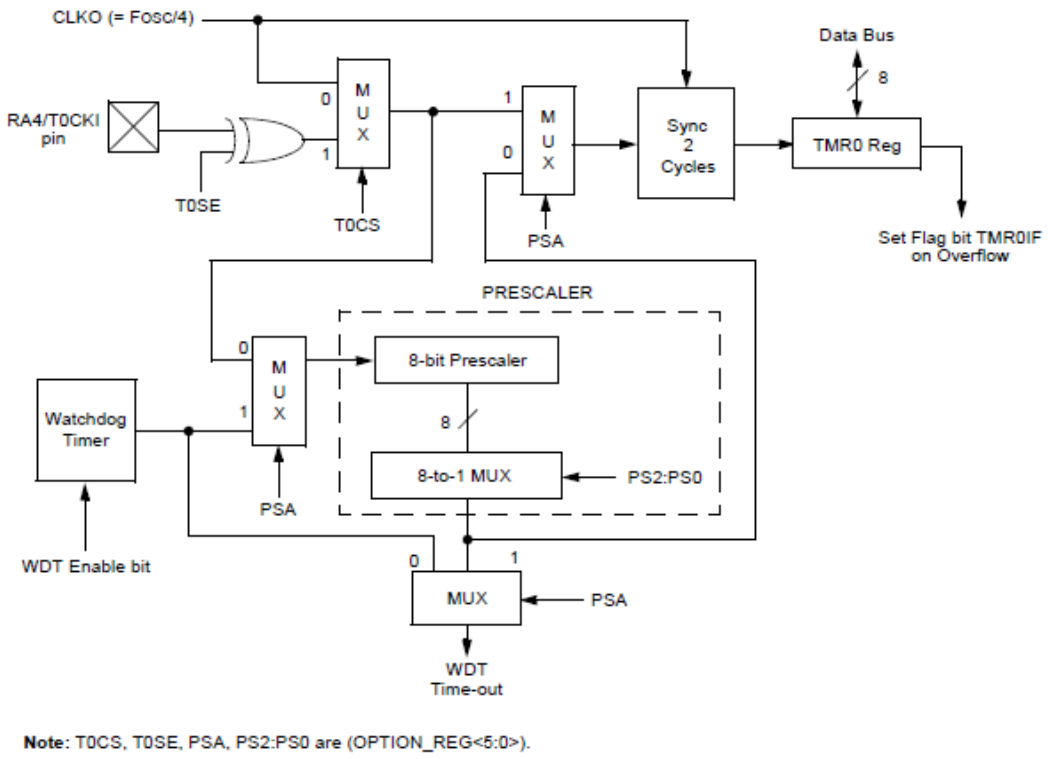

Fig. 3.6: Block diagram of Timer0 and the prescaler.

Fig. 3.7 is the flow chart of the Timer0 interrupt service routine, which is designed for square wave generation. In the interrupt routine, the interrupt flag is cleared, and the TMR0 is set to a given value according to the desired frequency.

When the frequency is set higher than 38 Hz, the product of the data in the TMR0 register and the data in the Timer0 prescaler register OPTION_REG determines the interval time between two interrupts. Because the status of the waveform output pins (pin 16 and 17 of the microcontroller) is changed from high to low or from low to high in each interrupt service routine, this interval time is half the cycle time of the

square waveform. Thus, the frequency of the square waveform can be calculated as follows:

$$f_{set} = f_{osc} /[2\times4\times (TMR0) \times(OPTION\_REG)] \quad (3.1)$$

where f_{set} is the frequency setting, and f_{osc} is the frequency of the crystal oscillator.

Accordingly, if the frequency setting and the frequency of the crystal oscillator are known, calculating the initial value of register TMR0 and the value of register OPTION_REG is straight forward.

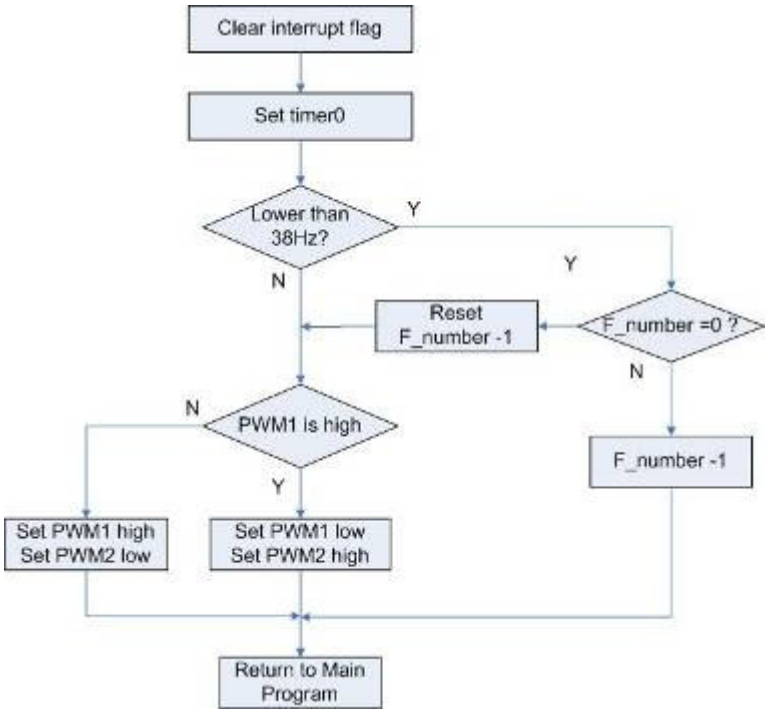

Fig. 3.7: Flow chart of Timer0 interrupt service routine.

To obtain enough resolution for a variety of square wave frequencies, the data in the prescaler register OPTION_REG is set according to the range of the setting frequency, as shown in Table 3.2.

Table 3.2 OPTION_REG setting

Frequency range	Value in OPTION_REG
38Hz ~ 76Hz	256
76Hz ~ 152Hz	128
152Hz ~305Hz	64
305Hz ~ 610Hz	32
610Hz ~ 1220Hz	16
1220Hz ~2441Hz	8
2441Hz ~ 4883Hz	4
4883Hz ~ 9700Hz	2

The data in the TMR0 register is calculated from

$$(\text{TMR0}) = f_{osc} / [8 \times f_{set} \times (\text{OPTION\_REG})] \quad (3.2)$$

When the frequency setting is lower than 38 Hz, the cycle time of the square wave is longer than the maximum interrupt interval time, which is $256 \times 256 \times 8 \times T_{OSC}$ (cycle time of the crystal oscillator). Therefore, according to equation (3.2), the value of (TMR0) would be larger than 256, the TMR0 register would overflow. Thus, another register (F number) is needed to comprise a 16-bit register with TMR0 register in order to store the result of equation (3.2). In the calculation of equation (3.2), the integer quotient is saved in F_number, and the remainder is saved in TMR0. In this case, the prescaler rate is fixed at 256, and the interval time between two interrupts is determined by the values in F_number and TMR0 registers. The setting frequency is expressed as

$$f_{set} = f_{osc} / [8 \times (\text{F\_number}) \times 256 \times 256 + 8 \times (\text{TMR0}) \times 256] \quad (3.3)$$

3.2.2 PWM wave generation

Two Capture/Compare/PWM (CCP) modules are used to generate two independent PWM waveform signals. Each CCP module contains a 16-bit register

that can operate as either a 16-bit capture register or a 16-bit compare register or a PWM master/slave duty cycle register.

When in PWM mode, the CPPx pin (pin 16 or 17) produces a PWM output with a resolution up to 10 bits. The PWM output, which has a time base (period) and a specific time when the output stays high (duty cycle), is shown in Fig. 3.8.

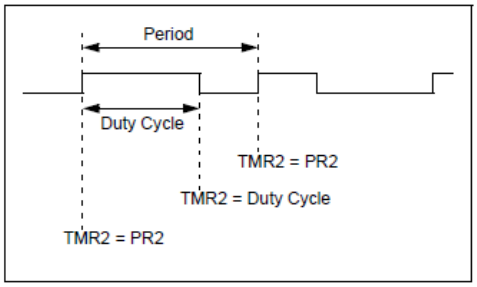

Fig. 3.8: PWM waveform at CCPx Output.

Fig. 3.9 shows a simplified block diagram of the CCP module in PWM mode. The Timer2 module is used as the PWM time base in PWM mode. Timer2 is an 8-bit timer with a prescaler and a postscaler as shown in Fig 3.10. PR2 is an 8-bit period register in the Timer2 module.

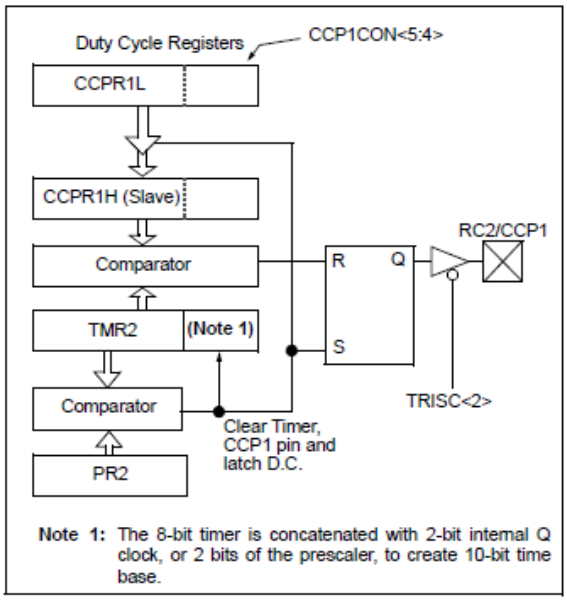

Fig. 3.9: Block diagram of CCP module.

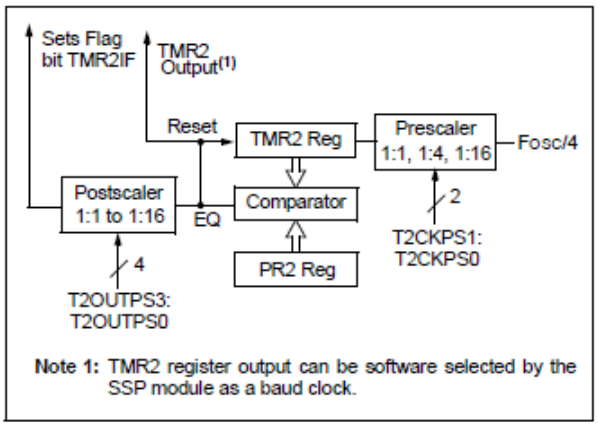

Fig. 3.10: Block diagram of Timer2 module.

The PWM period is a function of the data in the PR2 register and the value of the Timer2 prescaler (T2CON<1:0>). The PWM period of the PWM wave for the CPPx output can be calculated using the following formula:

$$\text{PWM period} = [(\text{PR2}) + 1] \times 4 \times T_{osc} \times (\text{Timer2 Prescaler Value}) \qquad (3.4)$$

The switching frequency of a PWM waveform is defined as 1/ [PWM period]. For a sinusoidal PWM waveform, the switching frequency of the PWM waveform is the product of the fundamental frequency and the frequency modulation ratio.

The fundamental frequency (f_s) and the frequency modulation ratio (m_f) can be set through the keypad. Thus, the PWM period is determined as following equation.

$$\text{PWM period} = 1/(\text{switching frequency})$$
$$= 1/[(\text{fundamental frequency}) \times (\text{frequency modulation ratio})] \qquad (3.5)$$

If the value of the Timer2 prescaler is preset in the microcontroller chip, the PWM period can be specified the value of (PR2).

The PWM duty cycle is determined by (CCPRxL:CCPxCON<5:4>) and the value of the Timer2 prescaler (T2CON<1:0>). The maximum resolution of the duty cycle is 10 bits. If the value of the Timer2 prescaler is determined, the PWM duty cycle can be specified by the CCPR1L (or CCPR2L for PWM2) register combining with CCP1CON <5:4> (or CCP2CON for PWM2) bits. The following formula is used to calculate the PWM duty cycle according to the data in these registers:

PWM duty cycle

$$= (\text{CCPRxL:CCPxCON<5:4>}) \times T_{osc} \times (\text{Timer2 Prescaler Value}) \qquad (3.6)$$

In the Timer2 module, the value of the PWM time base register TMR2 increases from 00h until it matches the value of PR2; once (TMR2) equals (PR2), a PWM interrupt routine is launched. In the interrupt routine, TMR2 is cleared, and the duty cycle of the next PWM cycle is specified through rewriting the data to CCPRxL:CCPxCON<5:4> from a pre-calculated discrete fundamental sinusoidal data form.

In the general purpose data memory area (SRAM) of the microcontroller, 50 bytes are specified as the pre-calculated discrete sinusoidal data form area for storing a half cycle of discrete sinusoidal data. Each discrete sinusoidal datum occupies two bytes, which is 16 bits. The size of the sinusoidal data form is flexible and is determined by the frequency modulation ratio (m_f). A Taylor series is used to calculate each datum in the sinusoidal data form. The Taylor series of the sine function is expressed as

$$\sin(x) = x - x^3/(3!) + x^5/(5!) - x^7/(7!) + \ldots = \sum\{[(-1)^n x^{(2n+1)}]/[(2n+1)!]\} \qquad (3.7)$$

where $-\pi < x < \pi$. n is the positive integer = 1,2 3,….

The error of the formula (3.7) to calculate sine function is less than $[(-1)^{n+1} x^{(2n+3)}]/[(2n+3)!]$.

If setting $x_p = (\pi/ m_f) \times (2p-1)$, p = 1, 2, 3… $m_f/2$, where m_f is the frequency modulation ratio and p is the positive integer, the discrete Taylor series expression of the sine function is expressed as:

$$\sin(x_p) = x_p - x_p^3/(3!) + x_p^5/(5!) - x_p^7/(7!) + \ldots = \sum\{[(-1)^n x_p^{(2n+1)}]/[(2n+1)!]\}$$
$$= \sum\{[(-1)^n((\pi/ m_f) \times (2p-1))^{(2n+1)}]/[(2n+1)!]\} \quad (3.8)$$

The discrete fundamental sinusoidal data form can be derived by calculating each $\sin(x_p)$ at each discrete x_p using equation (3.8). The size of the half-cycle sinusoidal data form in memory area of the microcontroller is $2\times (m_f/2)$. Another half-cycle sinusoidal datum is easy to calculate from the half-cycle sinusoidal data form.

The PWM duty cycle in each PWM period is then calculated from

$$\text{PWM duty cycle (at p cycle)} = m_a \times \sin(x_p) \times \text{PWM period} \quad (3.9)$$

where, m_a is defined as modulation index. In this thesis, the m_a is fixed at 0.87.

Once the PWM duty cycle in each PWM period is calculated, the data for CCPRxL:CCPxCON<5:4> in the pre-calculated discrete sinusoidal data form can be then calculated through the equation (3.6).

3.3 The output waveform of signal generator

Fig. 3.11 shows a photograph of the microcontroller-based trigger signal generator.

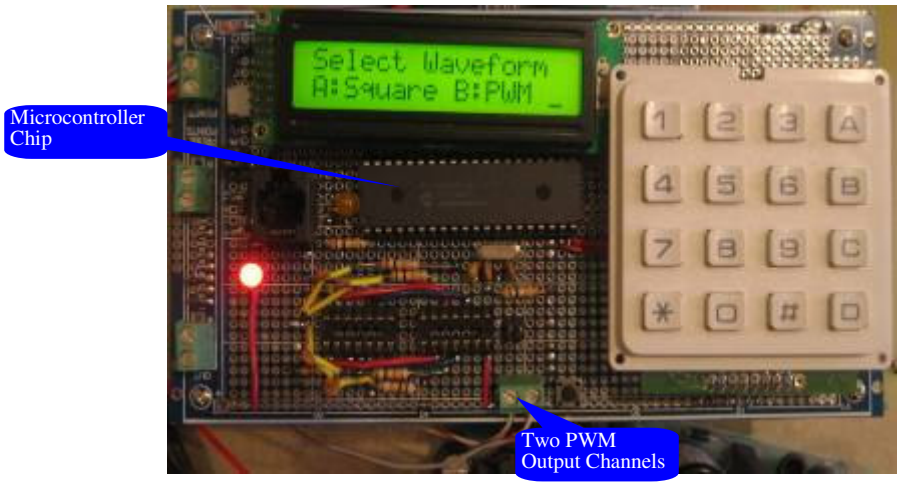

Fig. 3.11: Photograph of the waveform trigger signal generator.

The signal generator has two PWM output channels; PWM1 and PWM2. Each channel can produce a unipolar square wave or a PWM waveform. For the square wave signal, the two channels (1 and 2 in Fig. 3.12) are set to be opposite to each other. The difference between these two output signals is a bipolar square waveform, in which the peak value is twice the value of each channel (M in Fig. 3.12). For the PWM wave signal, the fundamental signals of these two output channels (1 and 2 in Fig. 3.13) are phase shifted 180° with respect to each other. The difference between these two output signals is a three level bipolar PWM waveform (M in Fig. 3.13).

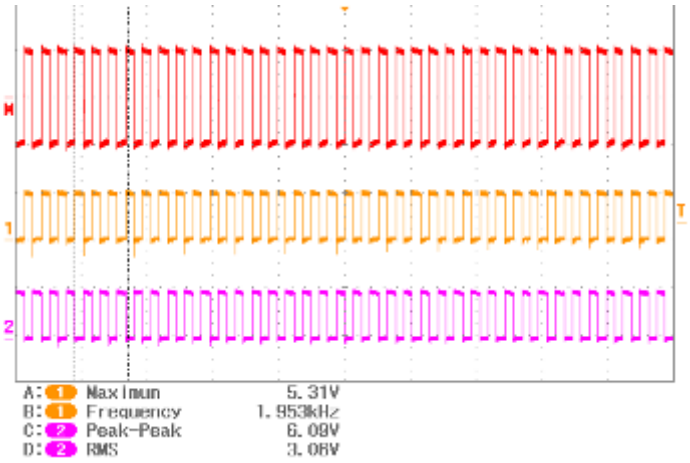

Fig. 3.12: Square wave output signals of the trigger signal generator.

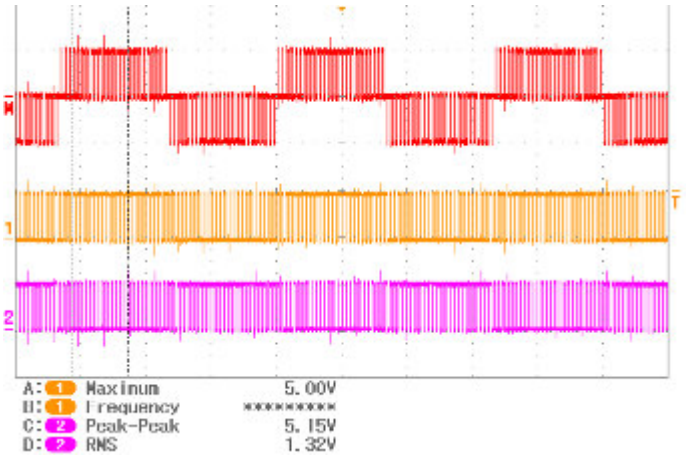

Fig. 3.13: PWM wave output signals of the trigger signal generator.

To generate a high voltage bipolar square waveform or a high voltage three-level bipolar PWM waveform, two improved cascade connection circuits (Fig. 2.5) are needed. The two output channels of the trigger signal generator are used to trigger these two circuits. The differential voltage of these two improved cascade connection circuits is a high voltage bipolar square waveform or a high voltage three level bipolar PWM waveform. The block diagram of high voltage bipolar square wave and PWM waveform generator is shown in Fig. 3.14.

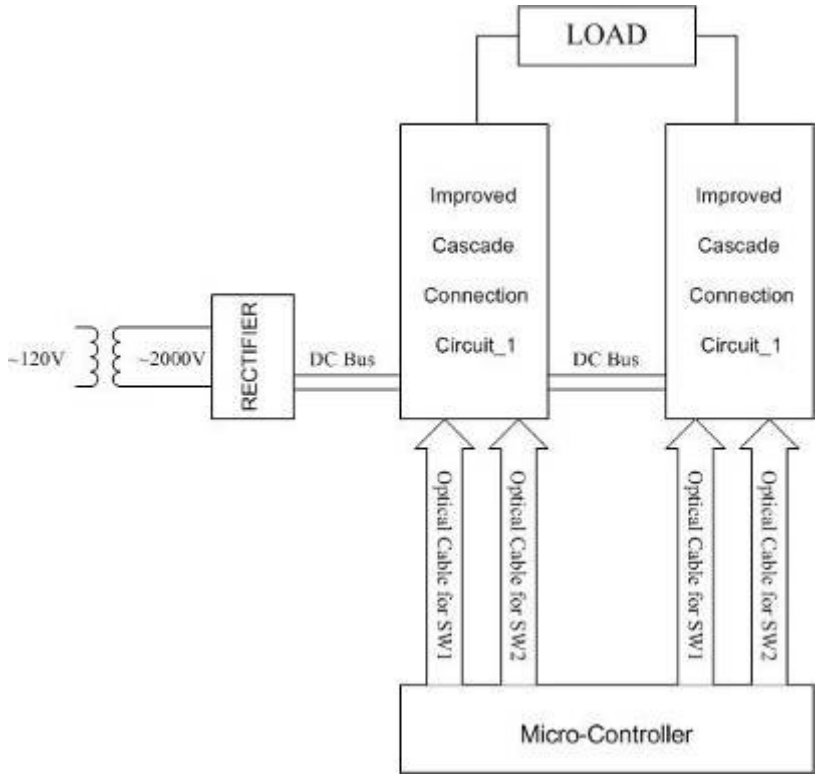

Fig. 3.14: Block diagram of bipolar square wave and PWM wave generator.

Chapter 4

Simulation and Experimental Results of the IGBT-Based Pulse Voltage Generator

This chapter presents the PSIM simulation results based on the PSIM software, and experimental results using the IGBT-based pulse voltage generator described in chapters 2 and 3. The PSIM simulations compare the performance of the series connection and the cascade connection and analyze the influence of the load on the output voltage waveforms. In the experimental tests, the performance of the generator was tested with different loads, such as a cable termination, a motor coil, and a coil sample bar. A 4 kV form-wound motor stator coil was tested with power frequency, exponential decay pulse, square and SPWM voltage waveforms, all with the same peak values. A discussion on the surface temperature rise caused by these voltage stresses is also presented.

4.1 Simulation results

Simulation software (PSIM) was selected in order to simulate the performance of the generator. The simulation can provide a theoretical understanding of the cascade connection. Due to the component limitation of the PSIM student version, a seven-stage generator was used in the simulation. Fig. 4.1 shows the simulation circuit, in which 7 waveform stages are cascade connected. Simulated oscilloscopes were used to record the total output voltage waveform (V_8) and the voltage waveforms at each switch (V_1-V_7). All IGBT switches were triggered by a common PWM trigger signal generator. Each stage was supplied by independent 1500 volts DC sources, and the DC sources were isolated from each other. Three cases that could occur under real operation conditions were studied using the simulated circuit.

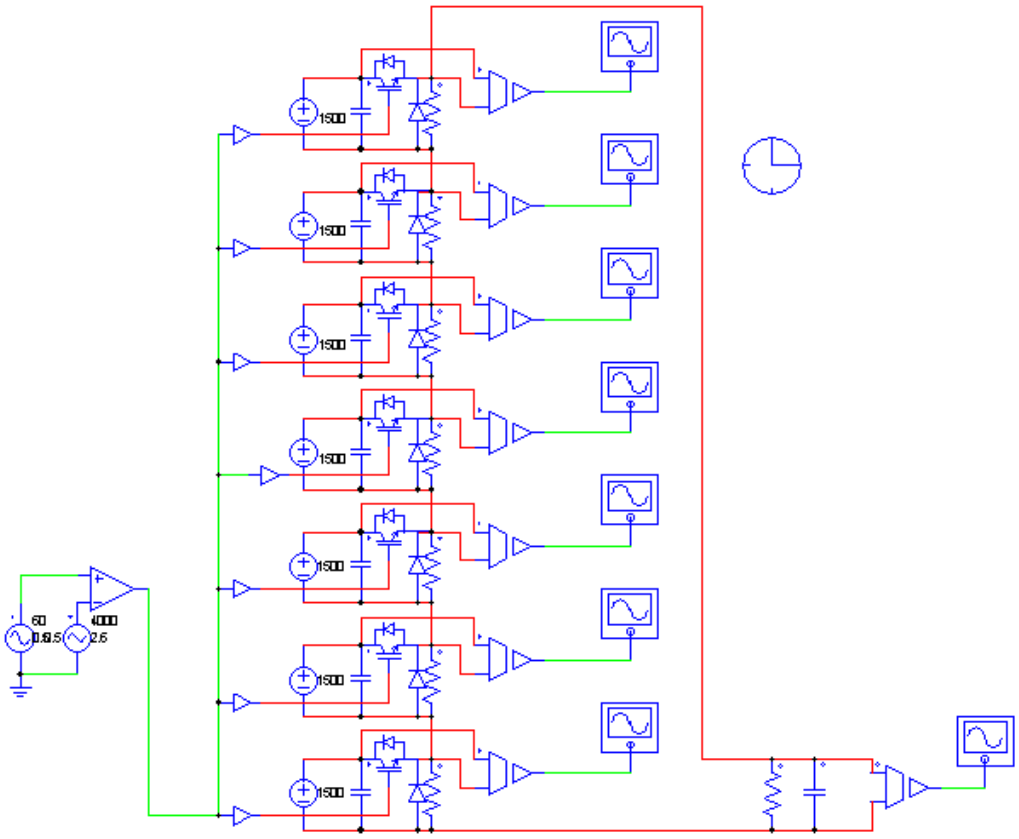

Fig. 4.1: Simulation circuit of the generator.

4.1.1 Study Case 1: A comparison of a series connection and a cascade connection

As mentioned in chapter 2, the main advantage of the cascade connection is that it can overcome the problems associated with series connected switches that may fail due to the unsynchronized switching operation. These problems are usually caused by electromagnetic interference from both inside and outside the generator. Fig. 4.2 shows two generators with different connection structures, namely, series and cascade, where both generators are connected to the same load. Under normal conditions, the switches in both connection structures run simultaneously. The output waveforms and the voltage waveforms at each stage of the two connection structures are almost the same, as shown in Figs. 4.3 and 4.4.

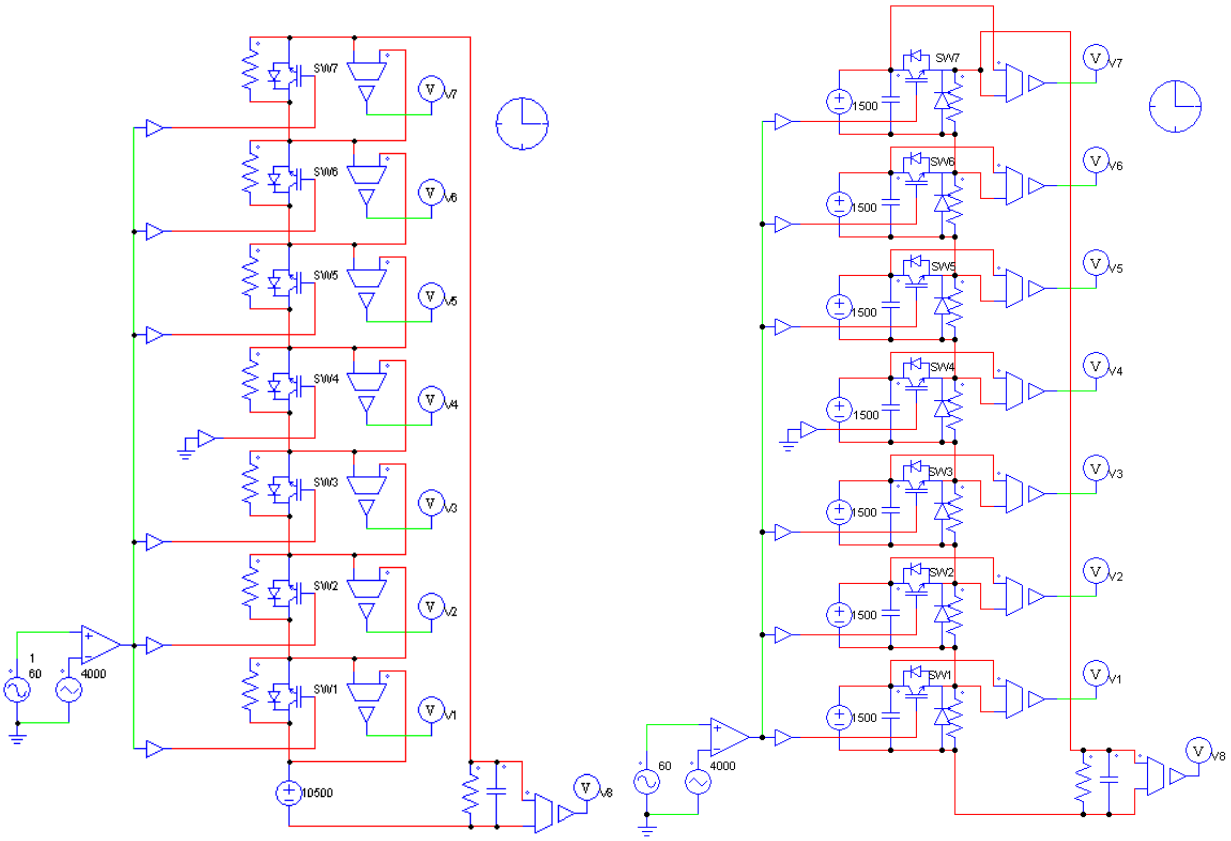

(a) Series Connection

(b) Cascade Connection

Fig. 4.2: Comparison of series connection and cascade connection.

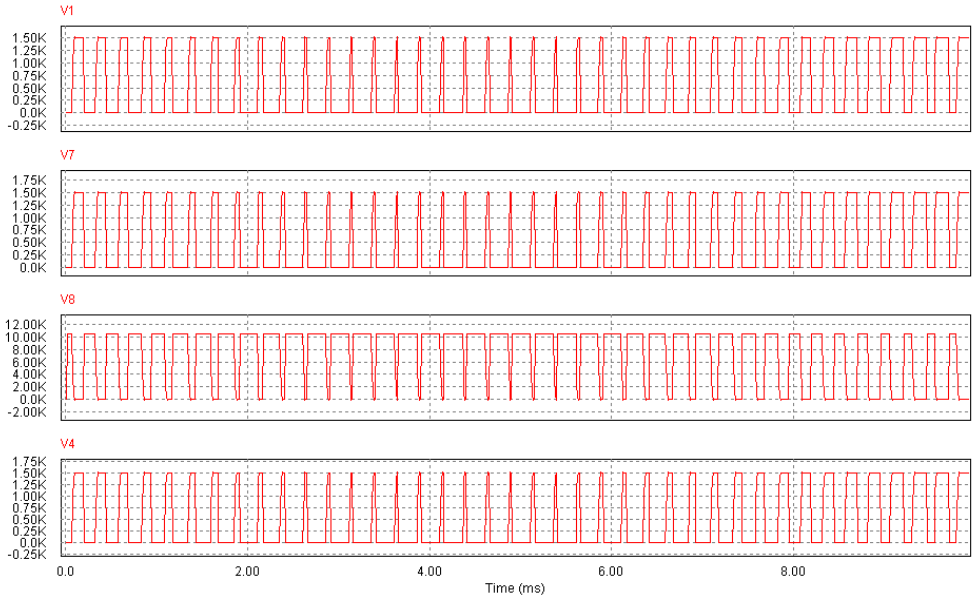

Fig. 4.3: Voltage waveforms at different points in series connection under normal operating condition.

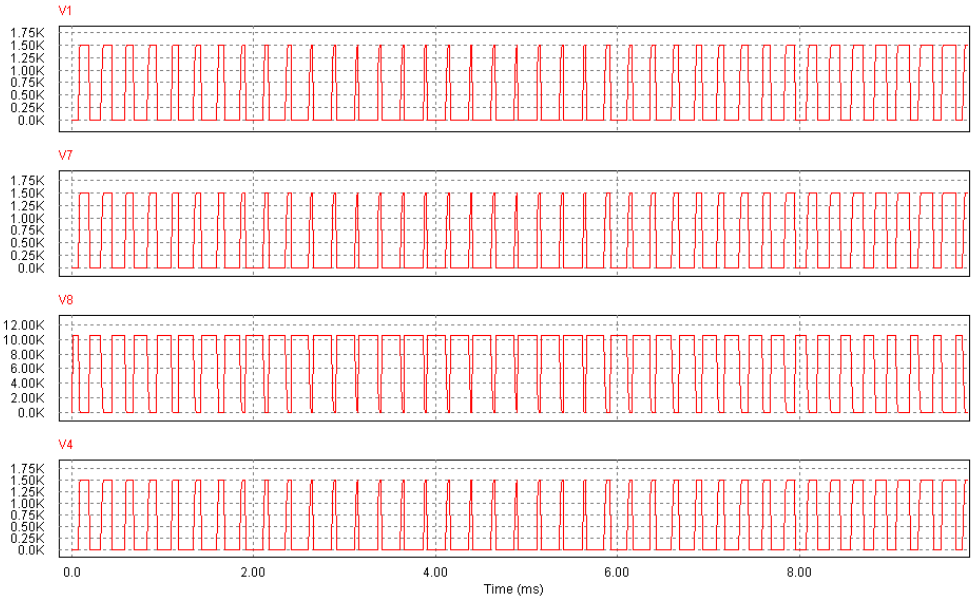

Fig. 4.4: Voltage waveforms at different points in cascade connection under normal operating condition.

However, when some of the switches lose synchronism, the conditions of the two connection structures are totally different. In the simulation circuits shown in Fig. 4.2, the trigger signal of one switch (SW4) in both generators is connected to ground in order to simulate the worst case operation. One of the switches in both connection structures fails to close and remains open for several cycles, while the other switches operate normally. The total output voltage waveforms and the voltage waveforms at the switches for both connection structures are shown in Figs. 4.5 and 4.6, respectively.

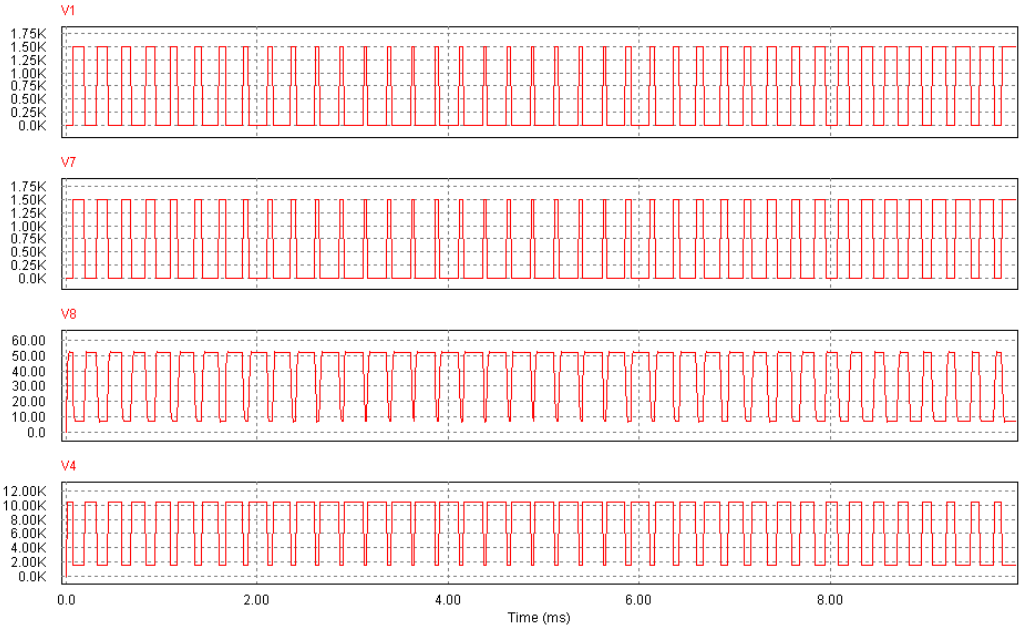

Fig. 4.5: Voltage waveforms at different points in series connection with one switch remaining open.

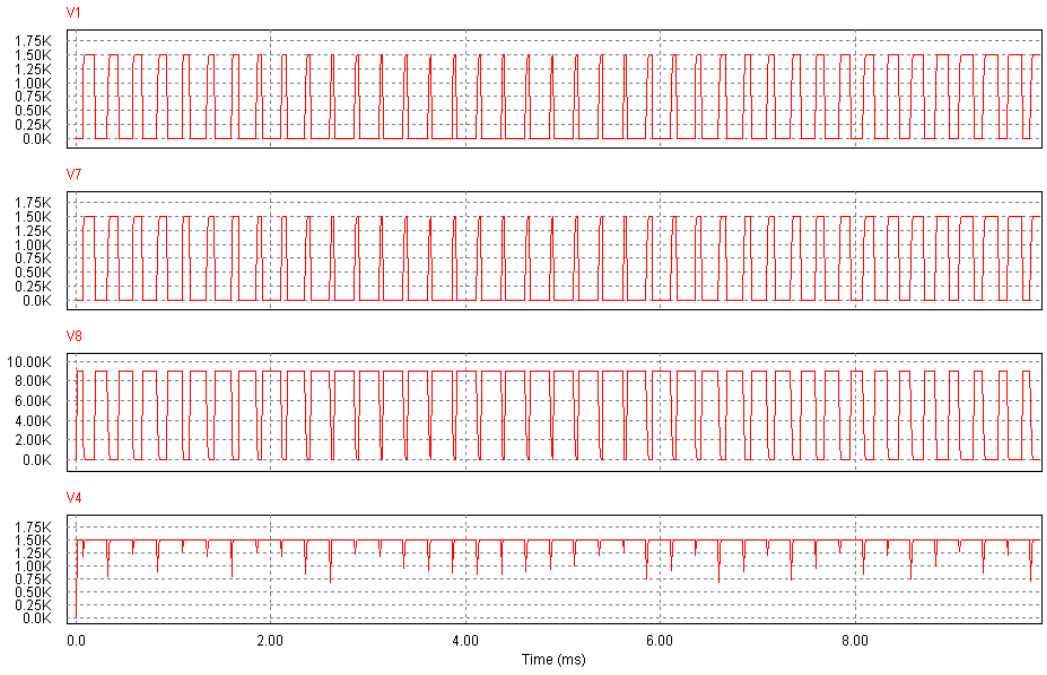

Fig. 4.6: Voltage waveforms at different points in cascade connection with one switch remaining open.

As shown in Figs. 4.5 and 4.6, when an unsynchronized operation problem occurs in the series connection, the total output voltage (V_8) drops significantly. The peak value of the output voltage drops from 10.5 kV in normal conditions (Fig. 4.2) to only 52 V in an unsynchronized condition (Fig. 4.5). Whereas, when the same unsynchronized problem develops in the cascade connection, the peak value of the output voltage drops from normal 10.5 kV to 9.0 kV, which is shown in Fig. 4.3 and Fig. 4.6. The voltage drop is exactly equal to the voltage of one stage.

The voltage across the switch (SW4) in the series connection is almost 10.5 kV, which is much higher than the rated operation voltage of the switch, as shown in Fig. 4.5. This voltage may damage the switch. As soon as one switch in the series connection is short circuited, all switches in the series connection may be damaged because the remaining switches must withstand the total high voltage which normally would be shared by all the switches. On the contrary, no such problem occurs in the cascade connection. Although the voltage waveform across the switch (SW4 in Fig. 4.6) in the cascade connection is seriously distorted, the peak value of the voltage across the switch is still within the range of the switch's operating voltage. Thus, the switch is safe from damage that might occur. Therefore, the whole generator has zero risk of failure due to unsynchronized operation.

The comparison of the simulation results for the two connection structures theoretically confirms that the cascade structure is a more reliable way to generate high voltage waveforms by using low voltage rated IGBT switches. The cascade connection structure avoids the unsynchronized operation problem that may cause damage to the switches in the series connection structure and therefore is safer, more reliable, and less costly.

4.1.2 Study Case 2: the load range of the generator

The equivalent parallel circuit representation of dielectric materials is shown in Fig. 4.7(a). The equivalent resistor of insulation materials is in the range of tens of MΩ to several GΩ, and the range of equivalent capacitance is from tens of pF to several nF.

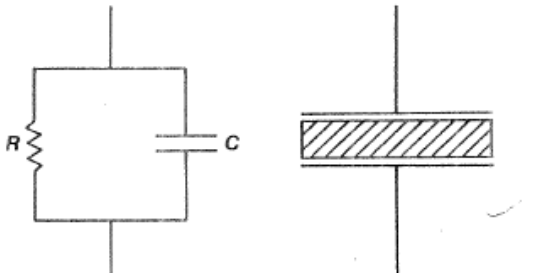

(a) Equivalent circuit (b) Dielectric insulation

Fig. 4.7: Equivalent circuit of a dielectric insulation.

It is clear that the test object has a significant influence on the wave shape of the pulse voltage produced by the generator, especially when connected to a load with a large capacitance. The wave shaping resistors (R_1 in Fig. 2.5) in the generator are selected to minimize this influence to a certain tolerance. These wave shaping resistors are connected in parallel with the load in the circuit. Based on the waveform generation mechanism in chapter 2, the rise time, the pulse width, and the fall time of the waveform are predicated by the values of R_{con}, C_1, R_1 and C_{tr}. The sum of the rise time, pulse width and the fall time determines the cycle of the square wave, so, R_{con}, C_1, R_1 and C_{tr} determines the highest switching frequency of the generator.

Considering most insulation materials and commercially available pulse capacitors, the value of C_1 is chosen to be 2 μF. For ten stages, the total capacitance is 0.2 μF, which is much higher than the capacitance of most test objects. So, C_1 can be neglected in calculating the rise time. The rise time is determined mainly by the product of R_{con} and C_{tr}. Since the value of R_{con} is very small, the rise time can be limited to less than several hundred nanoseconds.

The fall time is determined by $n\times(R_1//R_{load})C_{tr}$, where n is the number of stages in generator. Since R_1 is parallel to the load, the smaller the value of R_1, the less the influence caused by the load. However, low resistance causes high power consumption and low efficiency, and the pulse width will decrease with a smaller value of R_1. In this thesis, the value of the resistance used is 5 kΩ.

In the simulated circuit, the equivalent circuit model of a parallel combination of a resistor and a capacitor is used to imitate the any test object. Since $n\times R_1$ (50 kΩ) is much smaller than the equivalent resistance of test object (MΩ to GΩ), the load resistor can be neglected in the simulation. Figs. 4.8 and 4.9 show the voltage waveform at the test object which has an equivalent capacitance of 500 pF. As the frequency increases, the low part of the wave is "chopped" because there is not enough time available to decrease the voltage to zero.

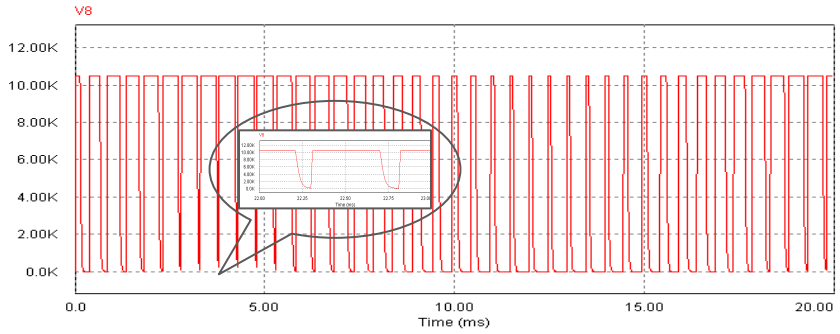

Fig. 4.8: Voltage waveform at a test object with a 500 pF equivalent capacitor at a switching frequency of 2 kHz.

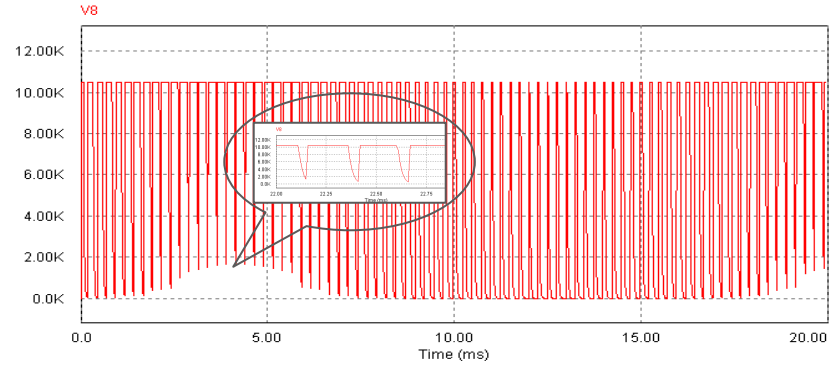

Fig.4.9: Voltage waveform at a test object with a 500 pF equivalent capacitor at a switching frequency of 4 kHz.

The maximum switching frequency that the generator can produce on different loads, before the waveform chops, is shown in Table 4.1. Fig. 4.10 shows the curve of maximum frequency *vs.* the equivalent capacitance of the test load.

Table 4.1 Maximum Switching Frequency of Generator with Different Test loads.

Equivalent Capacitance of Test Object (pF)	50	100	200	500	1000	2000	5000	10000
Maximum Switching Frequency (Hz)	7000	6400	4500	2000	1100	600	250	120

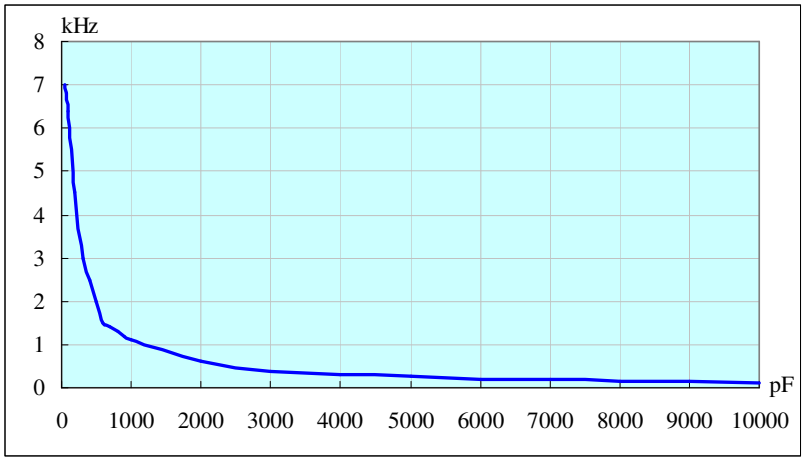

Fig. 4.10: Maximum frequency *vs.* equivalent capacitance of the test object.

As shown in Table 4.1 and Fig. 4.10, due to the long decay time, the maximum switching frequency that the generator can produce with a large capacitive load is very low. In order to decrease the decay time and increase the switching frequency for a large capacitive load, an auxiliary external resistor can be connected parallel to the load providing additional path to discharge the load. Table 4.2 shows the maximum switching frequencies for different loads when a 5 kΩ resistor is connected in parallel with the load. The disadvantages of this method are high energy consumption and low output efficiency.

Table 4.2 Maximum Switching Frequency of Generator with Different Test Objects paralleling with a 5kΩ Resistor.

Equivalent Capacitance of Test Object (pF)	50	100	200	500	1000	2000	5000	10000
Maximum Switching Frequency (Hz)	60000	50000	30000	12000	9000	5000	2000	1000

4.1.3 Study Case 3: testing with inductive loads

The simulated circuit for testing with an inductive load is shown in Fig. 4.11. A 500 Ω resistor is connected in series with the load in order to limit the output current.

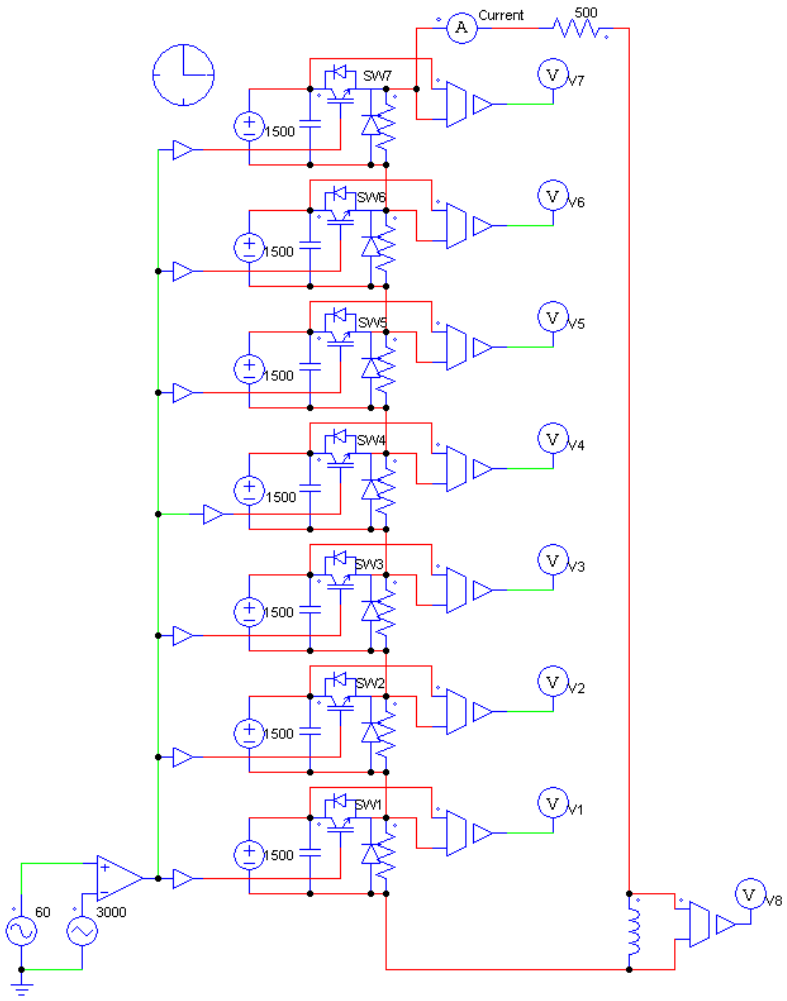

Fig. 4.11: Test with an inductive load.

Fig 4.12 shows the waveforms of the output voltage, the switch voltage, and the output current when the load inductance is 2 mH. Fig. 4.13 shows the waveforms when the inductance of the load is 2 H.

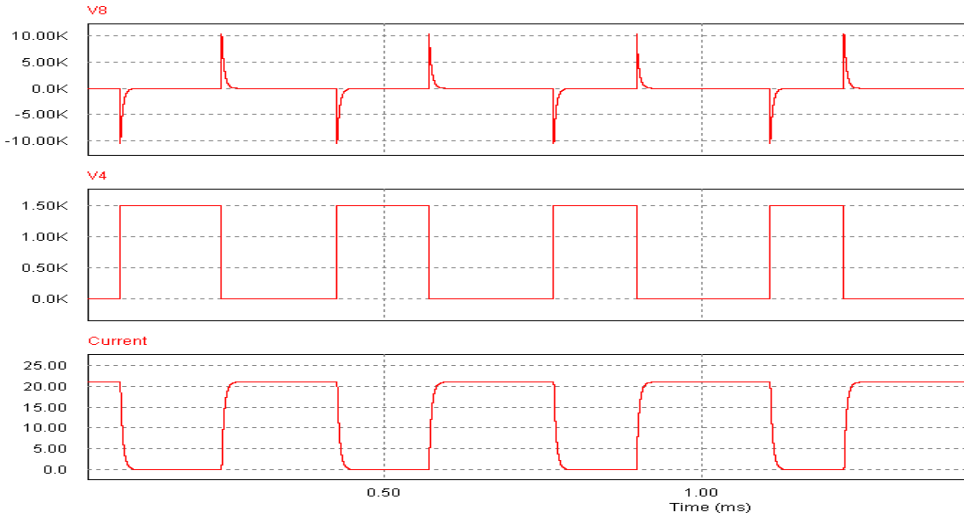

Fig.4.12: Test with a 2 mH inductive load.

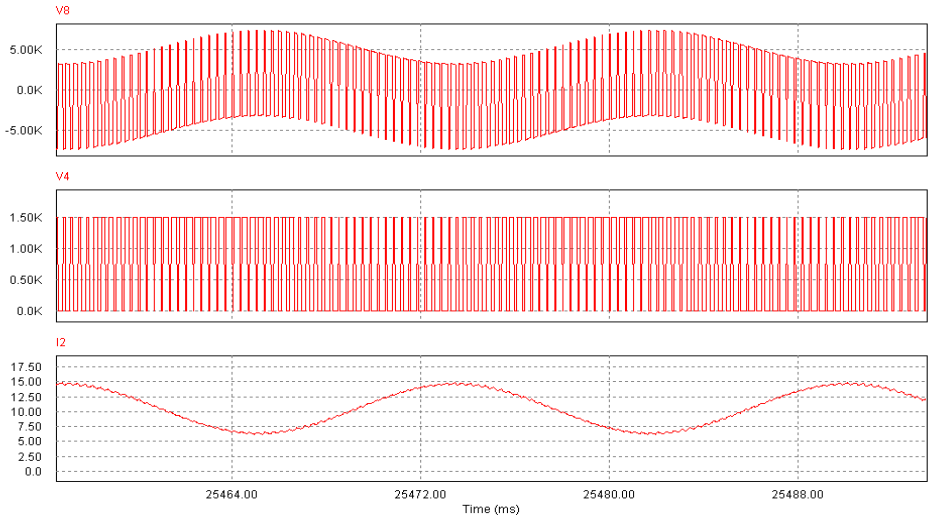

Fig. 4.13: Test with a 2 H inductive load.

When testing a low inductance load (2 mH), the output waveform is not a SPWM wave but a bipolar exponential decay waveform (Fig. 4.12). The exponential voltage pulse occurs at each IGBT switching period. When testing with a high inductive load (2 H), the test voltage waveform is a superimposed waveform consisting of a

fundamental sinusoidal waveform and PWM wave (Fig. 4.13). In both cases, the voltage at the switch is still a PWM waveform with a peak voltage of 1500 V, which is within the operating voltage range of each stage.

4.2 Experimental results

4.2.1 Open circuit waveforms:

Fig. 4.14 shows the open circuit output waveforms of the generator. The rising and the failing parts of the waveform are also shown in Fig. 4.14. Table 4.3 lists the rise time and fall time of the waveform at different peak values of the output voltage.

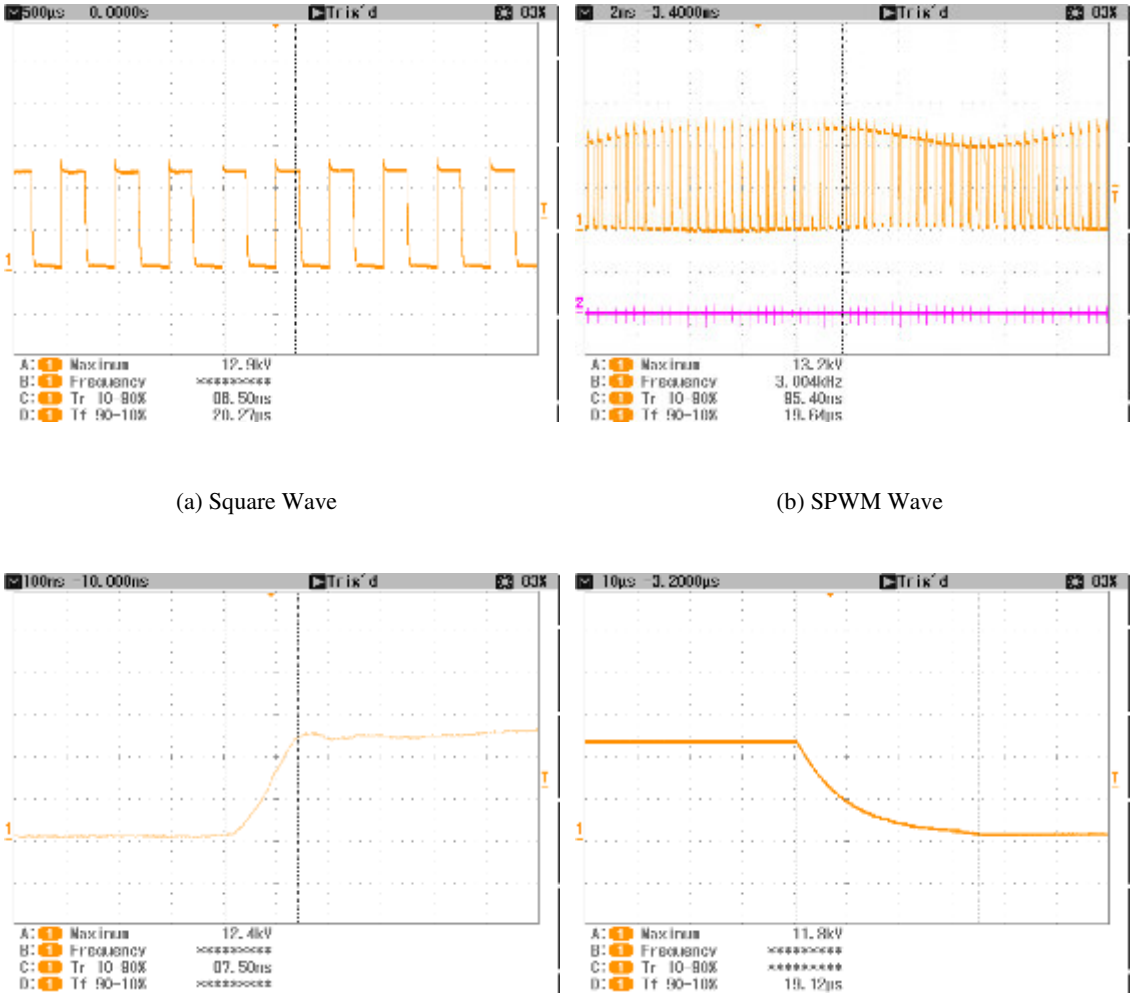

(a) Square Wave

(b) SPWM Wave

(c) Rise time

(d) Fall time

Fig. 4.14: Voltage and current waveforms with no load connected.

Table 4.3. Rise time and fall time of the waveform with no load connected

Peak Voltage(kV)	2.12	4.36	5.92	8.1	10.2	12.9
Rise time(ns)	156	148	134	134	136	140
Fall time(μs)	35	35.4	35.4	35.4	35.4	34.8

As evident from Table 4.3, the rise time and fall time remain at almost the same level for different peak values of the output voltage.

4.2.2 Tests with different test objects

Three typical test objects were selected for testing: a sample motor coil bar (13.8 kV rated voltage), a cable termination (14 kV rated voltage), and a motor stator coil (4 kV rated voltage), see Fig. 4.15. The equivalent capacitance and resistance of the test objects, which are measured at different frequencies, are listed in Table 4.4.

(a) Sample Bar

(c) Coil

(b) Cable termination

Fig.4.15: Test Objects.

Table 4.4 Equivalent capacitance and resistance of test objects.

Test object	Frequency	100	1k	10k	100k	1M
Cable termination	Rp	1.9G	1.2G	37M	2.4M	98k
	Cp	68p	65p	65p	64p	64p
Sample bar	Rp	294M	48M	4.7M	215k	4.7k
	Cp	552p	545p	541p	536p	518p
Coil	Rp	169M	21.6M	1.91M	79.8k	2.55k
	Cp	1000p	988p	979p	974p	202p

- Cable termination Test: The output waveforms of the generator when tested with the cable termination as its load are shown in Fig 4.16. The oscillation and overshoot at the front part of voltage waveform and the current waveform can be observed.

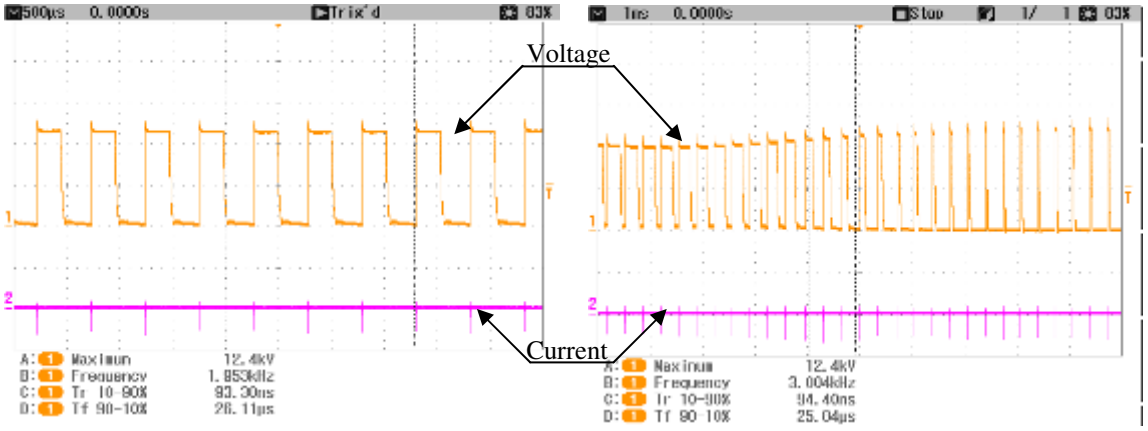

(a) Square Wave

(b) SPWM Wave

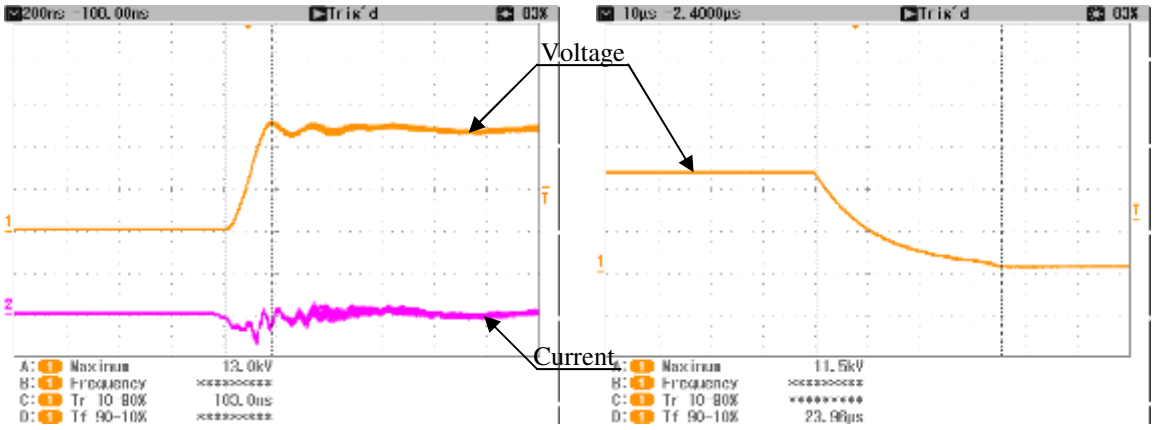

(c) Rising Part

(d) Falling Part

Fig.4.16: Voltage and current waveforms when tested with cable termination.

- Sample bar test: Fig. 4.17 shows the waveforms with the sample bar as the load. The oscillation and overshoot at the front part of voltage waveform and the current waveform are significantly greater compared with the open circuit waveform shown in Fig. 4.14.

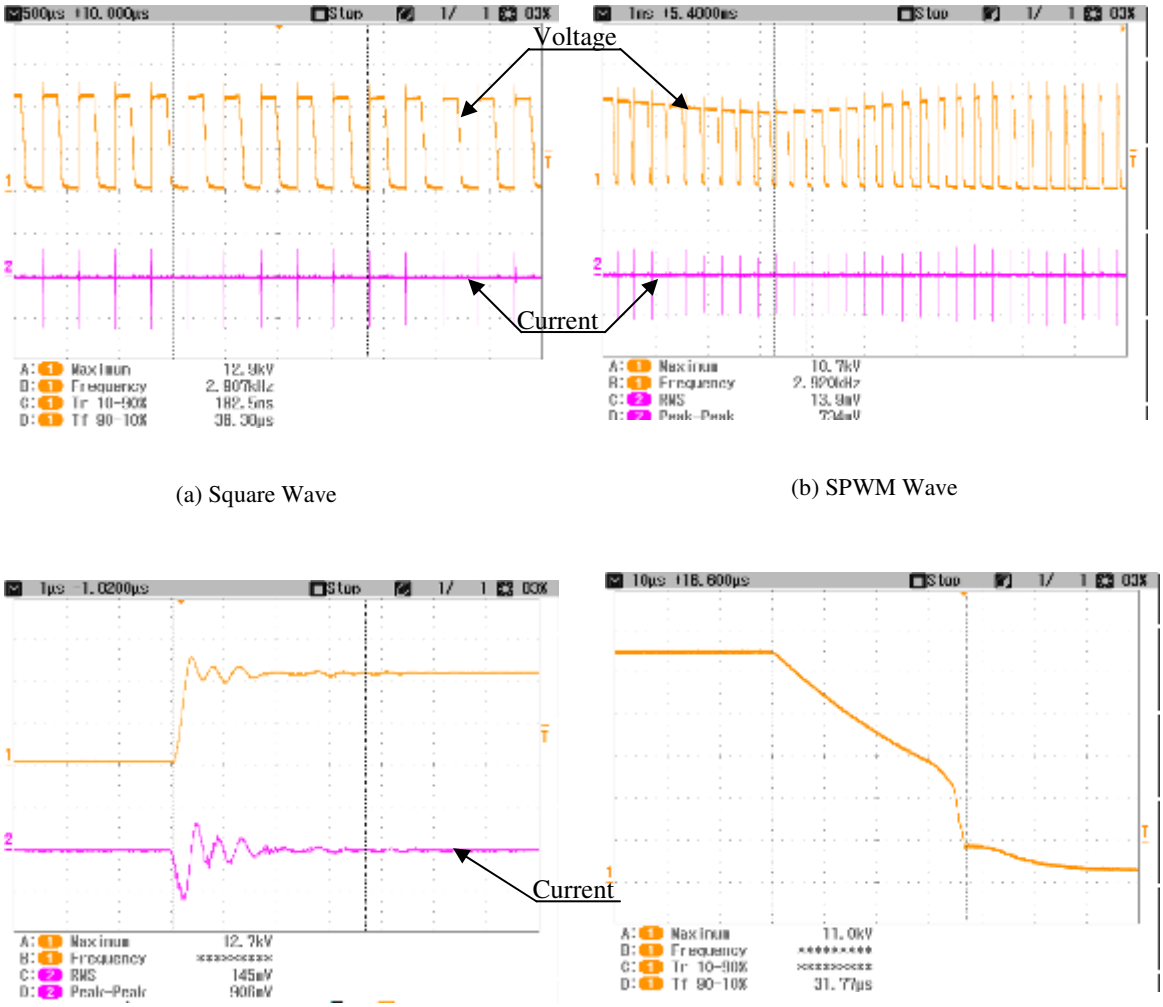

(a) Square Wave

(b) SPWM Wave

(c) Rising Part

(d) Falling Part

Fig.4.17: Voltage and current waveforms when tested with a sample bar.

- Coil test: A 4 kV form wound motor stator coil was tested with the generator; the output waveforms are shown in Fig. 4.18. As shown in the voltage and current waveforms, the durations (up to 20μs) of voltage and current oscillations are longer than all the other tests.

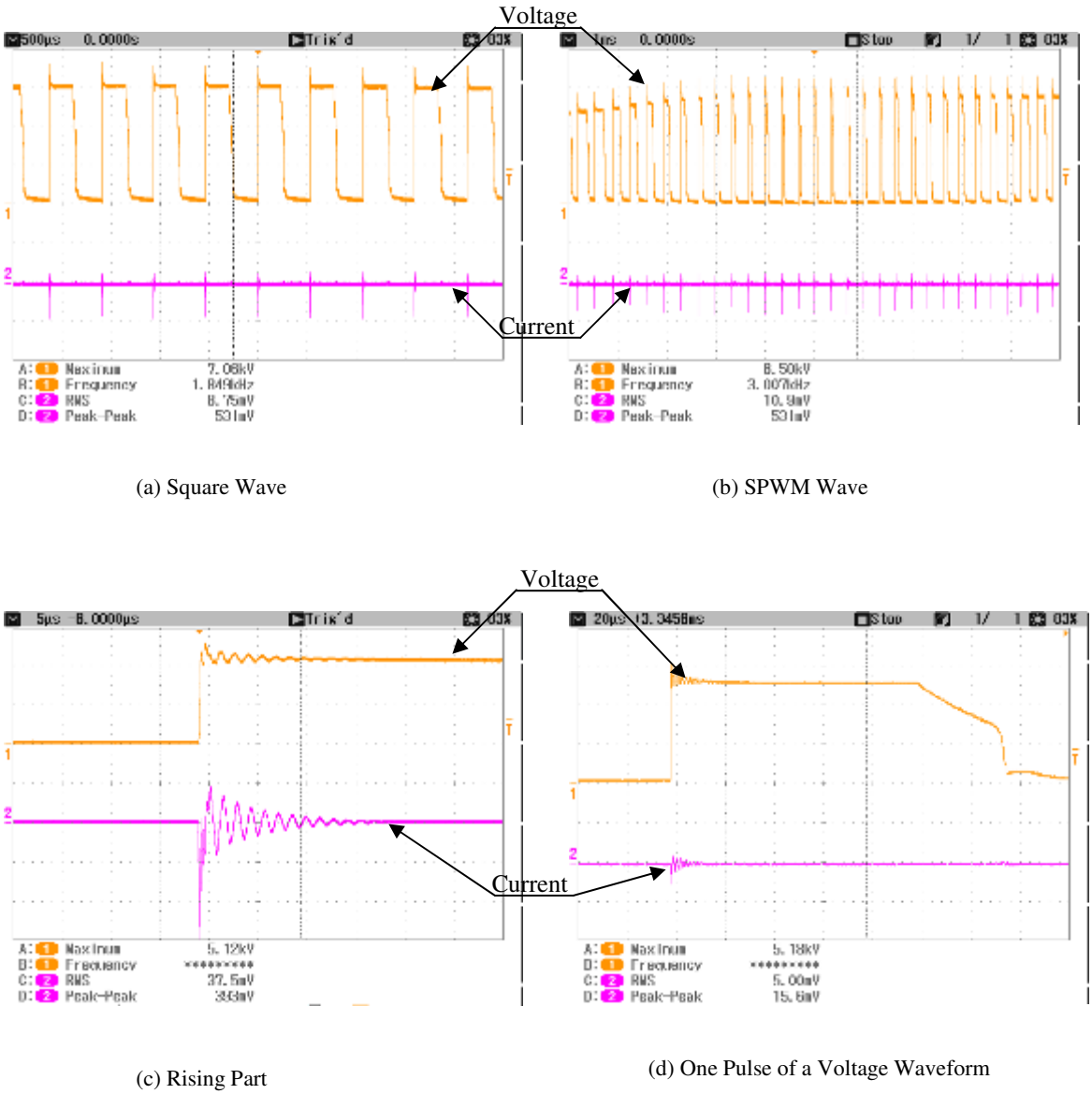

(a) Square Wave

(b) SPWM Wave

(c) Rising Part

(d) One Pulse of a Voltage Waveform

Fig. 4.18: Voltage and current waveforms when tested with a motor coil.

The upper waveforms show different responses for the various objects tested with the generator. These variations are due to the different parameters and characteristics of the test objects. The parameters of the test objects combined with the parameters of the connecting cable result in different shapes of the voltage and current waveforms, especially in the waveform fronts. Table 4.5 lists the parameters of the waveforms that were obtained from tests with different objects.

Table 4.5 Diversity of voltage waveform with different test objects.

Test Object	No Load	Cabel termination	Sample Bar	Form Wound Coil
Rise time (ns)	134	148	328	296
Fall time (μs)	35.4	35.6	36.4	37.4
Maximum Voltage Overshoot Amplitude (%)*	/	11.6	13	15.9
Oscillation Duration (μs)	/	1.5	6	20

* The maximum voltage overshoot amplitude is defined as $[V_{max}/(V_{max}- V_{top})]\times100\%$, where V_{max} is the maximum voltage of the waveforms and V_{top} is the top voltage of the waveform (the value of the flat part).

4.2.3 Insulation tests under different voltage stresses

A 4 kV_{rms} form-wound model stator coil (Fig. 4.15(c)) was tested under different voltage waveforms; namely, power frequency, exponential decay pulse, square wave, and SPWM wave. The middle part of the coil was clamped with two metal plates to simulate the motor core slot and the test voltages were applied between the coil terminal and the grounded metal plates.

In the test, a FLIR-SC500 infrared camera with an emissivity spectrum between 7.5 and 13 μm is used to measure the surface temperature of the coil. The temperature

image is displayed in a 320×240 pixel array. The sensitivity of the detector is 0.07 K at a temperature of 303 K and with an accuracy of 2 K over 273 to 773 K. The emissivity calibration was conducted on the sample at room temperature with a thermocouple reading as a reference. Fig. 4.19 shows the test setup for temperature measurement.

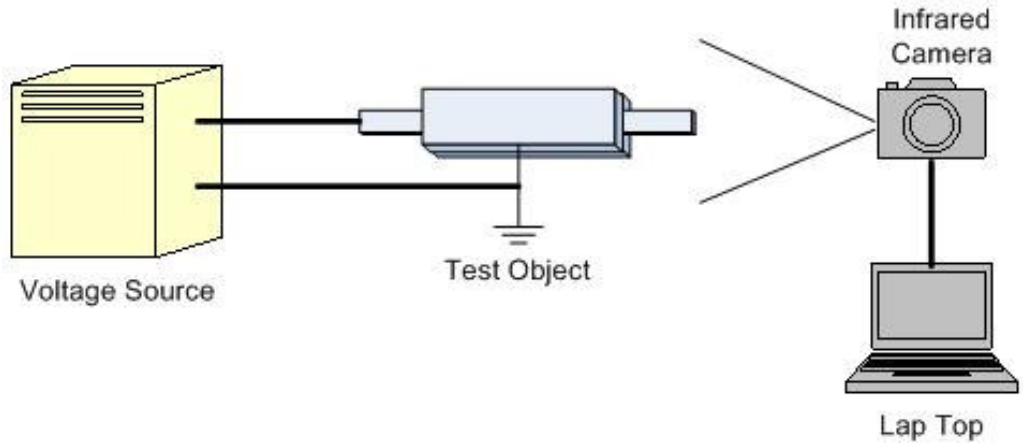

Fig. 4.19: Temperature measurement setup.

The four types of test voltage waveforms are shown in Fig. 4.20. The test waveform parameters corresponding to the four test voltage waveforms are given in Table 4.6.

Table 4.6 Parameters corresponding to the test voltage waveforms.

Test voltage used →	Power Frequency Voltage	Exponential decay pulse	Square wave	SPWM wave
Maximum voltage →	7.5kV	7.5kV	7.5kV	7.5kV
Frequency or repetition rate →	60Hz	3kHz	3kHz	60 × 50Hz
Rise time →	/	760ns	118ns	124ns
Fall time →	/	110μs	34μs	30μs

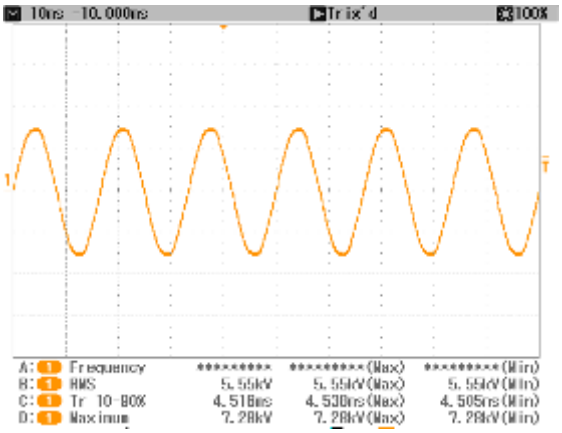

(a) Power Frequency Voltage

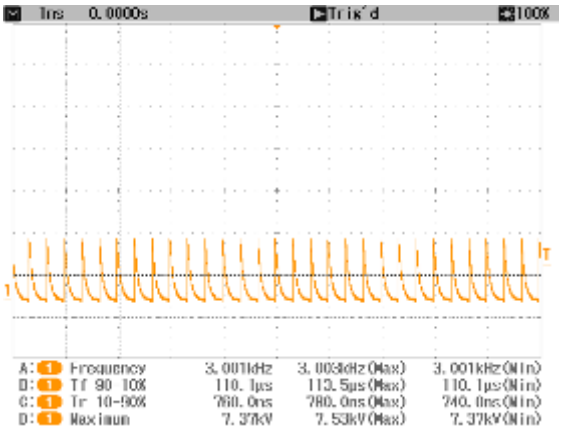

(b) 3 kHz Exponential Decay Pulse

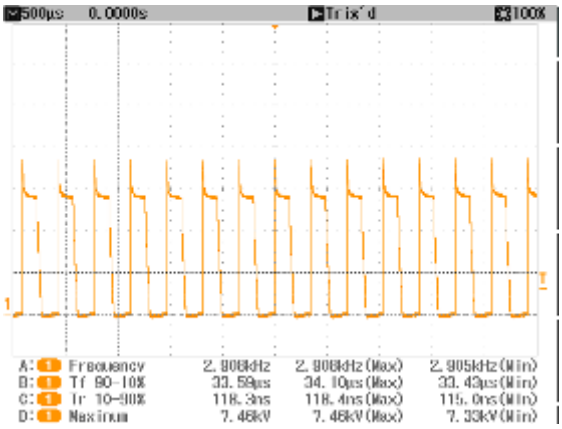

(c) 3 kHz Square Wave

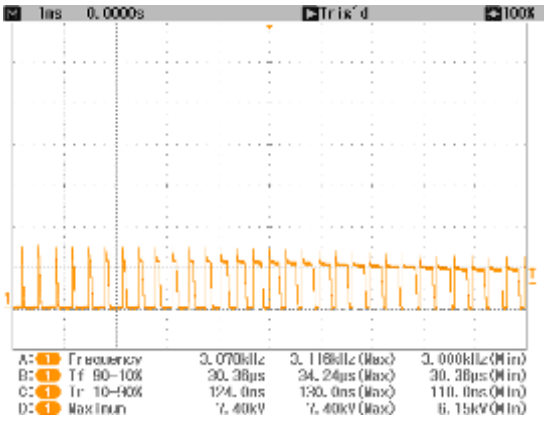

(d) 50×60Hz SPWM Wave

Fig. 4.20: Four types of test voltage waveforms.

The infrared images and surface temperature profiles on the surface of the coil at different stresses are shown in Figs. 4.21 - 4.24. Table 4.7 shows the maximum stable temperature rise of the motor coil under different voltage stresses, as mentioned previously.

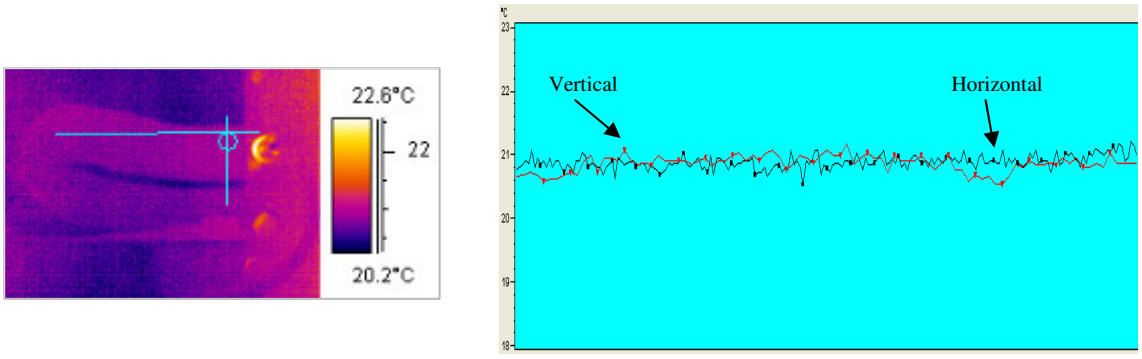

Fig. 4.21: Infrared image and surface temperature profile under a power frequency voltage of 60 Hz.

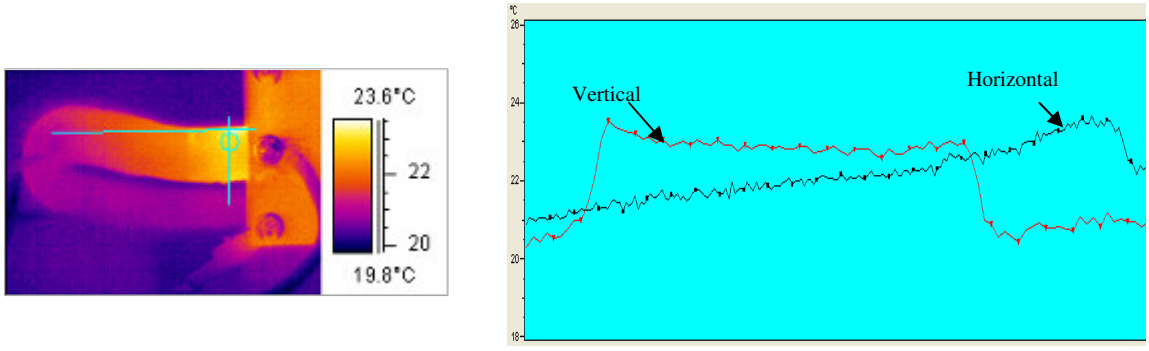

Fig. 4.22: Infrared image and surface temperature profile under an exponential decay pulse.

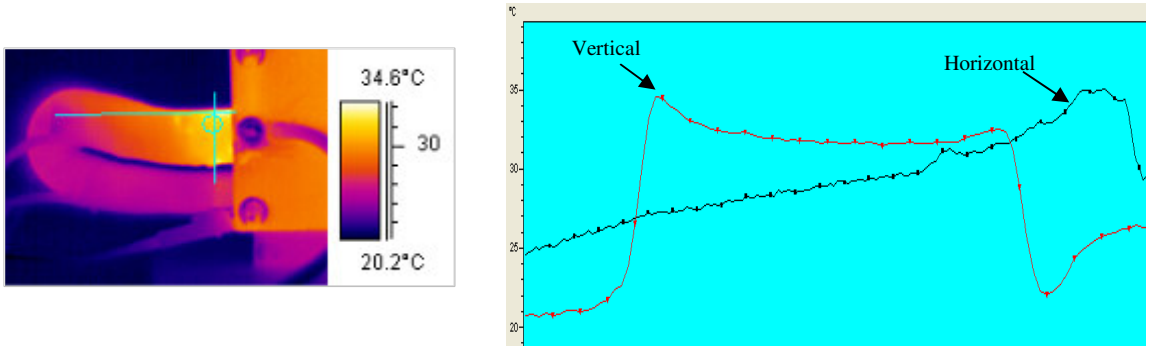

Fig. 4.23: Infrared image and surface temperature profile under a square wave voltage.

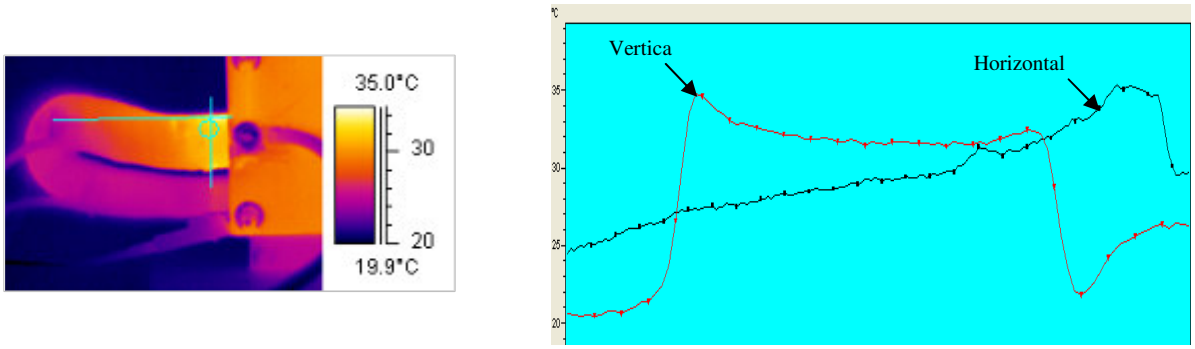

Fig.4.24: Infrared image and surface temperature profile under an SPWM voltage.

Table.4.7 Coil surface temperature rise

Maximum temperature rise (°C)			
Power frequency voltage	High repetitive exponential decay pulse	Square wave	SPWM
0.6	3.4	14.2	14.9

The above test results indicate that the temperature rise on the coil surface varies significantly depending on the type of voltage waveform used, although the peak values of these voltages are the same. From Table 4.7, it can be seen that the highest temperature rise is caused by the SPWM waveform showing a 15 °C rise above the ambient. The second highest temperature rise observed is for the case of the square wave, with a 14 °C rise. The high repetitive exponential decay pulse causes only a 3.5 °C temperature rise. Almost no temperature rise was detected in the case of the 60 Hz power frequency test.

It is difficult to predict the effects of a specific parameter, like rise time, or pulse width, on the observed temperature rise under square wave and SPWM wave due to the limited availability of a test data. However, it is easy to see that the stress due to these waveforms can be significantly severe compared to the other two voltage waveforms. The following paragraphs provide a possible explanation of the temperature profiles observed.

The peak value of the voltage overshoot produced by transient is a function of rise time, the pulse width, as well as the natural resonant frequency of the circuit. The first two are determined by the voltage source, and the latter one is determined by the impedances of the connecting cable and the coil. In the case where the pulse width matches the natural resonant frequency of the circuit, the overshoot reaches a maximum value that is considerably high in amplitude, and hence, the maximum *dv/dt*. As a result, the internal partial discharges can be triggered and cause a high temperature rise [33, 34].

Another factor that contributes to the significant temperature rise is the characteristics of the materials in the laminated insulation system of the motor. Some materials are sensitive to frequency, while others are not as sensitive. Fig. 4.25 shows the resistance-frequency curves of the two tapes used in the motor insulation system. The synthetic resin bonded mica tape (solid curve in Fig. 4.25), which is frequently used in making motor ground wall insulation, is sensitive to frequency. The curve shows that the tape resistance decreases significantly with an increase in frequency. In contrast, the conductive tape (dashed curve in Fig 4.25), which is used as a corona protector in the slot, is not sensitive to changes in the frequency. The resistance of conductive tape remains the same with the changing frequency.

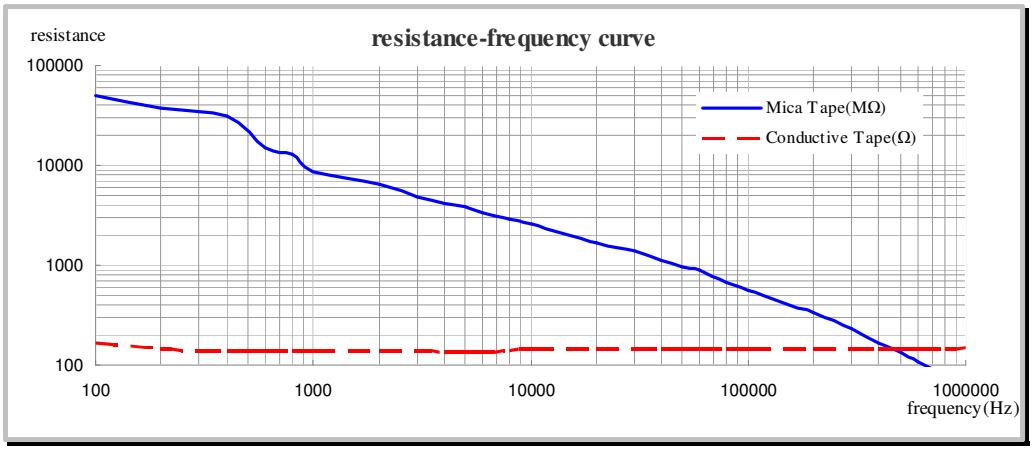

Fig. 4.25: Resistance-frequency curve of different insulation materials.

Fig. 4.26, Fig. 4.27 and Fig. 4.28 show the frequency spectra of various voltage waveforms used in this study. The frequency spectra of the SPWM, the square wave,

and the exponential decay pulse were obtained at a sample rate of 1MS/s. Compared to those of the exponential decay pulse, the harmonic components around the switching frequency and its multiples of the SPWM wave are significantly different. In Fig. 4.26, the spectrum is almost continuous in the high frequency area when compared to high frequency area of exponential decay pulse, Fig. 4.28. When these high frequency harmonic voltages are applied to the insulation system, the dielectric loss of frequency dependent insulation materials increases; thus, the heat generated due to dielectric loss can increase. When these high frequency harmonic voltages are applied to the insulation system, the dielectric loss of frequency dependent insulation materials increases; thus, the heat generated due to dielectric loss can also increase.

Additionally, the frequency response characteristic of different materials also changes the voltage distribution along the insulation layers in a laminated insulation system for motor coils. For some high frequency harmonic components in the applied voltage, a higher voltage is distributed at the conductive layer of the ground wall insulation, which results in an increase of heat generated by the conductive materials.

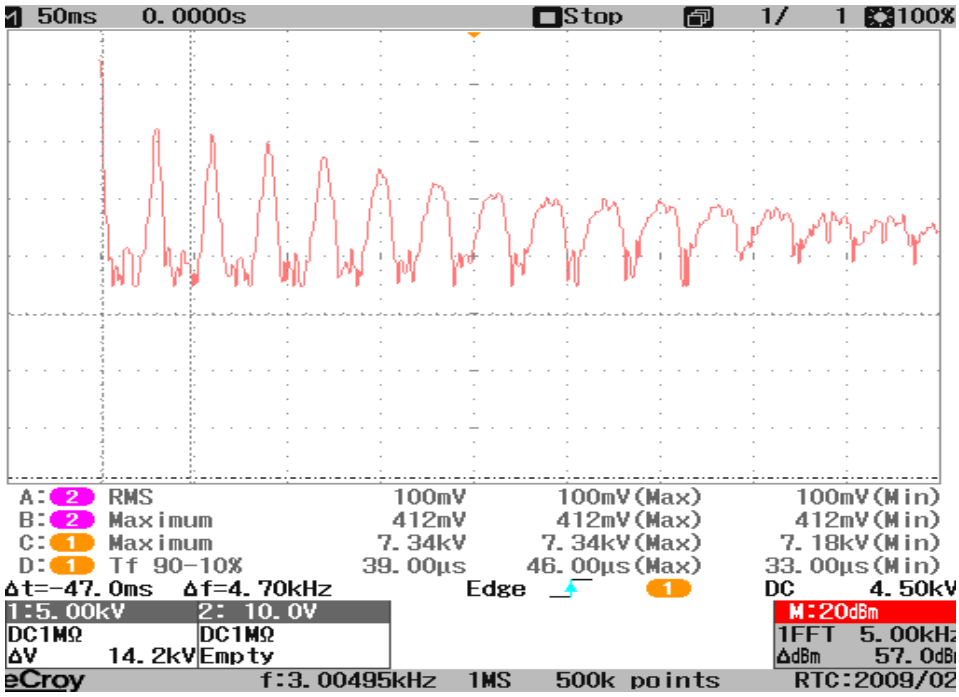

Fig. 4.26: Frequency spectrum of the SPWM waveform.

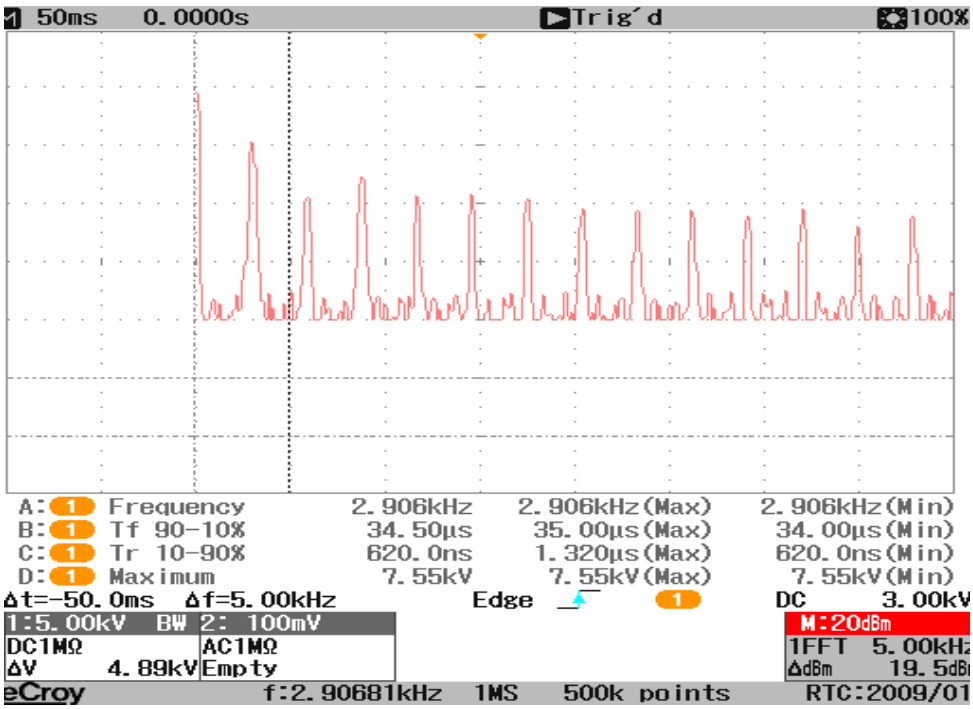

Fig. 4.27: Frequency spectrum of the square wave voltage.

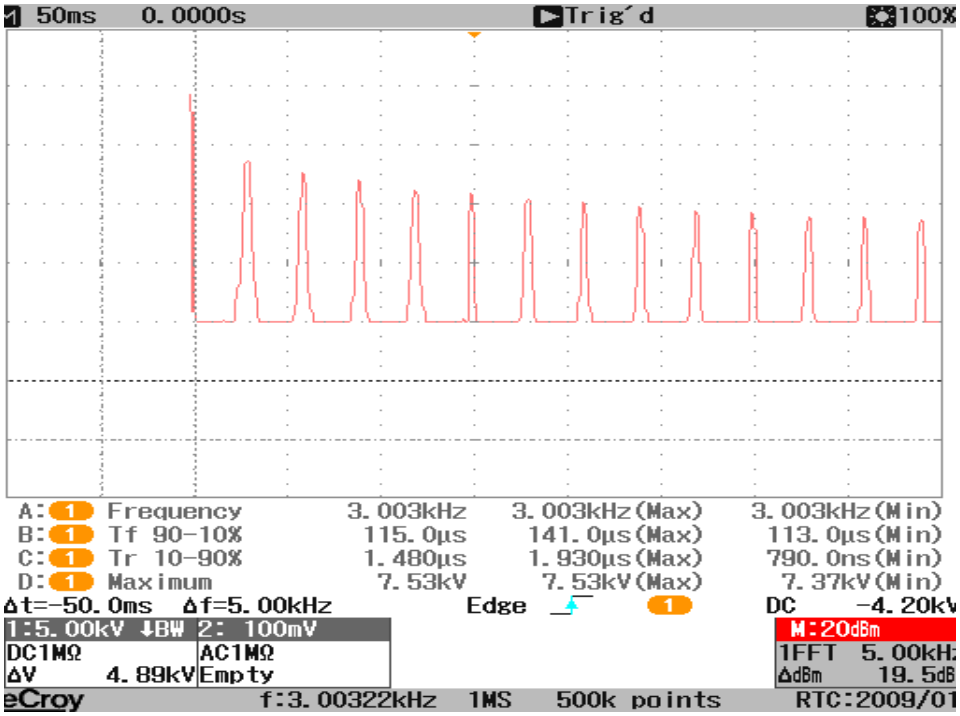

Fig. 4.28: Frequency spectrum of the exponential decay.

In summary, because the square wave or the SPWM voltage waveforms have varying pulse widths, faster rise time (200 ns as opposed to 500 ns for the exponential decay pulse), and higher frequency harmonic contents, the temperature rise caused by the square wave or the SPWM waveform is significantly higher than that produced by the other voltage sources. The fast repetitive exponential decay type pulsed-voltage [28] or the specific high frequency sinusoidal waveforms that are currently used to test the insulation performance do not reflect the actual conditions to which the VSC fed motors are exposed when in operation. Thus, these sources are not suitable for the qualification and acceptance tests of electric motor insulation systems fed by power electronic converters.

Since the square and SPWM voltage waveforms generate transients and enhanced stresses similar to those of the actual VSCs, it is recommended that square and SPWM voltage waveforms be used as a test source for the qualification and acceptance test of electric motor insulation systems fed by power electronic converters.

Chapter 5

Summary, Conclusions and Suggestions for Future Work

5.1 Summary and Conclusions

In recent years, pulse width modulated voltage source converters (PWM-VSCs) have dominated the market for motor drives. This is due to their compact size, high reliability and high efficiency. However, the PWM-VSCs cause enhanced electrical and thermal stresses on the motor insulation system resulting in premature failure of rotating electrical motors. The literature shows that the enhanced electrical and thermal stress is a result of a combination of factors, which include variations in pulse width, rise time, fall time, crest value, switching frequency of the PWM waveforms, and the impedance and frequency response characteristics of the feeding cable and the coil.

Unfortunately, within the motor manufacturing industry there is a lack of standards and proper insulation test facilities that can sufficiently deal with the enhanced stress caused by adjustable speed drives. Some tests are performed with high repetition rate exponential decay pulses or high frequency voltages. The results of these tests reveal their negative impact on both the motor insulation and the stress grading coating. However, in practice, the motor insulation is exposed to more complex waveforms than the high repetition rate pulses with an exponential decay or high frequency sinusoidal waveforms. It is necessary to test the insulation using a voltage waveform of similar complexity.

An IGBT-based pulse voltage generator has been developed in this work. The generator can produce high voltage square wave and SPWM waveforms, which are similar to the voltage waveforms feeding the motors when they are in operation. Low voltage IGBT switches (IXBT16N170) are selected for use in the generator. The generator consists of several stages connected in cascade; each stage is made of IGBT switches, a capacitor, and a wave shaping resistor. This special cascade connected structure allows the generator to operate in a stable condition. A microcontroller

based trigger signal generator is used to drive the power electronic switches in the generator. The control strategies of the firmware in the microcontroller make the generator flexible. In order to avoid the EMI problem, optical fibre cables are used to connect the microcontroller-based trigger signal generator to the switches, which are located in a high electric potential region.

The PSIM simulations compared the series connection and the cascade connection, and analyzed the load range of the generator in the project. Three types of test objects were selected to test the performance of the generator.

In order to test the motor insulation performance, a 4 kV form wound coil was tested under different voltage sources, namely, power frequency voltage, high repetition rate exponential decay pulse voltage, square wave, and SPWM waveform. Surface temperature rise were measured by an infrared camera during the tests.

The following conclusions can be drawn from the research presented in this thesis:

- An IGBT-based pulse voltage generator has been successfully developed. It can generate both square wave and SPWM waveform with a peak value up to 15 kV peak. The switching frequency range for both waveforms is 600 Hz to 6 kHz, and the fundamental frequency range of SPWM waveform is 20 Hz to 1200 Hz. The rise time is less than 200 ns. The pulse width can be varied from a few microseconds to several milliseconds.
- The simulations and experimental tests show that the cascade connection enables the generator to overcome the problems related to voltage division and synchronization of switches, which normally exist in a series connected structure.
- The improved cascade circuit design, which is based on “charging in parallel and discharging in series”, is utilized in the generator. The peak value of the output voltage can be boosted to several times of the common DC source input voltage, as a result of the design.
- A microcontroller-based trigger signal generator is used to generate the trigger signals for IGBT switches. The firmware of the microcontroller enables the generator to produce different waveforms with the same structural topology. In

addition, the test mode can be set through a keypad in order to satisfy the requirements for both standard and special tests. The modes include automatic test and manual test, long-term continuous aging tests, and cyclic aging tests with an adjustable time interval.

- The use of optical fibre cables to connect the microcontroller-based trigger signal generator to the switches, which are located in a high potential region, helps avoid the EMI problem.
- Based on the test results with a 4 kVrms form wound stator coil obtained under different voltage waveforms, it is concluded that both the square and SPWM voltage waveforms cause a significantly higher rise in temperature than the power frequency and exponential decay pulse voltage waveforms. The highest temperature rise is caused by the SPWM voltage waveform, which can be attributed to the high dv/dt transient voltage and the significantly complex high frequency harmonic content. Thus, it is recommended that the stator coil insulation be analyzed using SPWM voltage waveforms as they are similar to the waveforms generated by the VSCs.

5.2 Suggestions for future work

With regard to future work on the IGBT-based pulse voltage generator and the insulation test on rotating electrical machines fed by power electronic converters, the following directions are proposed:

- With the widely increasing applications of power electronics as well as modern communication signal techniques in power systems, modern electrical apparatuses are no longer operated under the stress of the power frequency sinusoidal voltage, but rather under that of a more complex voltage waveform. Accordingly, test facilities and equipment should be developed that match these changes and guarantee the safety and reliability of power systems. Based on the technique presented in this thesis, a multi-level SPWM voltage source or other voltage waveform related to power electronics can be developed as a next step toward the

end goal: the development of a multi-functional, flexible, and power electronic technique-based high voltage test facility.

- In IEC60034-18-42 "Qualification and acceptance tests for partial discharge resistant electrical insulation systems (Type II) used in rotating electric machine fed by voltage converts" [28], the recommended test waveform is a high repetitive exponential decay pulse. However, in this research, tests show that the temperature rise on the 4 kV_{rms} coil surface is significantly higher when tested with a square wave or a SPWM waveform than that tested with a high repetitive exponential decay pulse. More insulation tests should be performed on different coils with the IGBT-based pulse voltage generator and other sources in order to indicate which voltage waveform is most suitable as a standard qualification and acceptance test voltage for electrical insulation systems (Type II) used in rotating electric machines fed by voltage convertors.
- Future applications of the IGBT-based pulse voltage generator can be developed in other areas, which include nero fibre spinning, food treatment, and fault location on transmission lines, high voltage cables, or large motors.

References

[1] B. Sergelen, D. Sodnomdorj, D. Ulzii-Orshikh, N. Mergenbaatar, S. Turbat, "Energy saving by using variable speed drives with AC induction motors in industries". Strategic Technologies, IFOST 2008, Third International Forum, 23-29 June, 2008 pp. 564-567.

[2] F. Blaabjerg, J. K. Pedersen, S. Rise, and H. Hansen, "A Comparative study of Energy Saving Benefits in Softstarters for Three-phase Induction Motors", IEEE Industry Applications Conference, Vo1. 1, pp. 367-374, 1995.

[3] J.A.Oliver, and G.C.Stone, "Implications for the application of the applications of adjustable speed drive electronics to motor stator winding insulation". IEEE Elec. Insul. Mag. Vol. 11, pp.32-36, 1995.

[4] A. H. Bonnett, "Analysis of the impact of pulse-width modulated inverter voltage waveforms on AC induction motors" IEEE Transactions On Industry Applications, Vol. 32, No. 2, March/April 1996.

[5] M. Kaufhold, G. Borner, M. Eberhardt, and J. Speck, "Failure mechanism of the interturn insulation of low voltage electric machines fed by pulse-controlled inverters" IEEE Electrical Magazine, Vol. 12, No. 5, September/October 1996.

[6] M. Yano, S. Abe, E. Ohno, "History of power electronics for motor drives in Japan".

[7] T. Sawa, T. Kume, "motor drive technology --history and visions for the future", 35th Annual IEEE Power Electronics Specialists Conference, Anchen, Germany, 2004.

[8] E. P. Wiechmann, P. Aqeveque, R. Burgos, and J. Rodriguez, "on the efficiency of voltage source and current cource inverters for high-power drives", IEEE transactions of industrial electronics, Vol.55, No.4, April 2008.

[9] W. McDermid, "Insulation Systems and Monitoring for Stator Windings of Large Rotating Machines", Vol.9, issue 4, July/Aug 1993, pp. 7-15.

[10] M. Chapman, N. Forst, R. Bruetsch, “Insulation Systems for Rotating Low-Voltage Machines”, Electrical Insulation, ISEI 2008, Conference Record of the 2008 IEEE International Symposium on 9-12 June 2008, pp. 257-260.

[11] D. M. Hepburn, I. J. Kemp, and A. J. Shields, “Mica”, Vol. 16, Issue5, Sept.-Oct. 2000, pp. 19-24.

[12] A. O. Staub, E. L. Owen, “Solid-State Motor Controllers”, IEEE Transactions On Industry Applications, Vol. IA-22, No. 6, November/December 1986.

[13] M. Kaufhold, H. Auinger, M. Berth, J. Speck, and M. Eberhardt, “Electrical Stress and Failure Mechanism of Winding Insulation in PWM-Inverter-Fed Low-Voltage Induction Motors”, IEEE Transactions on Industrial Electronics, Vol.47, Np.2, April 2000.

[14] D. Fabiani, G. C. Montanari, A. Cavallini and G. Mazzanti, “ Relation Between Space Charge Accumulation and Partial Discharge Activity in Enamelled Wires Under PWM-like Voltage Waveforms”, IEEE Trans. on Dielectrics and electrical Insulation, Vol. 11, No.3, pp. 392-405, June 2004.

[15] D. Fabiani, G. C. Montanari, A. Contin, “ Aging Acceleration of Insulating Materials for Electrical Machine Windings Supplied by PWM in the Presence and Absence of Partial Discharges”, IEEE ICSD, Eindhoven, The Neatherlands, pp. 283-286, 2001.

[16] C. Hudon, N. Amyot, T. Lebey, P. Castelan, and N. Kandev “Testing of Low-Voltage Motor Turn Insulation Intended for PWM Applications”, IEEE Transaction on Dielectrics and Electrical Insulation, Vol. 7, No. 6, pp. 783-789, Dec 2000.

[17] D. Fabiani, and G. C. Montanari, “The Effect of Voltage Distortion on Ageing Acceleration of Insulation Systems under Partial Discharge Activity”, IEEE Electrical Insulation Mag., Vol. 17, No. 3, pp. 24-33, May/June 2001.

[18] N. Foulon, J. P. Lucas, G. Barré, R. Mailfert, J. Enon, “Investigation of the Failure Mechanism of Insulation Subjected to Repetitive Fast Voltage Surges”, IEEE/EIC-EMCW Conf., pp. 401-406, Sep 1997.

[19] IEEE Std 43™-2000(R2006), IEEE Recommended Practice for Testing Insulation Resistance of Rotating Machinery.

[20] IEEE Std C50.12™-2005, "**I**EEE Standard for Salient-Pole 50 Hz and 60 Hz Synchronous Generators and Generator/Motors for Hydraulic Turbine Applications Rated 5 MVA and Above".

[21] IEEE Std 112™-2004, IEEE Standard Test Procedure for Polyphase Induction Motors and Generators**.**

[22] IEEE Std 115™, IEEE Guide: Test Procedures for Synchronous Machines, Part 1—Acceptance and Performance Testing, Part II—Test Procedures and Parameter Determination for Dynamic Analysis.

[23] IEEE Std 433™-, IEEE Recommended Practice for Insulation Testing of Large AC Rotating Machinery with High Voltage at Very Low Frequency.

[24] IEEE Std 522™, IEEE Guide for Testing Turn-to-Turn Insulation on Form-Wound Stator Coils for Alternating-Current Rotating Electrical Machines.

[25] IEEE Std 1043™, IEEE Recommended Practice for Voltage-Endurance Testing of Form-Wound Bars and Coils.

[26] IEEE Std 1310™, IEEE Recommended Practice for Thermal Cycle Testing of Form-Wound Stator Bars and Coils for Large Generators.

[27] IEEE Std 1553™, IEEE Standard for Voltage-Endurance Testing of Form-Wound Coils and Bars for Hydro generators.

[28] IEC60034-18-42 Qualification and acceptance tests for partial discharge resistant electrical insulation systems (Type II) used in rotating electric machine fed by voltage converts.

[29] C. Abbate, G. Busatto, L. Fratelli, F. lannuzzo, B. Cascone, G. Giannini, "Series Connection of High Power IGBT modules for traction applications", Power Electronics and Applications, 2005 European Conference. P. 8.

[30] Data sheet: TD351. Available at web site: www.st.com

[31] Data sheet: "Versatile fiber optic connection". Available at web site: www.semiconnector.agilent.com

[32] Data sheet: 16F87xA. Available at web site: www.microchip.com

[33] C.Hudon, J.N.Seguin, N.Amyot, "Turn insulation aging of motors exposed to fast pulses of inverter drives", Digital Object Identifier, 22-25, Sept 1997.

[34] Y. Weijun, "Failure Mechanism of Winding Insulations in Inverted-Fed motors", IEEE Electrical Insulation Magazine, pp. 18-23, 1997.

[35] Y.Shakweh, "MV inverter stack topologies", IEE Power Engineering Journal, vol.15, pp. 139-149, June 2001.

[36] K. H. J. Chong, and R. D. Klug, "High Power Medium Voltage Drives", Conference on Power System Technology- POWERCON, Vol.1, pp. 658-664, Nov 2004.

[37] J. H. Kim, M. H. Ryu, B. D. Min**,** and G. H. Rim, '200KV Pulse Power Supply Implementation', Power electronics and applications, 2007 Europan Conference on 2-5, Sept 2007, pp. 1-5.

[38] W. J. Carey, and, J. R. Mayes, "Marx generator design and performance," 24th Power Modulator Symposium and High-Voltage Workshop, 2002, pp. 625 – 628.

[39] L. M. Redondo, J. F. Silva, E. Margto, 'Analysis of a modular generator for high-voltage, high-frequency pulsed applications, using low voltage semiconductors and series connected step-up transformers', Review of Scientific Instruments 78, 034702, 2007.

[40] J. Salmon, L. Wang, A. Krieger, "Comparison of Current Controllers that use Internal Feedback of the Controller PWM Signals to Produce a PWM-cycle Zero Average Current-error", Power Electronics Specialists Conference, 2005. PESC '05. IEEE 36th, 16-16 June 2005, pp. 2012 – 2018.

[41] S. R. Bowes, A. Midoun, "New PWM switching strategy for microprocessor controlled inverter drives", Electric Power Applications, IEE Proceedings B Volume 133, Issue 4, July 1986, pp. 237 – 254.

[42] G. Hua, F.C. Lee, "Soft-switching techniques in PWM converters", Industrial Electronics, IEEE Transactions on Volume 42, Issue 6, Dec 1995, pp. 595 – 603.

[43] Y. Konishi, M. Nakaoka, "Current-fed three-phase and voltage-fed three-phase active converters with optimum PWM pattern scheme and their performance evaluations", Industrial Electronics, IEEE Transactions on Volume 46, Issue 2, April 1999, pp. 279 – 287.

[44] A. Ruderman, “Three-phase multi-level PWM rectifier multi-carrier discontinuous voltage modulation strategy”, Power Electronics and Applications, 2007 European Conference on 2-5 Sept 2007, pp. 1 – 9.

[45] R. Panda, R. K. Tripathi, “A Novel Sine Wave Inverter with PWM DC Link”, Industrial and Information Systems, 2008. ICIS 2008. IEEE Region 10 and the Third international Conference on 8-10 Dec. 2008, pp. 1 – 5.

[46] J. Salmon, A. Knight, J. Ewanchuk, “Single phase multi-level PWM Inverter topologies using coupled inductors”, Power Electronics Specialists Conference, 2008. PESC 2008. IEEE 15-19 June 2008, pp. 802 – 808.

[47] H. Wu; Y. Deng; Y. Liu; X. He, “A new clew for research on PWM methods of multilevel inverters: principle and applications”, Power Conversion Conference, 2002. PCC Osaka 2002, Vol 3, 2-5 April 2002, pp.1251 – 1256.

[48] W. K. Lee, S. Y. Kim, J. S. Yoon, D. H. Baek, “A comparison of the carrier-based PWM techniques for voltage balance of flying capacitor in the flying capacitor multilevel inverter”, Applied Power Electronics Conference and Exposition, 2006. APEC '06. Twenty-First Annual IEEE 19-23 March 2006, p. 6.

[49] IEC 60034-18-41, “Evaluation and Qualification of Electrical Insulation Systems Used in Rotating Electrical Machines when Fed from Voltage Converters”, 2006.

[50] J.A. Allison, “Understanding the need for Anti-corona materials in High Voltage Rotating Machines”, 6th International Conference on Properties and Applications of Dielectric Materials, pp. 860-863, 2000.